

# **Stony Brook University**



OFFICIAL COPY

**The official electronic file of this thesis or dissertation is maintained by the University Libraries on behalf of The Graduate School at Stony Brook University.**

**© All Rights Reserved by Author.**

# **Much Ado About Antibacterials: Dynamics and Drug Design**

Dissertation presented

By

**Kanishk Kapilashrami**

To

The Graduate School

in partial fulfillment of the requirements

for the Degree of

Doctor of Philosophy

In

**Chemistry**

**(Chemical Biology)**

Stony Brook University

May 2012

Copyright by  
Kanishk Kapilashrami  
2012

**Stony Brook University**

The Graduate School

**Kanishk Kapilashrami**

We, the dissertation committee for the above candidate for the  
Doctor of Philosophy degree, hereby recommend  
acceptance of this dissertation.

**Peter J. Tonge – Dissertation Advisor  
Professor, Department of Chemistry**

**Daniel P. Raleigh - Chairperson of Defense  
Professor, Department of Chemistry**

**Jin Wang  
Professor, Department of Chemistry**

**Gunther Kern  
Principal Scientist, Bioscience, Infection I-Med, AstraZeneca R&D Boston,  
USA**

This dissertation is accepted by the Graduate School

Charles Taber  
Interim Dean of the Graduate School

## **Abstract of the Dissertation**

### **Much Ado About Antibacterials: Dynamics and Drug Design**

by

**Kanishk Kapilashrami**

Doctor of Philosophy

in

Chemistry

(Chemical Biology)

Stony Brook University

2012

The post genomic era has led to a glut of new putative targets. However, there is a serious dearth of novel chemotherapeutics. It has become clear in recent years that apart from optimizing the thermodynamics of a drug-target interaction, a cell-wide understanding of a drug's mode of action is indispensable to prevent the attrition commonly observed in the drug discovery pipeline.

The type II fatty acid biosynthesis (FASII) pathway is a validated target for antibacterial drug design. In this study we focus on two targets of the bacterial FASII; a *trans*-2-enoyl-ACP reductase and a  $\beta$ -ketoacyl-ACP synthase, both essential for bacterial survival. InhA is the enoyl-ACP reductase in *Mycobacterium tuberculosis*. SAR analysis based on a triclosan lead has resulted in a range of inhibitors with slow dissociation rates and hence long residence times on the target, which we believe to be important for *in vivo*

efficacy. A structural explanation of the slow-off kinetics is crucial for designing inhibitors with longer residence times. We have used NMR to explore the relationship between protein dynamics and enzyme inhibition.

KasA, the  $\beta$ -keto-acyl-ACP synthase in MTB, is targeted by various natural products including thiolactomycin (TLM) though with very modest activity *in vitro*. We have used inter-ligand NOEs to understand the relative orientation of TLM and a pantetheine fragment bound to KasA. Based on our data we have synthesized molecules with not only improved binding affinities but also longer residence times on KasA.

Lastly, we have addressed questions of target quantitation and turnover in bacteria and the effect of drugs on bacterial *homeostasis*. We have used a mass spectrometry based approach to quantify cellular target concentrations and their rates of synthesis and degradation. Our data has yielded insights into the mechanism of the post-antibiotic effect and the influence that drugs have on target levels in the cell. These data have helped us envision a utopian scenario where a drug with a long residence time on a target that has a slow turnover, would show potent *in vivo* efficacy.

*To my mum and dad:  
For everything they have done and more*



## Table of Contents:

List of Figures .....	xii
List of Tables .....	xv
List of Abbreviations.....	xvii
Acknowledgements.....	xxii
List of Publications.....	xxv

### Chapter 1:

Drug Discovery – A target, a lead and a drug .....	1
Historical trends .....	2
Drug discovery pipeline.....	5
Target identification and validation.....	7
Lead identification and optimization .....	8
Fatty acid biosynthesis – A novel pathway for drug discovery .....	9
Bacterial FASII – Enzymes, proteins and reactions .....	11
Inhibitors of fatty acid biosynthesis .....	14
Inhibition of enoyl-ACP reductase.....	15
Inhibition of $\beta$ -ketoacyl-ACP synthase .....	23
Summary .....	26

### Chapter 2:

$\beta$ -Ketoacyl-AcpM Synthase A .....	28
---	----



Introduction .....	29
Tuberculosis - a worldwide pandemic .....	29
$\beta$ -Ketoacyl-AcpM synthase A – Mycobacterium tuberculosis .....	32
$\beta$ -Ketoacyl-AcpM synthase A – Catalysis .....	33
Targeting KasA – essentiality .....	36
Inhibiting KasA – Thiolactomycin .....	38
Materials and Methods.....	42
Materials .....	42
C171Q Mutagenesis .....	42
Enzyme purification.....	42
Preparation of NMR samples .....	43
2D and 1D NOE Spectroscopy .....	44
Results and Discussion.....	45
Conclusions .....	55
<b>Chapter 3:</b>	
KasA Inhibition .....	57
Introduction .....	58
Thiolactomycin as a lead .....	58
Optimizing TLM.....	59
Materials and Methods.....	63

Materials .....	63
5R-TLM and analogs .....	63
Enzymes .....	64
Direct binding fluorescence titrations .....	64
Results and Discussion.....	65
Direct binding measurements and analysis .....	65
Rational Inhibitor design .....	70
Structure activity relationships .....	75
SetA.....	75
Set B.....	80
SAR of TLM analogs against other bacteria .....	88
Conclusions .....	92
<b>Chapter 4:</b>	
InhA – protein dynamics and ligand binding .....	95
Introduction .....	96
Trans-2-enoyl-AcpM reductase.....	96
Inhibition by isoniazid and resistance:.....	97
Lead optimization with triclosan .....	98
Slow onset inhibition with diphenyl ethers.....	100
Mechanism of time dependent inhibition in InhA.....	101

Methods to study conformational dynamics in InhA.....	103
Site directed mutagenesis.....	104
Fluorescence spectroscopy .....	104
Nuclear Magnetic Resonance spectroscopy .....	105
Materials and Methods.....	108
Preparation of the InhA mutants .....	108
Loop replacement experiments.....	109
Purification of enzymes – InhA and mutants.....	112
Synthesis of substrate.....	113
Enzyme kinetics .....	113
Inhibition of wild type and mutant InhA .....	113
Overexpression and purification of cyanophenylalanine incorporated InhA.....	114
Fluorescence binding experiments with F <sub>CN</sub> -InhA.....	114
Over-expression and purification of <sup>15</sup> N/ <sup>2</sup> H/ <sup>13</sup> C labeled InhA .....	114
NMR spectroscopy.....	116
Results and Discussion.....	117
Kinetic studies of mutant InhA .....	117
Inhibition studies with the InhA mutants.....	121
Fluorescence studies with F <sub>CN</sub> -InhA .....	123
Protein dynamics – NMR and SAXS.....	126

Conclusions: .....	139
--------------------	-----

**Chapter 5:**

Target quantitation and turnover .....	141
Introduction .....	142
Attrition in the drug discovery pipeline .....	142
Drug-target lifetime and pharmacology .....	143
Post antibiotic effect – target turnover.....	144
Mass spectrometry – target quantitation and turnover.....	145
Materials and Methods.....	147
Materials .....	147
Sample preparation.....	148
Cell cultures and growth conditions .....	149
Quantitation experiments .....	149
Turnover experiments .....	150
Mass spectrometry.....	151
MudPIT .....	151
1D (TSQ) .....	152
Turnover experiments .....	154
Results and Discussion.....	156
Target quantitation .....	156

Target turnover .....	167
Protein Degradation .....	167
Protein Synthesis .....	174
Conclusions .....	180
<b>References</b> .....	<b>182</b>

## List of Figures

Figure 1.1: Timeline of Antimicrobial drug discovery and resistance .....	3
Figure 1.2: Drug discovery pipeline.....	6
Figure 1.3: The Fatty acid biosynthesis type II pathway in <i>E. coli</i> .....	11
Figure 1.4: Inhibitors of bacterial FASII.....	15
Figure 1.5: INH-NAD adduct bound to InhA.....	17
Figure 1.6: Triclosan bound to <i>ec</i> FabI/NAD <sup>+</sup> complex.....	19
Figure 1.7: The X-ray crystal structure of InhA bound to PT70/NAD <sup>+</sup> .....	22
Figure 1.8: <i>E. coli</i> KASI and the catalytic triad .....	24
Figure 1.9: TLM bound to the malonyl-AcpM binding pocket of KasA.....	26
Figure 2.1: The FASII pathway in MTB .....	31
Figure 2.2: The active site of KasA and the conserved thiolase fold.....	33
Figure 2.3: Catalytic mechanism of KasA in the elongation step of FASII .....	34
Figure 2.4: Active site modification in acyl KasA.....	36
Figure 2.5: KAS inhibitors .....	38
Figure 2.6: <sup>1</sup> H NMR spectrum of TLM and PK940 in D <sub>2</sub> O at 700 MHz.....	46
Figure 2.7: 2D NOESY spectrum to detect ILOEs between TLM and PK940 .....	48
Figure 2.8: Overlay of <sup>1</sup> H NMR DPFGE 1D NOE spectra.....	50
Figure 2.9: NOE build up curves .....	52
Figure 2.10: Orientation of TLM and PK940 in the C171Q KasA active site .....	55
Figure 3.1: Time based inhibition of acyl KasA .....	61
Figure 3.2: Interactions between TLM with wild type and C171Q KasA.....	62

Figure 3.4: The direct binding curves for 3-demethylTLM.....	67
Figure 3.5: Time dependent inhibition of C171Q KasA by 3-propylTLM .....	68
Figure 3.6: Slow-onset kinetics of 3-propylTLM binding to C171Q KasA.....	70
Figure 3.7: Docked structure of the linked-fragment lead bound to KasA. ....	72
Figure 3.8: TLM as an iso-stere of malonyl-AcpM.....	73
Figure 3.9: Active site residues stabilizing a hydrogen bond donor/acceptor at C3 .....	74
Figure 3.10: Hydrophobic pocket in C171Q KasA occupied by an acyl chain.....	75
Figure 3.11: Hydrogen bond network stabilizing the TLM:KasA complex .....	77
Figure 3.12: Docked structures of TLM9 bound to KasA .....	82
Figure 4.1: The catalytic mechanism for the enoyl-AcpM reductase in MTB. ....	97
Figure 4.2: Activation of Isoniazid by KatG .....	98
Figure 4.3: Diphenyl ether lead and inhibitors.....	99
Figure 4.4: The two step mechanism for time based inhibition of InhA.....	101
Figure 4.5: Substrate binding loop and slow onset inhibition .....	103
Figure 4.6: The reaction catalyzed by InhA.....	118
Figure 4.7: UV-CD scans for wild type InhA and mutants. ....	120
Figure 4.8: Quenching of $F_{CN}$ fluorescence by chloride ions.....	124
Figure 4.9: Quenching of $F_{CN}$ fluorescence by $NAD^+$ and DMSO .....	124
Figure 4.10: Emission scans of A201 $F_{CN}$ InhA upon binding to inhibitors. ....	125
Figure 4.11: $^{15}N/^{1}H$ HSQC of wild type InhA and inhibitor bound InhA .....	127
Figure 4.12: Analysis of the $^1H$ detect DOSY spectra .....	129
Figure 4.13: SAXS data of wild type InhA and InhA bound to the inhibitors.....	132

Figure 4.14: Overlay of the $^{15}\text{N}/^1\text{H}$ TROSY HSQC spectra .....	135
Figure 4.15: $^{15}\text{N}/^1\text{H}$ TROSY-HSQC of InhA bound to PT70 at 40 °C .....	137
Figure 4.16: $^{15}\text{N}/^1\text{H}$ TROSY-HSQC spectrum of (-) His <sub>6</sub> InhA bound to PT70 ..	138
Figure 5.1: MRM transitions for <i>ecFabX</i> . .....	154
Figure 5.2: Calibration curves for AQUA standard for <i>ecFabX</i> quantitation .....	157
Figure 5.3: Calibration curves for the new AQUA standards.....	161
Figure 5.4: Changes in copy-number/cfu in <i>ecFabX</i> upon treatment with triclosan. .....	163
Figure 5.5: Changes in copy-number/cfu in <i>ecFabX</i> upon treatment with TLM.	165
Figure 5.6: Degradation of <i>ecFabX</i> using the steady state assumption .....	169
Figure 5.7: Degradation of <i>ecFabX</i> using the non-steady state assumption.....	172
Figure 5.8: The amount of $^{15}\text{N}$ protein synthesized as a function of time.....	175
Figure 5.9: Synthesis of the three FASII proteins .....	176
Figure 5.10: Isobaric interference of the $^{13}\text{C}$ isotope of the FabF standard.....	179



## List of Tables

Table 1.1: Diphenyl ether inhibitors targeting <i>M. tuberculosis</i> .....	21
Table 2.1: Primers for C171Q KasA Quikchange mutagenesis .....	42
Table 3.1: MIC ( $\mu\text{g/ml}$ ) values for thiolactomycin against various bacteria. ....	59
Table 3.2: C4 analogs of TLM (Set A; TLM 21-24) .....	79
Table 3.3: Binding parameters for C3 TLM analogs to free enzyme and the acyl- KasA mimic.....	87
Table 3.4: KASI and KASII enzymes in various bacteria .....	88
Table 3.5: MIC values of TLM analogs against a different bacterial strains. ....	91
Table 4.1: The forward and the reverse primers for mutagenesis.....	111
Table 4.2: Kinetic parameters for wild type InhA and mutants .....	119
Table 4.3: IC <sub>50</sub> data for PT04 and triclosan for wild type InhA and mutants.....	122
Table 4.4: Radius of gyration calculated from the Guinier analysis.....	133
Table 5.1: Peptides from FASII enzymes used as M.S standards. ....	148
Table 5.2: Details of the MRM analysis for the turnover experiments. ....	156
Table 5.3: Target concentrations and copy-number per cfu.....	158
Table 5.4: Copy-number/cfu and concentrations of ecFabX enzymes.....	159
Table 5.5: Changes in copy-number/cfu of ecFabX after treatment with triclosan. .....	162
Table 5.6: Changes in copy-number/cfu of ecFabX post treatment with TLM...	164
Table 5.7: The cytosolic volume of <i>E.coli</i> cell. ....	166
Table 5.8: Rates of degradation of FabX (steady state assumption) .....	170

Table 5.9: Anti-correlation of protein abundance/cfu as a function of time.....	171
Table 5.10: Rates of degradation of FabX (non-steady state assumption) .....	173
Table 5.11: The rates of synthesis of ecFabX.....	177

## List of Abbreviations

TB: Tuberculosis

FDA: U.S Food and Drug Administration

*S. aureus*: *Staphylococcus aureus*

*N. gonorrhoeae*: *Neisseria gonorrhoeae*

*S. pneumoniae*: *Streptococcus pneumoniae*

*P. aureginosa*: *Pseudomonas aureginosa*

*M. tuberculosis*, MTB: *Mycobacterium tuberculosis*

W.H.O: World Health Organization

ADME/Tox: Absorption, Distribution, Metabolism, Excretion/ Toxicity

FASII: Fatty acid biosynthesis type 2

FASI: Fatty acid biosynthesis type 1

*E. coli*: *Escherichia coli*

AccABCD: acetyl-CoA carboxylase

FabD: Malonyl-CoA:ACP transacylase

FabH:  $\beta$ -ketoacyl-ACP synthase III

FabB:  $\beta$ -ketoacyl-ACP synthase I

FabF:  $\beta$ -ketoacyl-ACP synthase II

FabG:  $\beta$ -ketoacyl-ACP reductase

FabA and FabZ:  $\beta$ -hydroxyacyl-ACP dehydrases

FabI: *trans*-2-enoyl-ACP reductase

ACP: Acyl carrier protein

CoA: Coenzyme-A

NADH: Nicotinamide adenine dinucleotide reduced

NAD<sup>+</sup>: Nicotinamide adenine dinucleotide oxidized

INH: Isoniazid

InhA: *trans*-2-enoyl-ACP reductase in *M.tuberculosis*

K<sub>i</sub>: Inhibition constant

PDB: Protein data bank

SAR: Structure activity relationships

*P. falciparum*: *Plasmodium falciparum*

MIC: Minimum inhibitory concentration

KatG: Mycobacterial catalase-peroxidase

KAS: β-ketoacyl synthase

*E. faecalis*: *Enterococcus faecalis*

*H. influenzae*: *Haemophilus influenzae*

TLM: Thiolactomycin

NMR: Nuclear magnetic resonance

AIDS: Acquired immune-deficiency syndrome

MDR-TB: Multiply drug resistant TB

XDR-TB: Extensively drug resistant TB

AcpM: Acyl carrier protein in MTB

KasA: β-ketoacyl-ACP synthase I in MTB

KasB: β-ketoacyl-ACP synthase II in MTB

K<sub>a</sub>: Acid-dissociation constant

*M. smegmatis*: *Mycobacterium smegmatis*

NOESY: Nuclear Overhauser effect spectroscopy

ILOE: Inter-ligand nuclear Overhauser effect

DPFGSE: Double pulsed field gradient spin echo

O.D<sub>600</sub>: Optical density at 600nm

Rpm: Revolutions per minute

HMQC: Heteronuclear multiple quantum correlation

HMBC: Heteronuclear multiple bond correlation

T<sub>mix</sub>: Mixing time

*S. marcescens*: *Serratia marcescens*

*S. flexneri*: *Shigella flexneri*

*S. enterides*: *Salmonella enterides*

*S. typhi*: *Salmonella typhi*

*S. paratyphi*: *Salmonella paratyphi*

*K. pneumonia*: *Klebsiella pneumoniae*

$k_{obs}$ : Rate constant of time dependent quenching

$k_b$ : Rate constant of photobleaching

$k_{off}$ : Rate constant of dissociation of inhibitor from the Enzyme-inhibitor complex

$k_{on}$ : Forwards rate constant of transition from EI\* to EI

PEG: Poly ethylene glycol

*Y. pestis*: *Yersinia pestis*

*B. pseudomallei* (*B.pm.*): *Burkholderia pseudomallei*

*B. thailandensis* (*B.t.*): *Burkholderia thailandensis*

*F. tularensis (F.tu): Francisella tularensis*

SDR: Short-chain dehydrogenase/ reductase

IC<sub>50</sub>: 50% inhibition constant

BSA: Bovine serum albumin

IPTG: Isopropyl  $\beta$ -D-1-thiogalactopyranoside

F<sub>CN</sub>: Cyanophenylalanine

TROSY: Transverse relaxation optimized spectroscopy

HSQC: Heteronuclear single quantum coherence.

CD: Circular dichroism

DMSO: Dimethyl sulfoxide

FRET: Förster resonance energy transfer

DOSY: Diffusion ordered spectroscopy

R<sub>h</sub>: Radius of hydration

R<sub>g</sub>: Radius of gyration

SAXS: Small angle X-Ray scattering

P(r): pair-distance distribution function

PAE: Post-antibiotic effect

MS: Mass spectrometry

LC: Liquid chromatography

SILAC: Stable isotope labeling by amino acids in culture

ICAT: Isotope coded affinity tags

iTRAQ: Isobaric tags for relative and absolute quantitation

AQUA: Absolute quantitation

SDS: Sodium dodecyl sulfate

PAGE: Polyacrylamide gel electrophoresis

PMSF: Phenylmethyl sulfonyl fluoride

MudPIT: Multidimensional protein identification technology

FA: Formic acid

LTQ: Linear trap quadrupole mass spectrometer

TSQ: Triple stage quadrupole mass spectrometer

ESI: Electrospray ionization

MRM: Multiple-reaction monitoring

ACN: Acetonitrile

Cfu: Colony forming unit

emPAI: exponentially modified protein abundance index

PK/PD: Pharmacokinetics/ pharmacodynamics

## Acknowledgements

As I sit down to write my dissertation, a lot is going through my mind. These 6 odd years I've been at Stony Brook, the places I've been to and the people I've met have added so much to my life that I find myself overwhelmed and at a loss of words to express myself. These few pages would perhaps be a meager attempt on my part to acknowledge those people who I am indebted to for making me the person I am today.

For starters I must thank my advisor, Prof. Peter Tonge, for being an excellent boss. At the risk of going into rhetoric, I really do feel blessed to be a part of the Tonge lab and to be under his able tutelage. Pete has played a key role in allowing me to stand on my own two feet in the scientific arena. Allowing me to explore my own research interests, he has been pivotal in honing my creativity and making me an independent researcher. To his patient support ("*teething issues*"??!!), his encouragement and his vision, I owe the successful completion of my Ph.D.

I must also thank the chair of my committee – Prof. Dan Raleigh. Dan has helped me immensely throughout my Ph.D. through his brilliant and timely scientific advice and constant support. Our brief *tête-à-têtes* in the 6<sup>th</sup> floor corridor always kept me going and would indeed be quite memorable!



Thinking about these past few years in Stony Brook, a lot of people cross my mind; people that came into my life and became an integral part of my being. Though I am rarely vocal with my acknowledgements (perhaps to many people's chagrin), I feel a rather foreign urge to thank them all for adding so much to my life and making me the person I am. Derek Middlemiss, Marian Fernando, Kellie Aldi, Lucienne Buannic, Allison Hiagney, Carl Machutta, Jacek Kuzniar – I really appreciate you guys being in my life, seeing me through the thick and thin. Sajjad Hossain, Kajal Gulati – you guys came into my life as friends but very quickly became family, I must thank you for being with me in flesh and/or in spirit. Joseph Hein, I must thank him for standing by me and for his exceptional care and support.

Last but not the least, I must *must* acknowledge my family to whom I owe not just this degree or any future success but also my life. *Ma* and *papa*, for all the sacrifices they have made, all the selfless love and blessings they have showered me with and for the relentless faith, even at times when I perhaps faltered. To them, for all they have done, with or without knowing, I dedicate this dissertation. *Baidi* and *Abhinav jijaji*, for being a constant source of inspiration and sound advice and of course for all the fun times (*kweed* sessions anyone??!!). *Anu di* and *Amit jijaji*, for loving me despite my tantrums (I swear you can sleep in the room next time around!), for lovely times and of course for all the help with formatting!! Finally, my adorable niece, *Ahana* - you should

know that you are loved and that we are ecstatic for being blessed with you in our lives.

I thank you all for all you have done with or without knowing and please know that all the fights and tantrums aside I cherish being your son, your brother and your friend – and I wouldn't have it any other way...

## List of Publications

1. “Transient 1D NOE NMR Spectroscopy for Fragment-Based Inhibitor Discovery: Application to the Development of Thiolactomycin-Based KasA Inhibitors.” **Kanishk Kapilashrami**, Gopal Reddy Bommineni, Carl Machutta, Pilho Kim, Cheng-Tsung Lai, Carlos Simmerling, Francis Picart, Peter J. Tonge (Submitted).
2. “Slow Onset Inhibition of bacterial  $\beta$ -ketoacyl-acyl carrier protein synthases by Thiolactomycin.” Carl Machutta, G.R Bommineni, Sylvia Luckner, **Kanishk Kapilashrami**, Bela Ruzsicska, Peter J. Tonge. *J. Biol. Chem.* 2010, (285), 6161-9.
3. “One-Dimensional Inter-ligand Nuclear Overhauser Effect – fragment based drug discovery targeting *M.tuberculosis* KasA” **Kanishk Kapilashrami**, Carl Machutta, Francis Picart, B. Gopal Reddy, Peter J. Tonge *FASEB* April, 2010
4. “Protein target quantitation and turnover in bacterial Fatty acid biosynthesis type II pathway” **Kanishk Kapilashrami**, Antonius Koller, Robert Reiger, Peter J. Tonge (in preparation).
5. “Design and synthesis of potent analogs of TLM targeting Mycobacterium tuberculosis – a Fragment based approach.” **Kanishk Kapilashrami**, Gopal Reddy Bommineni, Susan Knudson, Richard Slayden, Jason Cummings, Yang Lu, Peter J. Tonge (in preparation)
6. “Probing protein dynamics in InhA upon binding slow onset inhibitors.” **Kanishk Kapilashrami**, Kaushik Dutta, Francis Picart, Daniel P. Raleigh, Bowu Luan, Peter J. Tonge (in preparation)

# Chapter 1

*Drug Discovery – A target, a lead and a drug*

*Historical trends:*

Drug discovery, as we know it today, really began in the 19<sup>th</sup> century with Paul Ehrlich postulating the existence of “chemoreceptors” on organisms. He suggested that differences in these chemoreceptors on organisms from homologs in host tissues could be therapeutically exploited. This can be perhaps considered the birth of chemotherapy, that laid the foundation for significant therapeutic triumphs in subsequent years (1). Before the advent of antibiotics in the 1940s, patients with bacterial infections, caused by organisms such as *Streptococcus pneumonia* and *Mycobacterium tuberculosis*, had a very low chance of survival. In fact, with the lack of antimicrobials, tuberculosis (TB) had a mortality rate of almost 50% (2, 3). However, by the late 19<sup>th</sup> century chemistry had reached a level of maturity that allowed the use its theories and practices to systems outside its realm (1).

Subsequently, Ehrlich’s identification of anti-syphilitic and anti-trypanosomal “magic bullet” drugs ushered in the modern era of chemotherapy based on chemically synthesized molecules that sustained the dye industry (1, 4). It was then that Fleming’s discovery of penicillin brought about the ‘Golden age’ of antibacterial drug discovery with a shift from solely synthetic efforts to the exploitation of scaffolds found in natural products. This was the era, spanning roughly two decades from 1940 through 1960, when most of the antimicrobial classes now in clinical use were first characterized (4). Over the next few

decades most drug design efforts were focused more on medicinal chemical modification of these scaffolds instead of discovery. Since the proverbial golden days, the pace of discovery of novel and clinically useful classes of antibiotics has slowed drastically. Though daptomycin (lipopeptide) and linezolid acid (oxazolidinone) were approved by the FDA in 2003 and 2000 respectively, these antibiotic classes were first discovered in the 80s (4) (Figure 1.1). The lack of novel classes of antibiotics can be attributed, amongst other things, to the shift in the paradigm of antibiotic discovery away from discovery of new scaffolds.

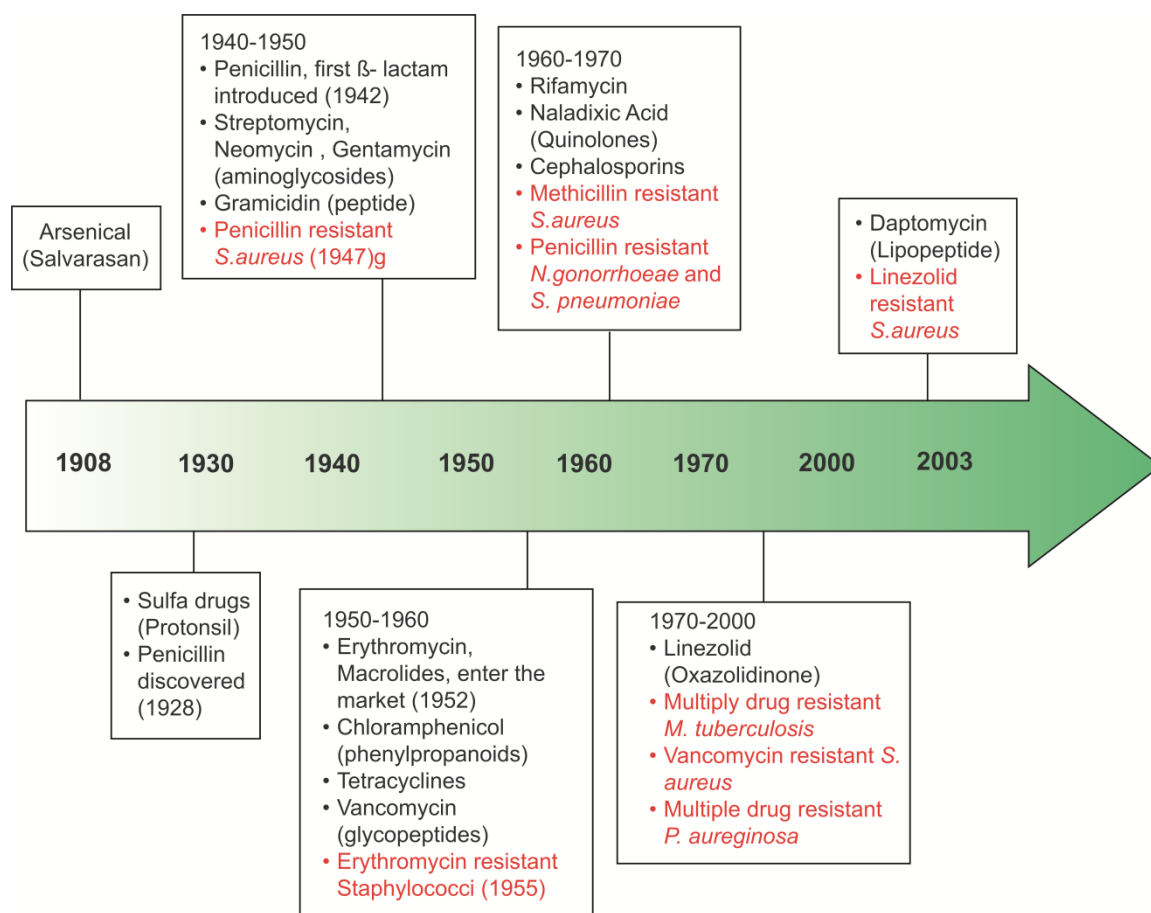


Figure 1.1: Timeline of Antimicrobial drug discovery and resistance.

Adapted from (4, 5)

Moreover, along with the successes of the *golden-age* came a degree of complacency where the pharmaceutical companies diverted their efforts in other therapeutic areas (6). In this time period while all antibiotics in the market were modifications of existing scaffolds and no novel antibiotic was introduced, bacteria developed resistance to commonly used antibiotics with each year seeing more strains resistant to different lines of medicinal assault (2, 4, 7). While antibiotic resistance has always been a problem and a driving force for drug discovery programs, the increase in the number and the diversity of resistant pathogens continues to pose a severe threat to public health worldwide (4). In fact, multidrug resistant strains of organisms such as *Klebsiella pneumoniae* and *Acinetobacter baumannii* are virtually untreatable by currently available antibiotics (4, 8, 9). The emergence of resistant strains is a massive clinical problem for anti-TB programs around the world. In 2011, The World Health Organization (W.H.O) estimated emergence of 440,000 new cases of multidrug resistant TB every year where the pathogen is resistant to the two most effective drugs, isoniazid and rifampicin (first line drugs). There has also been an emergence of extensively drug resistant strains which show resistance to not just the first line of treatment but also to many second line drugs (amikacin, kanamycin or capreomycin) and fluoroquinolones (W.H.O., Global T.B control report, 2011, (10-12)).

Resistance has been reported against drugs such as vancomycin that was considered the 'drug of last resort' for a variety of bacterial infections including

multidrug resistant *Staphylococcus aureus* (13). Irrespective of the origin, environmental or commensal, these 'superbugs' have devised different ways to develop resistance against the available drugs. This may include bypassing the drug target, increasing the antibiotic efflux and reducing the influx and/or inactivation of the drug by expression of specific modifying enzymes (4, 14).

Hence, there is a great need to design novel antibiotics with a distinct mode of action to combat the problem of resistance. This of course includes discovering and validating new targets, discovering new natural scaffolds and using medicinal chemistry to optimize promising moieties. That being said, it is of utmost importance to invest in and understand bacterial physiology especially in states of latency. It is these 'dormant' states that are predominant in bacterial populations and are highly resistant to antibiotic treatments (2, 15). This dissertation sheds light on at different levels of the drug-discovery process in order to aid the development of novel chemotherapeutics.

#### *Drug discovery pipeline:*

The discovery and development of new drugs is an arduous process that could take easily up to a decade if not more. Typically, modern day drug discovery programs (**Figure 1.2**) involve years of pre-discovery that prelude the discovery and development of novel chemotherapeutics. Various bottlenecks in this process include not just target and hit identification but also lead optimization



and the size of the medicinal chemistry effort that can be mounted (16). A major source of attrition during the development of new drugs comes from a severe disconnect between *in vitro* performance and *in vivo* efficacy. It is therefore very important to consider the difference between drug behavior in a closed *in vitro* system and an open *in vivo* system. It is quite widely accepted that understanding a drug's mode of action, including the lifetime of the drug-target complex (17) can help improve *in vivo* drug activity.

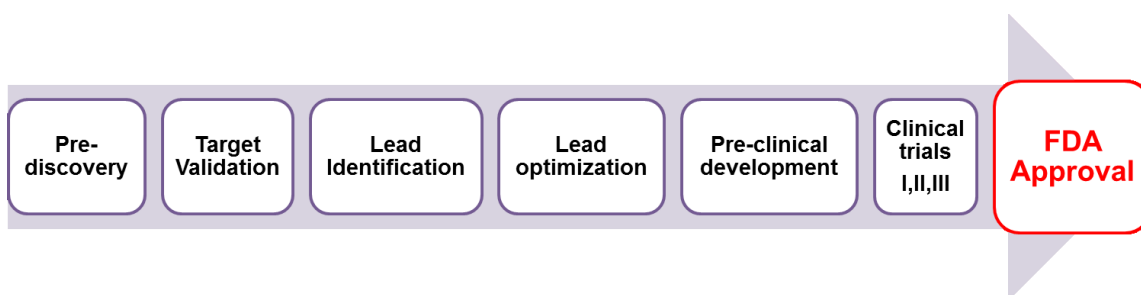


**Figure 1.2: Drug discovery pipeline.** Adapted from (18-20). Each of these stages typically involves an interdisciplinary approach with both biologists and chemists working in close harmony.

While all of these stages have equal contribution to a successful launch of a new drug, this dissertation focuses on the earlier stages of drug discovery ranging from pre-discovery through lead optimization.

### *Target identification and validation:*

At the very onset of any drug discovery program, it is indispensable to understand the etiology and the pathogenesis of the disease and the molecular mechanisms underlying them. This pre-discovery phase would include an in-depth understanding of the changes in the pathogen at the genetic and the proteomic level and how these changes result in the disease pathology. Armed with this knowledge, a researcher would choose a 'druggable' target protein or gene for drug development (19). However, just because a target is hypothetically linked to a disease does not necessarily make it a relevant point of intervention for novel drugs. Therefore, a target must be validated before embarking on the drug discovery program. Target validation has major implications in the success or failure of a drug. As a starting point one should expect a reproducible, dose dependent phenotypic change in live cells induced by the drug. The validation is greater if the same phenotype can be observed in an animal model that has disease relevant characteristics (1, 20). However, procurement or development of an *in vivo* model relevant to the human disease in question is challenging as animal models, if available, might not replicate all elements of human disease pathogenesis (20, 21). Hence, it is not uncommon, especially for human diseases, that the validation occurs relatively late in the drug-discovery pipeline, at the time of phase III clinical trials (20).

### *Lead identification and optimization:*

The next step after having identified and validated a target is to look for the 'lead compound' that can interact with the target, modulate target activity and alter the course of the disease. Traditionally, different methods have been used to identify 'hits' and subsequently lead molecules, including de-novo design and high throughput screening methods. Also, a wide variety of pharmaceutical compounds have been derived from natural sources. The use of natural product leads traces back to the isolation of penicillin by Alexander Fleming from a soil fungus – *Penicillium notatum*. Microorganisms found in nature continue to evolve myriad pathways to synthesize complex bio-active molecules (4). While, natural products have fallen out of favor in the past few years, quite a few drug companies such as Wyeth, Bayer and Merck have successfully launched drugs based on natural product scaffolds (22).

Once identified, a lead is optimized to make it more selective and specific for the target and to optimize the pharmacokinetic (ADME/Tox) properties. Optimization typically involves medicinal chemists and biologists working closely, making modifications to the lead and testing the effect of these alterations on the biological activity of the compound. Subsequent stages of optimization include evaluation of drug formulations, synthetic feasibility and scaling-up costs. A lead compound that successfully endures these rigorous tests would subsequently

move on to the preclinical and clinical trials followed by review and, in a perfect world, approval by the FDA.

*Fatty acid biosynthesis – A novel pathway for drug discovery:*

In light of growing antibacterial resistance there is a desperate need for drugs that inhibit different bacterial targets and have a novel modes of action. Advances in gene sequencing have resulted in a very large number of possible drug targets though this does not correlate with a greater efficiency of the drug discovery process (23, 24). Ideally, a combinatorial approach with genomic, proteomic and the more recent metabolomic components is likely to be more successful in delivering a 'druggable' target (23).

Traditionally, metabolic enzymes have been lucrative targets due to their role in molecular physiology and conservation in various pathogens. Also, the availability of enzyme assays is very useful at the stage of lead identification and optimization (6, 25). As the currently used antibiotics target only a subset of these enzymes, they might represent an untapped source of many more targets. However, recent *in vivo* studies in *Salmonella* have suggested a paucity of new metabolic targets for broad-spectrum antibacterials and a need to refocus our attention on previously known but unexploited targets (25).

Fatty acid biosynthesis (FAS) has been shown to be a valid target for antibacterial drug discovery through extensive research in *Escherichia coli* (26, 27). While, fatty-acid biosynthesis is relatively underexploited, it is highly conserved amongst bacteria and is essential for its survival. Also, bacterial FAS is distinct from the mammalian FAS (FASI) wherein the various steps are catalyzed by the different domains of a large polypeptide (28). Apart from gene knock out/ knock down experiments, the bacterial FAS pathway has been validated by the effectiveness of drugs such as isoniazid and triclosan which target a key component of this pathway (29, 30). Moreover, various bacteria, unable to scavenge fatty acids from the host, have to synthesize this indispensable component of the cell membrane *de novo* (31, 32). The essentiality of this pathway coupled with the major differences with mammalian FASI make it a lucrative target for broad-spectrum antibiotic discovery (28).

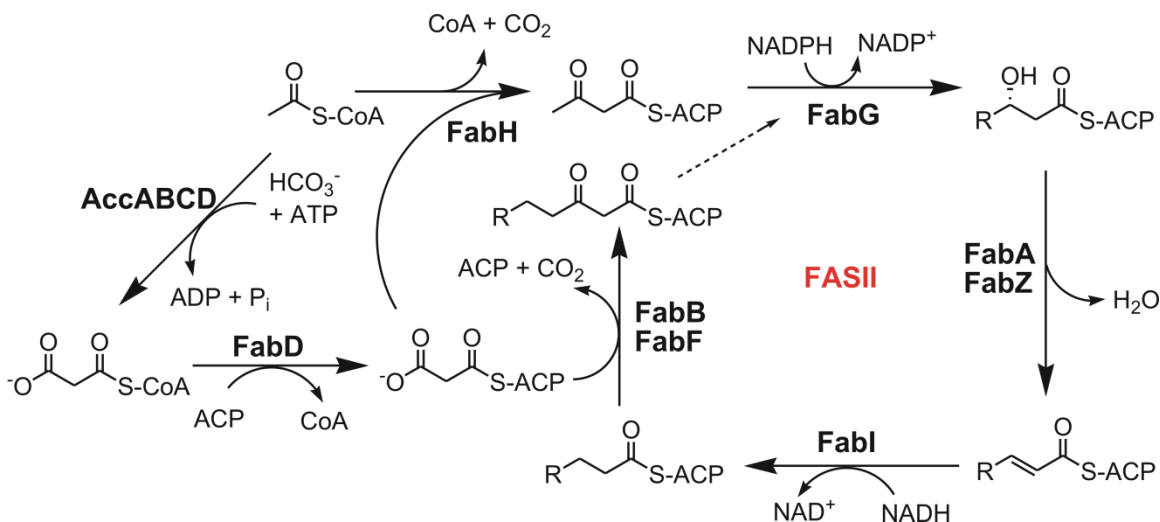


**Figure 1.3: The Fatty acid biosynthesis type II pathway in *E. coli*.** AccABCD is the acetyl-CoA carboxylase; FabD is the malonyl-CoA:ACP transacylase; FabH, FabB and FabF are  $\beta$ -ketoacyl-ACP synthases; FabG is the  $\beta$ -ketoacyl-ACP reductase; FabA and FabZ are  $\beta$ -hydroxyacyl-ACP dehydrases and FabI is the *trans*-2-enoyl-ACP reductase. The initial condensation of acetyl-ACP with malonyl-ACP is carried out by FabH while further rounds of elongation are carried out by FabB and FabF.

*Bacterial FASII – Enzymes, proteins and reactions:*

FASII (**Figure 1.3**) has been extensively studied in *E. coli* where it forms the basis of our understanding of this pathway in bacterial systems (33). Different bacteria exhibit slight differences in their FASII pathways. However, most of the homologs of *E. coli* FASII enzymes are very well conserved in all bacteria (34).

The initiation of FASII involves reactions that provide the substrates for the first chain elongation step. Condensation of an acceptor C2 unit (acetyl-CoA or ACP) with malonyl-ACP to form acetoacetyl-ACP marks the first step of FASII. Synthesis of malonyl-CoA is catalyzed by the acetyl-CoA carboxylase (ACC) protein complex. In contrast to the multifunctional protein in mammals, the bacterial ACC is composed of four separate proteins with the reaction divided into two steps. The first step involves the activation of the CO<sub>2</sub> moiety in bicarbonate and its transfer to biotin to form carboxybiotin by AccC. The second step involves transfer of the CO<sub>2</sub> group to acetyl-CoA to form malonyl-CoA catalyzed by AccA and AccD. Substrate channeling between these two half reactions is provided by AccB which has the biotin cofactor covalently attached to it (35-37). Subsequently, malonyl-CoA:ACP transacylase (FabD) catalyzes the conversion of malonyl-CoA to malonyl-ACP. The transthioesterification reaction is catalyzed via a ping-pong mechanism where the malonyl group, from malonyl-CoA, is attached to the active site serine and the CoA is eliminated. A nucleophilic attack from the thiol of the acyl carrier protein (ACP) results in the formation of malonyl-ACP (30, 38).

The elongation step is initiated by a decarboxylative Claisen condensation of malonyl-ACP with acetyl-CoA catalyzed by FabH ( $\beta$ -ketoacyl-ACP synthase III). The reaction involves formation of an acyl enzyme intermediate by the attack of the cysteine sulfhydryl to the acetyl group. Subsequently, malonyl-ACP undergoes decarboxylation resulting in the formation of a carbanion. The

condensation of the carbanion with the acetyl group results in formation of acetoacetyl-ACP (30, 39, 40).  $\beta$ -Ketoacyl-ACP (acetoacetyl-ACP) is then reduced at the C3 position to form  $\beta$ -hydroxyacyl-ACP by FabG, the  $\beta$ -hydroxyacyl-ACP synthase. FabG utilizes a Ser-Tyr-Lys triad and an NADPH cofactor similar to the short chain alcohol dehydrogenase/reductase superfamily of proteins (30, 41, 42). The next step in FASII is the dehydration of 3-hydroxyacyl-ACP to *trans*-2-enoyl-ACP by 3-hydroxyacyl-ACP dehydrase (FabZ or FabA). These proteins are characterized by a His-Asp/Glu dyad where the histidine abstracts the C2 proton of the substrate while the acidic residue promotes the removal of the hydroxyl group (43, 44).

The last step in this cycle is catalyzed by FabI (*trans*-2-enoyl-ACP reductase) with the reduction of *trans*-2-enoyl-ACP to acyl-ACP. Unlike FabG, in *E. coli*, this protein uses an NADH cofactor and a Tyr-Tyr-Lys triad (45-47). Once, the optimal chain length is reached a thioesterase cleaves the fatty acid for cell-wall synthesis. Further elongation of the acyl chain is catalyzed by FabB or FabF ( $\beta$ -ketoacyl-ACP synthases) depending on the chain length. The mechanism of catalysis for FabB (KAS I) and FabF (KAS II) is similar to FabH (Kas III) in the formation of an acyl enzyme intermediate with the elongating acyl chain and the enzyme. This is followed by a decarboxylative claisen condensation between malonyl-ACP and growing acyl chain resulting in formation of  $\beta$ -ketoacyl-ACP.



It is important to note that the growing acyl chain is shuttled between enzymes via a highly acidic acyl carrier protein (ACP). This *acpP* gene product is the most abundant protein in the cell and carries the acyl chain via a phosphopantetheinyl group (48-50).

*Inhibitors of fatty acid biosynthesis:*

The essentiality of FASII and its differences from the mammalian homologs presents enzymes in this pathway as lucrative targets for antibacterial drug discovery. Moreover, since these enzymes are conserved through all bacteria, targeting FASII can result in discovery of successful broad spectrum antibiotics. Various inhibitors that target the FASII enzymes have been described (**Figure 1.4**) including isoniazid which is a first line drug against tuberculosis.

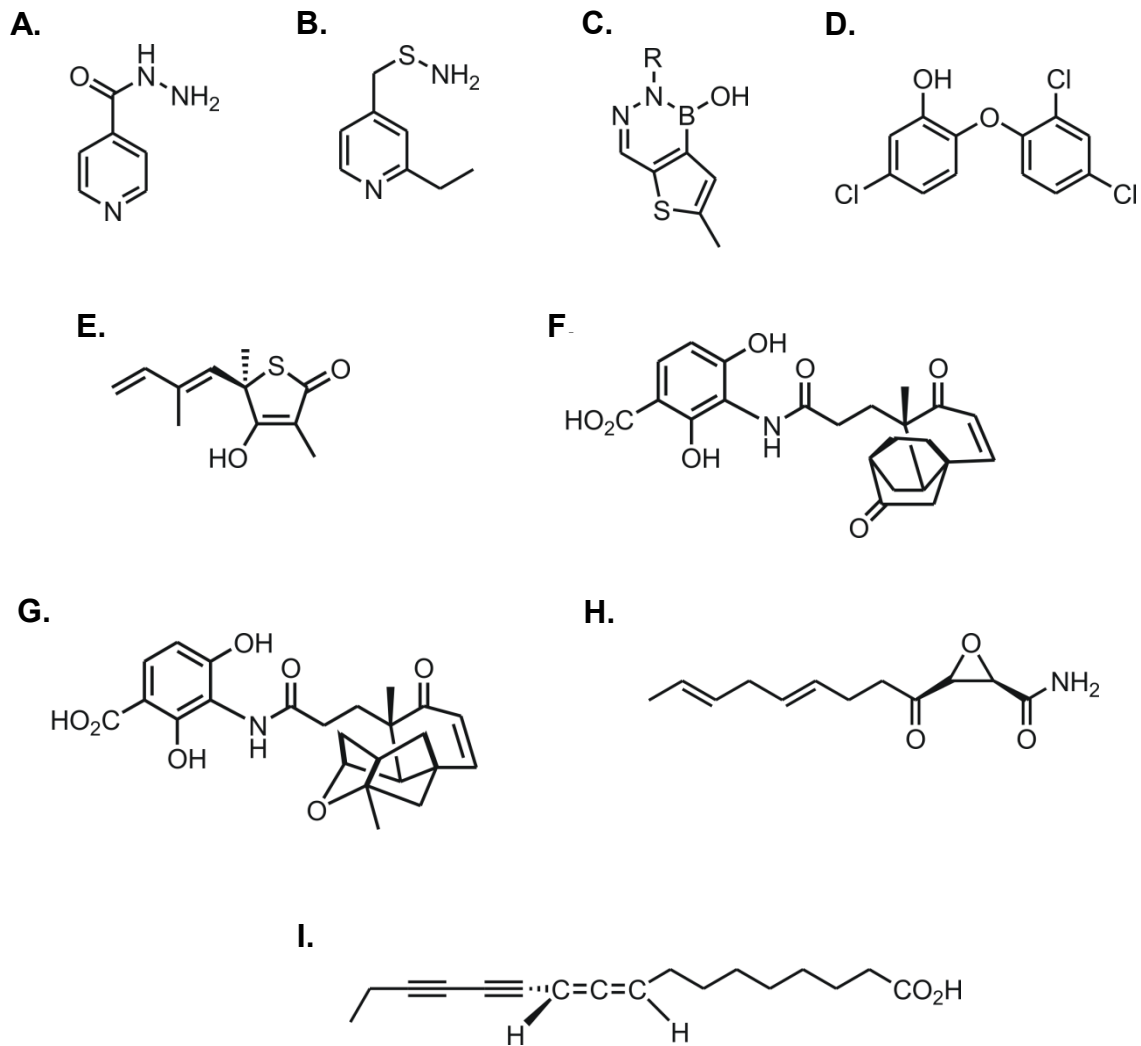


**Figure 1.4: Inhibitors of bacterial FASII: A)** Isoniazid; **B)** Ethionamide, **C)** Diazaborines where the R group is variable, **D)** Triclosan, **E)** Thiolactomycin, **F)** Platencin, **G)** Platensimycin, **H)** Cerulenin, **I)** Phomallenic acid C.

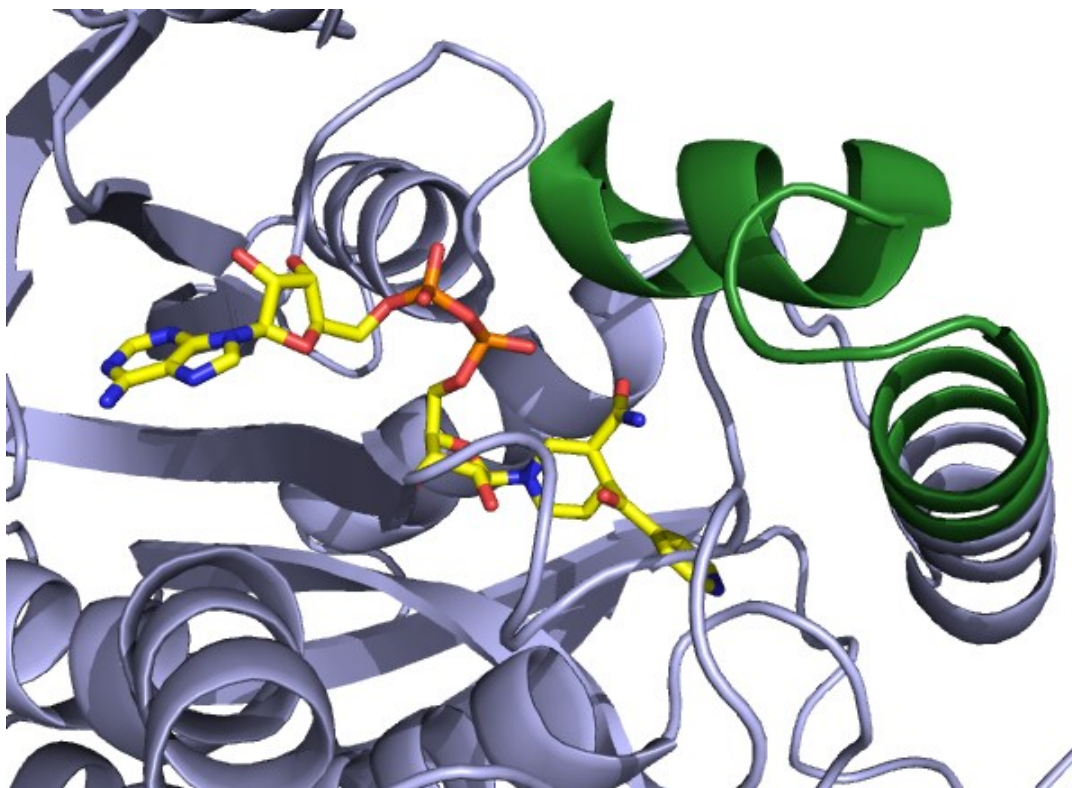
*Inhibition of enoyl-ACP reductase:*

The last step of the FASII pathway is catalyzed by the *trans*-2-enoyl-ACP reductase, involves the reduction of the double bond between C2 and C3 of the

growing acyl chain. This NADH dependent enzyme is encoded by the *fabI* gene and was first shown to be essential by Bergler *et al* (51). FabI enzymes are members of the short-chain dehydrogenase/reductase family that is characterized by a catalytic triad that includes a Tyr and a Lys residue. In reductases the third residue is a Tyr or a Phe as compared to a Ser in dehydrogenases (52, 53). Homologs of FabI from different bacterial species show a very high structural similarity apart from a mobile loop region commonly referred to as the substrate binding loop as it covers the active site (52).

Various inhibitors of FabI are currently available including two broad classes, those that covalently modify the NAD cofactor and those that non-covalently bind the enzyme-cofactor binary complex (52). Amongst the first class are diazaborines, heterocyclic boron-containing compounds that form a covalent bond with the boron and the 2'-hydroxyl of the NAD<sup>+</sup> ribose (54). Anti-tuberculosis drugs isoniazid (INH) and ethionamide also belong to this class. Isoniazid, a prodrug that is activated by the mycobacterial catalase-peroxidase KatG to form the INH-NAD adduct, has a complex mode of action (55, 56). While, this adduct is a tight binding inhibitor of mycobacterial FabI (InhA), the complexity in the mode of action of INH implies that this drug could have multiple targets inside the cell. In fact the INH-NAD(P) adducts has been shown to bind tightly to dihydrofolate reductase along with a number of other proteins in mycobacteria (57, 58). The INH-NAD adduct exhibits slow-onset inhibition to InhA with an

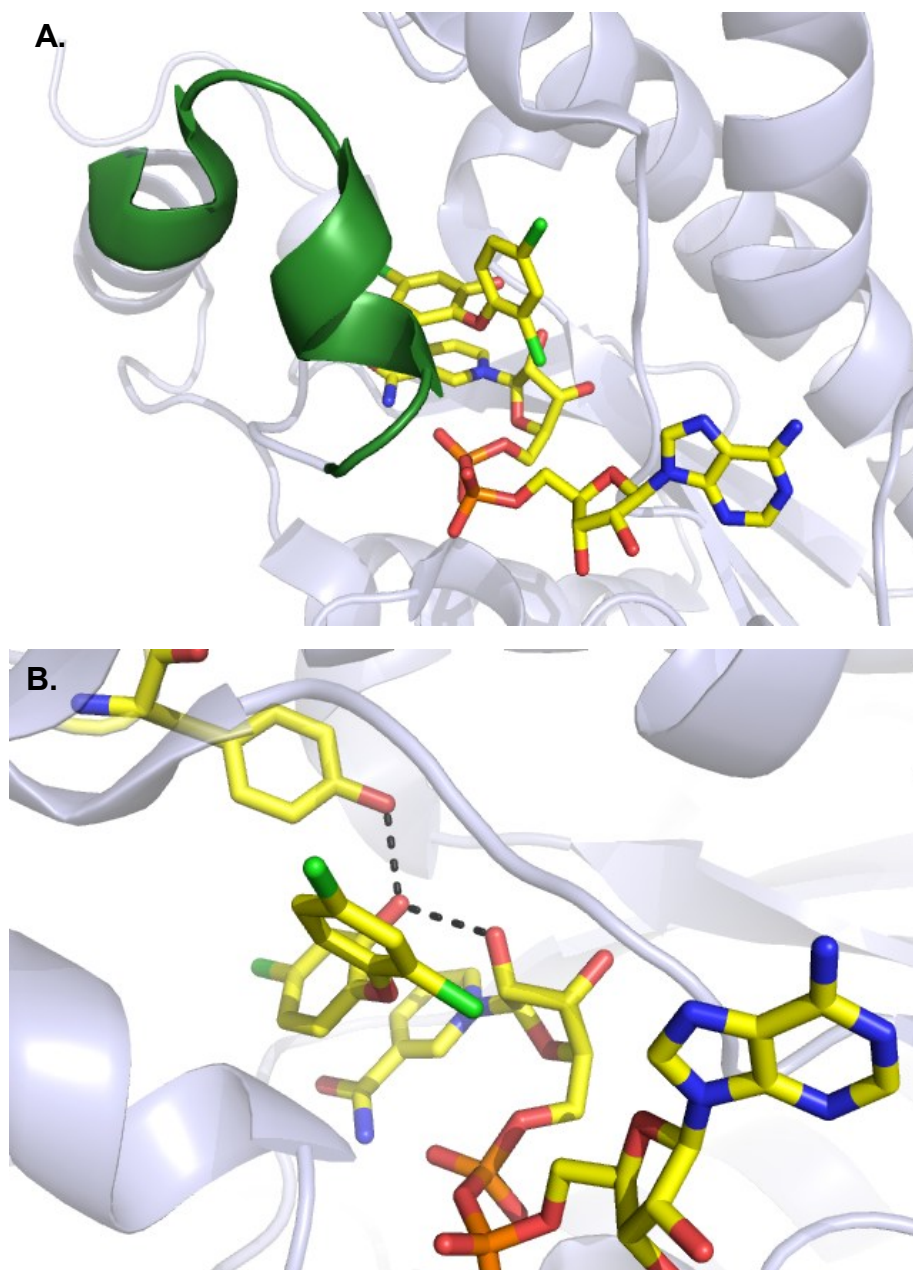
overall  $K_i$  of 0.75 nM. The binding event results in a conformational change in the enzyme wherein the substrate binding loop becomes ordered (**Figure 1.5**).



**Figure 1.5: INH-NAD adduct bound to InhA (1zid.pdb) (59).** The ordered substrate binding loop is shown in green.

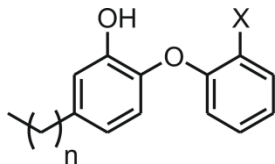
The second class of inhibitors includes those that non-covalently interact with the enzyme-cofactor binary complex. Triclosan, a broad spectrum antibiotic, has been shown to be a potent inhibitor of FabI enzymes for different organisms (60, 61). Triclosan binds to ecFabI/NAD<sup>+</sup> binary complex with an overall  $K_i$  of 7 pM (61, 62) with the phenol ring forming stacking interactions with the oxidized nicotinamide and the hydroxyl group involved in hydrogen-bonding interaction

with the Tyr156 and 2' hydroxyl of NAD<sup>+</sup> ribose (**Figure 1.6**). Despite the fact that the substrate binding loop of ecFabI is smaller than its mycobacterial homolog, the loop also becomes ordered upon triclosan binding resulting in slow onset inhibition similar to binding of the INH-NAD adduct to InhA (52, 59).



**Figure 1.6: Triclosan bound to ecFabI/NAD<sup>+</sup> complex.** **A)** Ordering of the substrate binding loop (green) upon triclosan binding, **B)**  $\pi$  stacking between triclosan phenol and the nicotinamide ring of NAD<sup>+</sup>, hydrogen bonding interactions between Tyr156, phenolic hydroxyl of triclosan and 2'-hydroxyl of NAD<sup>+</sup> ribose.

While triclosan is very effective against FabI enzymes from *E. coli*, *S. aureus* and *P. falciparum*, it shows a much weaker  $K_i$  and a modest MIC<sub>99</sub> against *M. tuberculosis* (12.5 µg/ml for H37<sub>Rv</sub>). However, developing potent triclosan analogs through extensive SAR could yield potentially useful therapeutics against isoniazid resistant strains of TB. Resistance against INH primarily arises due to mutations in KatG peroxidase-catalase which is responsible for activation of the pro-drug. Since triclosan does not require activation by KatG, its analogs could be very useful in fighting INH resistance in TB (52). Extensive structure-activity-relationship (SAR) studies based on triclosan have resulted in some very potent slow, tight binding inhibitors against *M. tuberculosis* (**Table 1.1**) (11, 59, 63). The SAR efforts with the diphenyl ether inhibitors have been greatly aided by crystallography and structural studies of these inhibitors bound to InhA. Careful analysis of X-ray crystal structures has suggested that the time dependent inhibition of the enzyme is coupled to ordering of the substrate binding loop (**Figure 1.7**).

Table 1.1: Diphenyl ether inhibitors targeting <i>M. tuberculosis</i>						
Compound Name						
	n	X	K <sub>i</sub> (nM)	Slow Onset	K <sub>i</sub> <sup>*</sup> (nM)	MIC (H37 <sub>Rv</sub> ) μg/ml
PT05	7	H	1.1	No	-	1.9
PT04	5	H	9.4	No	-	2.1
PT70	5	CH <sub>3</sub>	7.8	Yes	0.044	3.1

**Table 1.1: Diphenyl ether inhibitors targeting *M. tuberculosis*.** The binding affinities against InhA and MIC<sub>99</sub> are given (64).



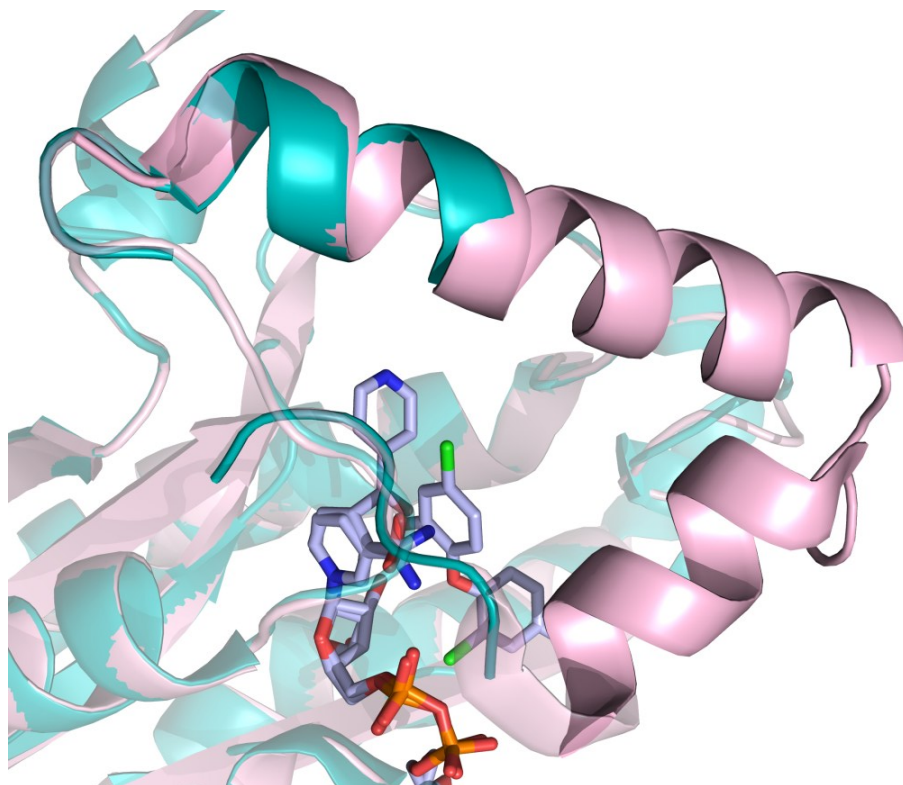


**Figure 1.7: The X-ray crystal structure of InhA bound to PT70/NAD<sup>+</sup>** (purple, pdb.2X22) (64) in comparison to InhA bound to triclosan/NAD<sup>+</sup> (blue, pdb.2B35) (59). While the substrate binding loop is ordered in the case of the PT70 structure, which is a slow onset inhibitor, it is dynamic in the case of the triclosan bound structure. Crystallographic analysis and MD simulations (Tonge P.J., not published) implicate the substrate binding loop in the slow onset binding of various inhibitors.

### *Inhibition of $\beta$ -ketoacyl-ACP synthase:*

The first step of each elongation cycle of the FASII includes the formation of a carbon-carbon bond via decarboxylative Claisen condensation (65). The enzymes responsible for this, termed condensing enzymes, belong to the thiolase superfamily of proteins that was first characterized in *Saccharomyces cerevisiae* in a degradative thiolase (66). *E. coli* has three different  $\beta$ -keto-acyl synthases (KAS), KASI, II and III commonly also referred to as FabB, FabF and FabH respectively. KAS enzymes are characterized by a catalytic triad that is composed of a Cys, His and another His/Asn. While, FabH (KASIII) has a Cys-His-Asn triad and accepts only coenzyme substrates, FabB and FabF (KASI and II) have a Cys-His-His triad (**Figure 1.8**) and accept only ACP substrates (65, 67). Importantly, as a conserved feature, the active site Cys is present at the N terminus of an  $\alpha$ -helix resulting in lowering of the  $pK_a$  of the sulfhydryl due to the helix dipole effect (68, 69).

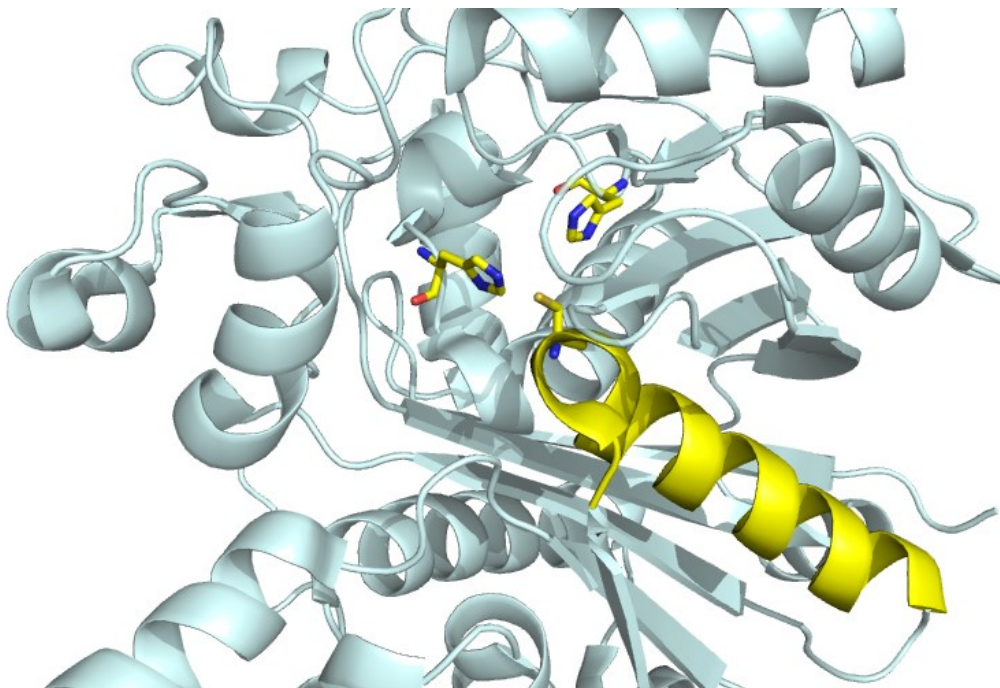


**Figure 1.8: *E. coli* KASI and the catalytic triad.** KASI (FabB) from *E. coli* with the active site Cys-His-His triad (yellow) (PDB 2VB9) (70). The active site Cys is present at the N terminal of an  $\alpha$ -helix.

While KAS inhibitors are not in clinical use, a slew of natural products have been identified that inhibit these enzymes, (**Figure 1.4 E-I**) suggesting that they may be lucrative drug targets. Cerulenin, first isolated from the fungus *Caephalosporium caerulens*, is a suicide inhibitor that selectively targets FabB and FabF over FabH in *E. coli* (30). Drug discovery efforts using cerulenin as a lead were thwarted by its cross reactivity with hFASI.

Natural product screening using an antisense RNA assay afforded various new potential KAS inhibitors such as platensimycin, platencin and phomallenic

acid (29, 71, 72). Platensimycin, first isolated from *Streptomyces platensis* (73), has been shown to be effective against Gram-positive bacteria such as *S. aureus*, *E. faecalis* and *S. pneumonia* (29). Platensimycin binds in the malonyl-ACP binding pocket, showing slow onset kinetics, to the acyl-enzyme intermediate of saFabF.

A natural product analog of platensimycin, platencin inhibit both FabF and FabH comparably and also is effective against various antibiotic resistant bacteria such as vancomycin-resistant *Enterococcus faecium* (74). The same antisense technology resulted in the isolation of phomallenic acids that show good inhibition of the FabH/F enzymes (71, 72). These inhibitors show antibacterial activity against methicillin resistant *S. aureus*, *B. subtilis* and *H. influenza* with selectivity for FabF/H enzymes.

Another natural product thiolactomycin (TLM), first identified in *Nocardia* sp. (75-77), is a highly selective KAS inhibitor. TLM shows activity against both Gram-positive and Gram-negative bacteria (75, 78) and MTB (68). Moreover, TLM has low toxicity, fairly high solubility and is selective for bacterial KAS enzymes in *in vitro* assays. Because of its favorable properties, TLM has great potential as a lead molecule despite the fact that it inhibits all three types of KAS enzymes.

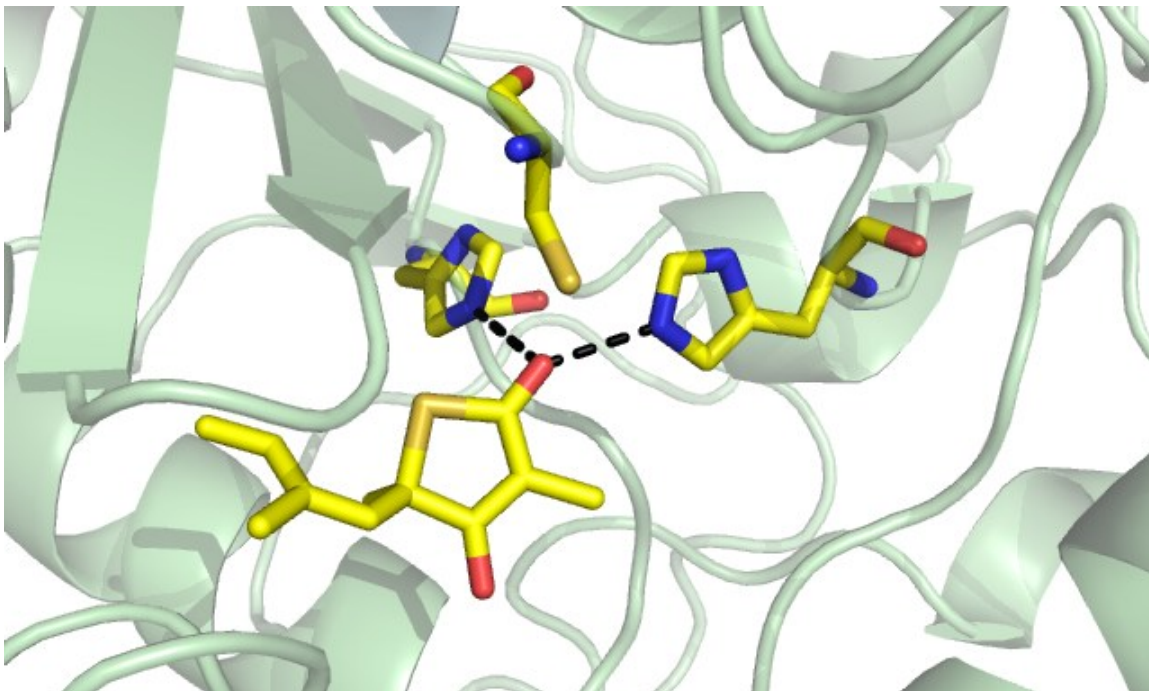


**Figure 1.9: TLM bound to the malonyl-AcpM binding pocket of KasA** (MTB KASI, pdb. 2WGG (69)). The keto group of the thiazole ring is stabilized by hydrogen bonding interactions with His304 and His311.

TLM mimics the binding of the malonyl-ACP substrate (**Figure 1.9**) and shows slow onset kinetics with the acyl-enzyme intermediate of various KASI enzymes. Optimization of the TLM lead is discussed in detail in chapters 2 and 3.

*Summary:*

Aggressive efforts must be made to develop novel chemotherapeutics to keep pace with the rapidly emerging resistant strains and to fill the gap in antibacterial research and development. The inhibitor discovery efforts described

in this dissertation attempt to take into account a broader view of the drug discovery process.

In **Chapters 2** and **3** we have used inter-ligand NOEs to direct a fragment based approach to optimize the binding of TLM to KasA. We have been able to obtain the relative orientation of TLM and a pantetheine analog bound to KasA by measuring transient NOE build up between these fragments. These data have helped us design and test molecules that have not only improved binding affinities but also have longer residence times on KasA. In **Chapter 4** we have used solution state NMR and SAXS experiments to understand the mechanism of slow-onset inhibition in InhA. While this project is currently in progress, we have obtained crucial information about the mode of action for our diphenyl ether inhibitors. Moreover, we have been able to optimize our system to allow acquisition of quality spectra and make the 120 kDa enzyme amenable to NMR measurements. Lastly, in **Chapter 5** we have used a mass-spectrometry based approach to quantify target concentration and turnover in a bacteria cell and address the effect of drugs on bacterial *homeostasis*. While we have studied three *E. coli* FASII targets; FabB/F and FabI, we intend to extrapolate this method to other targets and organisms.

# Chapter 2

## *$\beta$ -Ketoacyl-AcpM Synthase A*

## **Introduction:**

### *Tuberculosis - a worldwide pandemic:*

Tuberculosis (TB), caused by the organism *Mycobacterium tuberculosis* (MTB) is a serious public health concern with about 9 million new TB cases in reported in 2010 (WHO Report 2011, Global TB Control). This disease kills an overwhelming two million people annually worldwide with about two billion people infected and is a leading co-infection in patients with AIDS (12). Moreover, propelled by lack of patient compliance to lengthy treatments, there has been an emergence of multi-drug resistant (MDR-TB) and extensively drug resistant (XDR-TB) strains of TB making it a public health menace. MDR-TB is simultaneously resistant to the frontline drugs, isoniazid and rifampicin. XDR-TB is resistant to frontline drugs along with fluoroquinolones and at least one of the three injectable second line drugs, capreomycin, kanamycin or amikacin. Exacerbated by the absence of an effective vaccine, there is a desperate need for novel chemotherapeutics to combat TB. A lot of work is being done not just in drug research and development and finding better drug targets but also in the fields of more sensitive detection methods for the bacteria. The latter is a severe bottleneck in the treatment for TB especially because of the difficulty in detecting latent mycobacteria.



An acid fast bacterium, MTB thrives and multiplies inside human macrophages under conditions where the other bacteria are usually destroyed (12). This property is attributed to the presence of a complex, protective cell envelope around the mycobacterium which also provides a permeability barrier to various hydrophobic antibiotic substances, making a large number of antibiotics ineffective (12, 79-84). This lipid rich cell wall is composed of C<sub>60</sub>-C<sub>90</sub> α-alkyl β-hydroxy fatty acids called mycolic acids. Unlike other bacteria, mycobacteria require two distinct pathways for fatty acid synthesis: a eukaryote-like FASI for *de-novo* fatty acid synthesis and a dissociative FASII pathway for elongating the C<sub>14-16</sub> FASI end product (85, 86). The FASII system is responsible for elongation of the shorter chain fatty acids to about 56 carbons, that serve as precursors for mycolic acids (87).

Most of the FASII enzymes in the mycobacterium are important for bacterial viability (88). Moreover, processes that alter the cell wall constitution, plasticity and permeability, including mycolic acid synthesis, are active even during periods of non-replication (89). Therefore, the fatty acid biosynthesis (FAS) pathway is a lucrative target for drug discovery (**Chapter 1**). In most bacteria and plant cells FAS occurs as a dissociated type II pathway consisting of at least nine separate proteins disparate from a type I polypeptide found in mammalian systems. However, in MTB the *de novo* synthesis of the fatty acids up to C<sub>16</sub> occurs by a FASI multi-functional polypeptide and the elongation (up to C<sub>60</sub> – C<sub>70</sub>) occurs via FAS II pathway (**Figure 2.1**) mediated by an acyl-carrier

protein – AcpM. The reaction results in the addition of two carbons to the growing fatty acid chain per cycle.

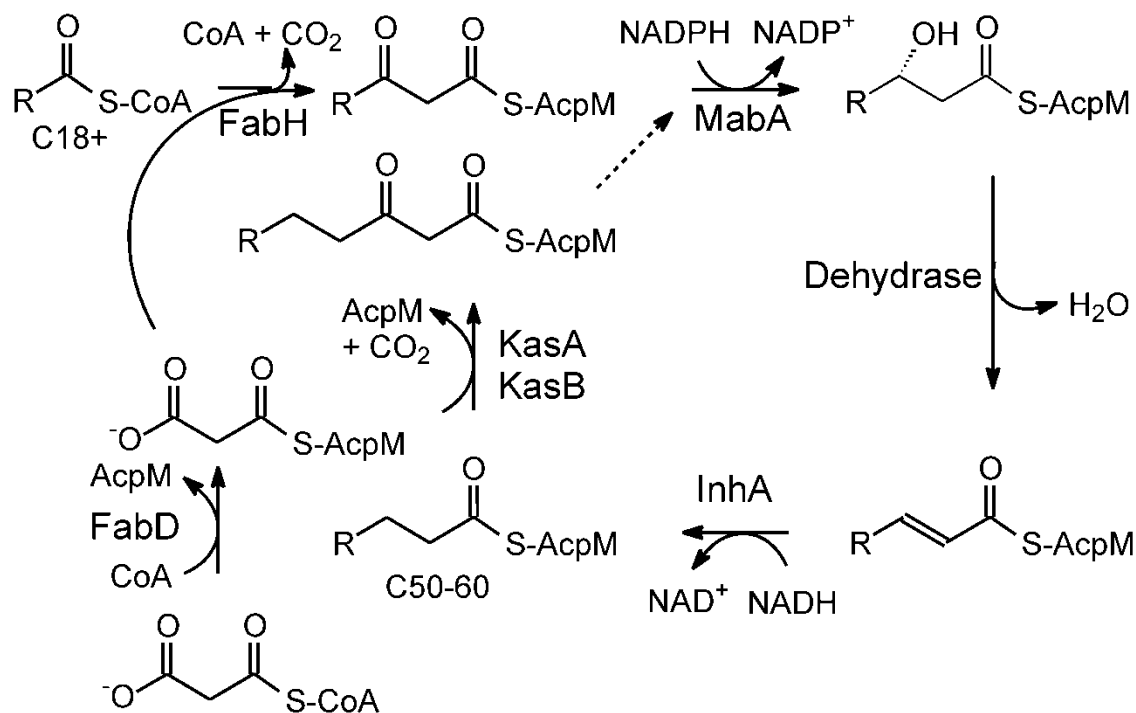


**Figure 2.1: The FASII pathway in MTB.** The  $C_{18+}$  Acyl-CoA provided by the FASI pathway is condensed with malonyl-AcpM by FabH providing a  $\beta$ -ketoacyl AcpM. This product is reduced to  $\alpha$ -hydroxyacyl-AcpM by MabA which is dehydrated by an unknown dehydrase to *trans*-2-enoyl-AcpM. The double bond is subsequently reduced by an NADH-dependent enoyl-AcpM reductase, InhA (FabI in *E. coli*) to yield a saturated acyl-AcpM. Subsequent rounds of elongation are catalyzed by KasA/KasB (FabB/FabF in *E. coli*) involving a decarboxylative Claisen condensation with malonyl-AcpM yielding a  $\beta$ -ketoacyl-AcpM longer by two carbon atoms (59).

*β-Ketoacyl-AcpM synthase A – Mycobacterium tuberculosis:*

Carbon–carbon bond formation in the biosynthesis of natural products such as fatty acids and polyketides is carried out via a decarboxylative Claisen condensation (65). The enzymes responsible for this reaction are collectively referred to as condensing enzymes. While there are numerous members in this superfamily, including enzymes that catalyze both decarboxylating and non-decarboxylating reactions, they share a common three dimensional fold called the thiolase fold. Interestingly, while they share very little similarity at the amino acid level, their active sites are strikingly similar (65, 90). Enzymes in the thiolase family form dimers where each monomer can be divided into N and C terminal halves each having βαβαβαββ topology (90, 91) (**Figure 2.2**).

The KAS family of proteins belongs to the decarboxylating class of this superfamily. This includes the “initiation” condensing enzymes KASIII (FabH) and the “elongation” condensing enzymes KASI and KASII (KasA and KasB respectively). While both of these classes catalyze the same reaction mechanistically, there are differences in substrate specificity and the catalytic triad. KASI and II have a Cys-His-His triad and exclusively utilize ACP thioesters while KASIII has a Cys-His-Asn triad and use CoA primers for catalysis (65, 67).

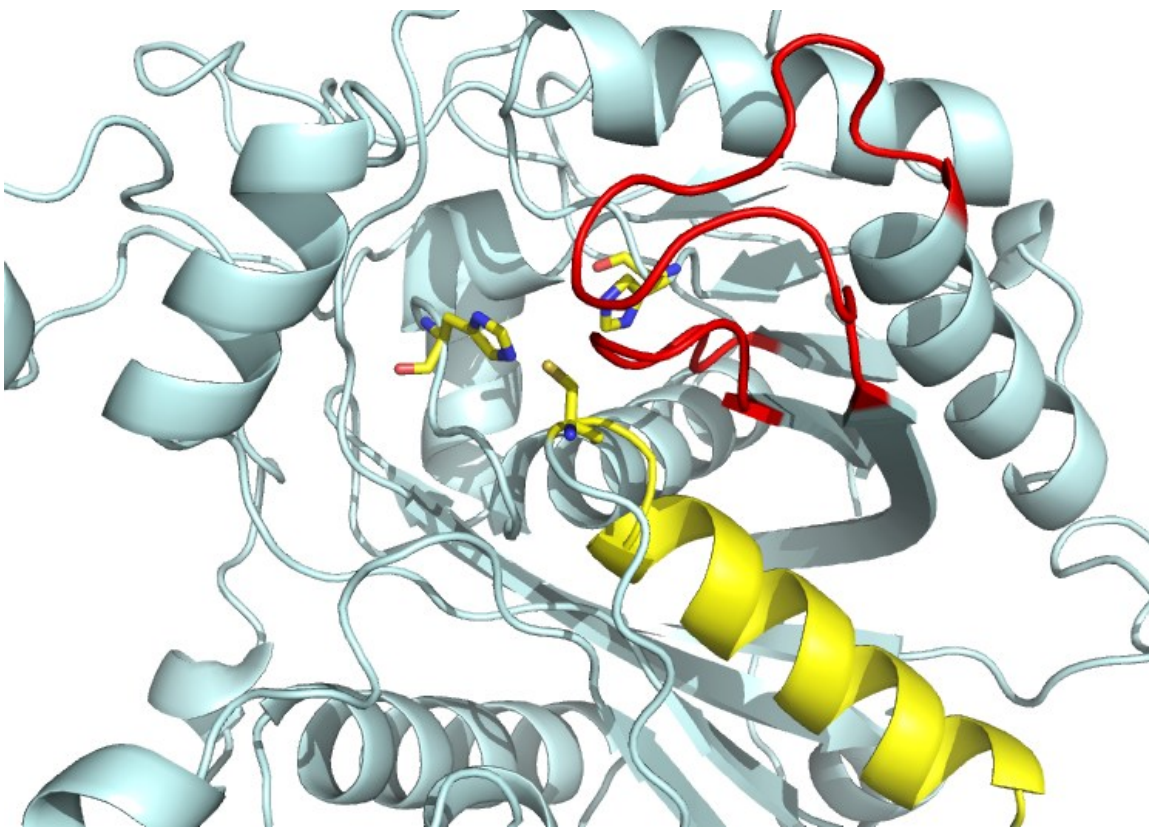


**Figure 2.2: The active site of KasA and the conserved thiolase fold** (PDB: 2WGD (69)). The Cys-His-His catalytic triad is shown (sticks) along with the catalytic helix N $\alpha$ 3 (yellow). The substrate binding loops of the thiolase family (C $\beta$ 4-C $\beta$ 5 and C $\beta$ 3-C $\alpha$ 3) are shown in red.

*$\beta$ -Ketoacyl-AcpM synthase A – Catalysis:*

$\beta$ -ketoacyl-AcpM synthase A (KasA) is involved in the decarboxylative Claisen condensation of acyl-AcpM with malonyl-AcpM thus resulting in elongation of the fatty acid chain by two carbon units. The mechanism of action of KasA is shown in **Figure 2.3** (65, 68). The reaction follows a ping-pong

mechanism wherein the acyl group is first transferred to the active site cysteine followed by the dissociation of the apo-AcpM. The formation of the acyl-KasA intermediate is followed by decarboxylation of malonyl-AcpM and condensation of the resulting carbanion with the acyl chain.

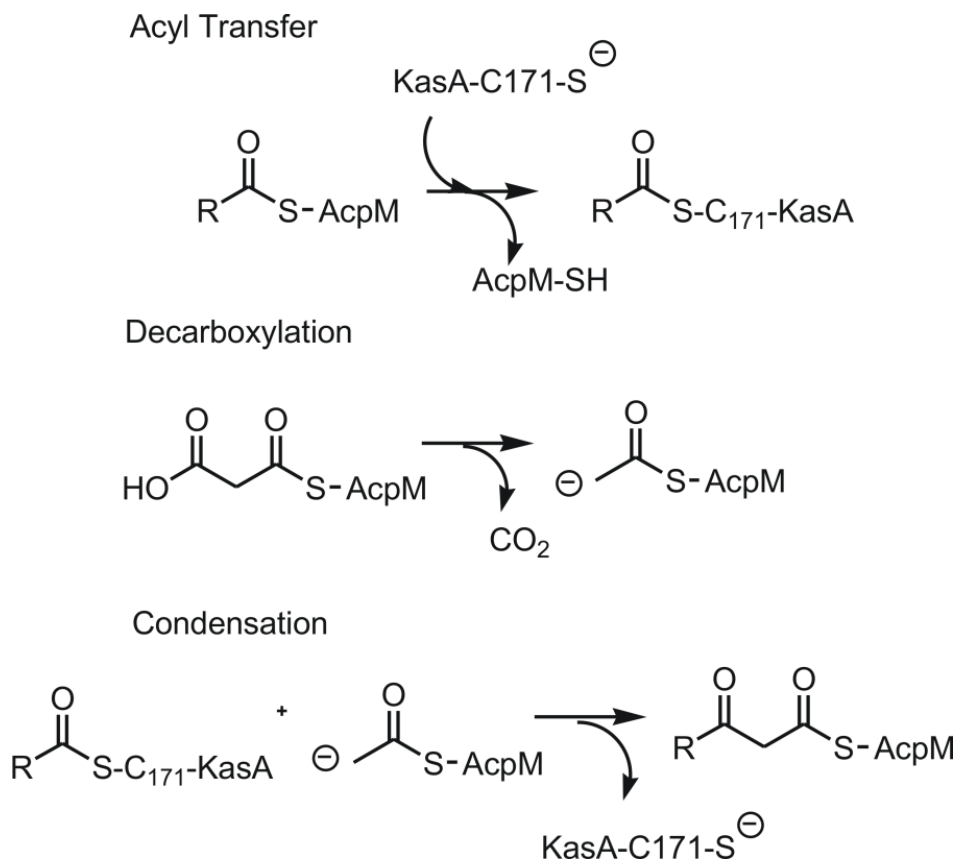


**Figure 2.3: Catalytic mechanism of KasA in the elongation step of FASII.**

The reaction mechanism involved the formation of an acyl enzyme intermediate.

The reactivity of the active site Cys (C171 in KasA) is assisted by an  $\alpha$ -helix dipole. The active site Cys is present at the N-terminus of helix N $\alpha$ 3 which

lowers its  $pK_a$  thereby increasing its nucleophilicity (92, 93). The decarboxylation of malonyl-AcpM and a stabilization of the resultant carbanion is assisted by the active site His residues (His311 and His345) (94). The nucleophilic attack and carbon-carbon bond formation is promoted by the stabilization of the negatively charged thio-oxide tetrahedral intermediate by an oxyanion hole formed by the backbone amides of the active site Cys (C171) and a conserved Phe (F404) (65, 95, 96).

The reaction is characterized by the formation of a stable acyl enzyme intermediate. This intermediate plays an important role in not just KasA catalysis but also inhibition. Previously, it has been shown that decarboxylation of malonyl-AcpM occurs at a much slower rate when the acyl substituent is not present. Perhaps, this reflects the importance of generating the reactive carbanion species only in the presence of the recipient acyl chain on the active-site Cys residue (97). Witkowski *et al.* have shown that an active site Cys to Gln mutant mimics the acyl-KASI (*ecFabB*) intermediate and converts the keto-acyl synthase into a malonyl decarboxylase. They postulate that the side chain carbonyl of the Gln mimics the thioester in acyl-KASI and the enzyme assumes a conformation analogous to the acylated enzyme (97) (**Figure 2.4**). The similarity of the wild type acyl-KasA and the mutant side chains are shown in **Figure 2.4**. In the acyl enzyme, the role of the oxyanion hole in increasing the acyl-enzyme thioester's susceptibility to nucleophilic attack renders this structure unstable to base catalyzed hydrolysis. However, the Cys to Gln mutant is a highly stable acyl-

enzyme mimic and allows for studies where long term stabilization of the wild type acyl-enzyme thioester is unrealistic.

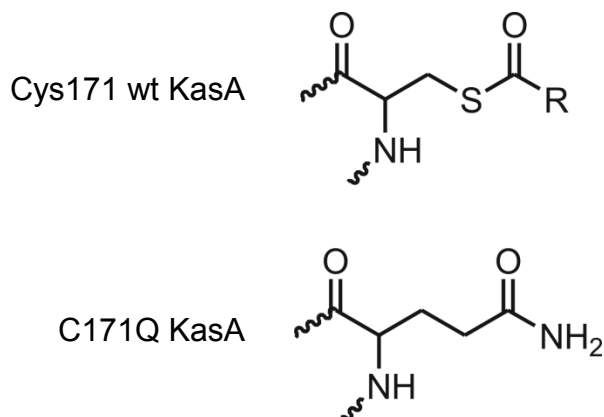


**Figure 2.4: Active site modification in acyl KasA.** C171Q KasA mimics the acyl enzyme intermediate.

KAS inhibitors such as platensimycin and TLM (**Figure 2.5**) have been shown to preferentially bind to the acyl enzyme (96, 98) and also the Cys to Gln acyl-enzyme mimic. Hence, for measurements of binding affinities and kinetics, the Cys to Gln mutant (C171Q for KasA) is a very useful substitute for the acyl enzyme.

#### *Targeting KasA – essentiality:*

KAS enzymes have been shown to be essential in a very wide variety of pathogens including *E. coli*(92), *S. aureus* (98), and *P. falciparum* (99). KasA was shown to be important for mycobacterial growth using transposon-site

hybridization (100). Also, conditional depletion of KasA in *M. smegmatis* was shown to induce cell lysis implying the influence of this enzyme on membrane integrity (101). Along with the essentiality of KasA, the isolation of various natural product inhibitors of KAS enzymes like TLM (102, 103), platensimycin (98) and cerulenin (104, 105) (**Figure 2.5**) has spurred a renewed interest in drug discovery targeting KasA. Although KAS inhibitors are not in clinical use, many KAS inhibitors have shown efficacy against TB (106) and other pathogens *in vitro* further validating KAS enzymes as attractive targets for drug discovery. The details of these different KAS inhibitors can be found in **Chapter 1**.



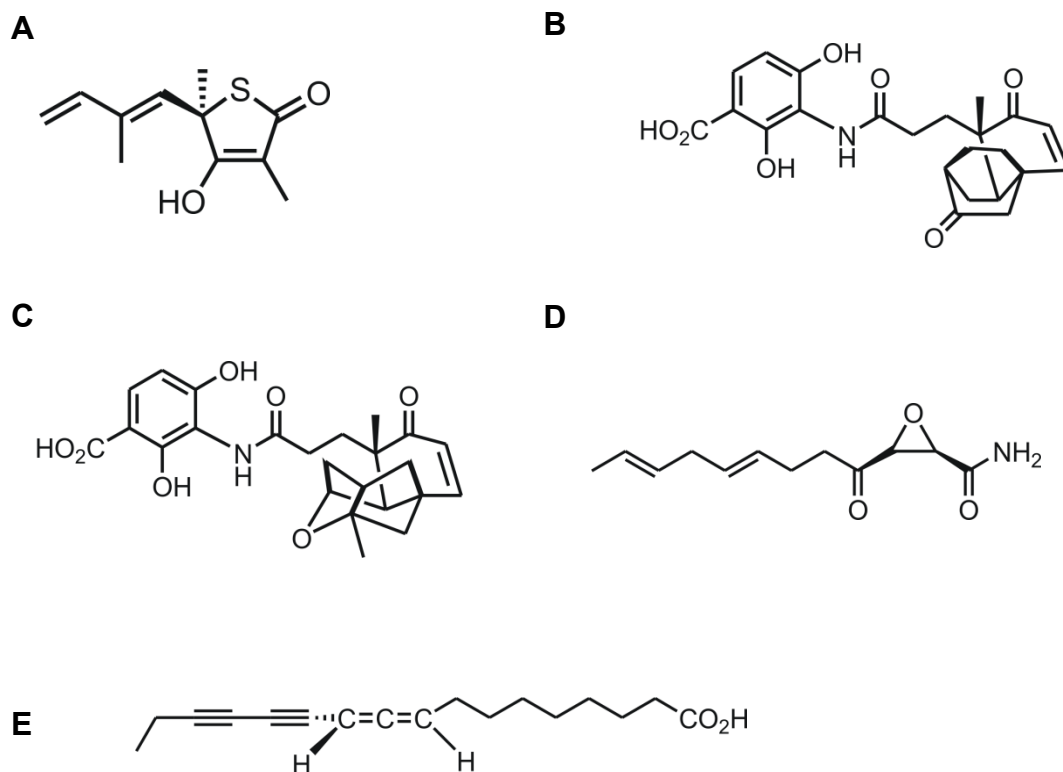


**Figure 2.5: KAS inhibitors. A)** Thiolactomycin (102, 103), **B)** platencin, **C)** platensimycin (98), **D)** cerulenin (104, 105), **E)** phomallenic acid C (71, 72).

*Inhibiting KasA – Thiolactomycin:*

Thiolactomycin (TLM, **Figure 2.5A**), a broad spectrum antibiotic, was first isolated from a strain of an actinomycetes (*Nocardia sp.*) by Oishi *et al* (107). The structure of KasA is known to have two adjacent active sites; an acyl transferase site responsible for forming the acyl-enzyme intermediate and a decarboxylation site where the malonyl-ACP binds. TLM is a competitive

reversible inhibitor and is known to bind to the malonyl ACP binding site (65). A natural product thiolactone, TLM shows broad spectrum antibacterial activity against Gram positive, Gram negative bacteria and mycobacteria (107, 108). Despite moderate MIC values, TLM is a promising lead molecule for the development of potent KasA inhibitors due to its favorable physicochemical properties, low cytotoxicity, high bioavailability and activity in animal infection models (68, 92, 106-110). TLM binds ~100-fold more tightly to the KasA acyl-enzyme intermediate, consistent with the knowledge that TLM is a mimic of the malonyl group (68). However, given that TLM inhibits wild type KasA with a  $K_i$  of only about 200  $\mu\text{M}$  (68), there is interest in optimizing the interactions between TLM and the enzyme to improve both affinity and selectivity. Ultimately this must be accomplished by retaining the slow onset component of the inhibition characteristic of TLM binding to the acyl-enzyme.

In order to develop an inhibitor with improved affinity for KasA we have employed a fragment based approach, by realizing that TLM and the pantotheine arm of the Malonyl ACP bind adjacent to each other. Interligand NOEs (ILOEs) between small molecule ligands can be used as a powerful tool to aid and guide fragment based drug discovery (111-113). If two or more small molecules bind to a macromolecule in close proximity to each other, the strong negative ILOEs that develop in their bound complex geometries can be observed even in the presence of sub-stoichiometric amounts of the target provided that there is a rapid exchange between the bound and free state (113). Pairs of suspected

weak inhibitors can be chosen as prospects for binding to a protein either based on structural characteristics or by screening chemical libraries. Protein mediated ILOE can then assist in pharmacophore identification, and can guide the design and synthesis of bidentate ligands using these weak binding fragments as building blocks.

2D NOESY techniques are the methods of choice for investigating structural relationships in large biological molecules, primarily because all of the data is collected at once and the expected NOEs are large and negative. However, interligand NOEs between small molecules can be very weak, and difficult to detect and differentiate due to chemical shift overlaps and background issues typical of 2D NOESY experiments (114). Such issues can adversely limit the application of the method, and the ability to obtain and interpret NOE data. Overcoming these limitations would require longer mixing times (beyond 500 msec) thereby excluding the early time points of the NOE build-up that are crucial for distance measurements.

In partial mitigation of these issues, we sought to extend traditional ILOE NMR by use of the selective 1D NOE technique pioneered by A.J Shaka *et al* (114, 115) and later refined by Krishnamurthy *et al.* (116). Here, as opposed to the conventional steady state approach, the transient NOEs arising only from selectively inverted resonances are detected. Pairs of selective pulses and pulsed field gradients are used in a double pulsed field gradient spin echo (DPFGSE) sequence to cleanly select and invert specific resonances such that

only those signals related to NOEs originating from the inverted signal are detected. Background and chemical shift overlap issues are therefore removed (114, 115). Selective 1D NOE experiments enable significantly increased sensitivity per unit of data collection time, effectively extending NOE detection and distance limits, and better supporting systems with short lifetimes. In addition NOE build-up curves can easily be constructed to include shorter mixing times.

In this chapter we demonstrate the use of this technique for detecting ILOEs between two ligands bound to KasA. We have previously shown that TLM is a slow onset inhibitor of the KasA acyl enzyme, consistent with the knowledge that TLM mimics the malonyl group of malony-AcpM, the second substrate in the ping pong reaction catalyzed by KasA. Structural data suggested that TLM might bind to KasA in the presence of ligands that occupy the pantetheine binding channel (69). To test this hypothesis we synthesized a pantetheine analog (PK940) and used ILOE NMR spectroscopy to analyze the interaction of this compound with TLM and KasA. Based on the ILOE and structural data, we then synthesized TLM analogs that have higher affinity for KasA than the parent compound.

## Materials and Methods:

### *Materials:*

5(±)-Thiolactomycin was obtained from Sigma Aldrich Chemical Co. and enantiomerically pure 5R-thiolactomycin was synthesized by Gopal Reddy Bommineni. Pantoylamide analog PK940 was synthesized by Pilho Kim.

### *C171Q Mutagenesis:*

Cys 171 was mutated to a Gln using Quikchange mutagenesis. The primers that were used are shown in **Table 2.1**.

<b>Table 2.1: Primers for Quikchange mutagenesis</b>	
Forward primer	acc ccg gtg tcg gcc cag tcg tcg ggc tcg gaa
Reverse primer	ttc cga gcc cga cga ctg ggc cga cac cgg ggt

**Table 2.1: Primers for C171Q KasA Quikchange mutagenesis.**

### *Enzyme purification:*

Wild type and C171Q KasA were purified from *Mycobacterium smegmatis* mc<sup>2</sup>155 strain as described (68) with a few important modifications. Briefly, the

pFPCA1 vector containing the KasA gene was transformed into electro-competent *M. smegmatis* cells and the overexpression of KasA was induced at an O.D<sub>600</sub> of 0.8 with 1 ml of 44% acetamide. After shaking the cultures at 35.5°C for 24 hours, the cells were harvested by centrifugation at 5000 rpm (4 °C) for 20 minutes. The resulting pellet was re-suspended in 40 ml binding buffer (50 mM Tris HCl, 800 mM NaCl, 5 mM imidazole, pH 6.8) and subsequently sonicated 5 times for 45 seconds, with a minimum pause of 1 minute between each round. The cell debris was pelleted by centrifugation at 33000 rpm (4 °C) for an hour. The supernatant was then filtered with a 0.45 micron filter and loaded onto a 5 ml Ni-NTA His tag column. The column was washed with 40 ml binding buffer and about 150 ml wash buffer (50 mM Tris HCl, 800 mM NaCl, 60 mM Imidazole, pH 6.8). Soluble KasA was subsequently eluted using an imidazole gradient from 60 mM to 1 M. The fractions containing KasA (500 imidazole) were concentrated and exchanged into the storage buffer (50 mM Tris HCl, 150 mM NaCl, pH 8.5) via a Sephadex size-exclusion column. KasA fractions from the size-exclusion column were pooled and concentrated to ~50 µM and stored at 4 °C. The protein was used within 1 week after preparation.

*Preparation of NMR samples:*

C171Q KasA was exchanged into 50 mM NaH<sub>2</sub>PO<sub>4</sub>, 0.15 M NaCl, (D<sub>2</sub>O, pH 8.9) buffer. 5*R,S*-Thiolactomycin (Sigma Aldrich) and PK940 were dissolved in the phosphate buffer with final concentrations in the experiment being ~8 mM

and ~4 mM, respectively. The concentration of enzyme in the experiments was 30  $\mu$ M.

*2D and 1D NOE Spectroscopy:*

All NMR data were acquired on standard bore 700 MHz and 900 MHz Brüker Avance NMR instruments in D<sub>2</sub>O at 15 °C and processed with Brüker TOPSPIN 2.1 software. 2D NOESY spectra were collected at 700 MHz over a range of mixing times (50 – 900 ms) using a spectral width of 7716.05 Hz in F2 and 2048 complex data points for an acquisition time of 0.133 s with a 2 s recycle delay. 256 points were collected in the indirect F1 dimension for a 0.0166 s acquisition time. 40 scans were collected per F1 increment and F1 quadrature detection was achieved using the States-TPPI method (117). Time domain data were *apodized* using squared sine bell functions in both dimensions and zero-filled in the indirect dimension to a final data matrix size of 1024 (F1) x 2048 (F2) after Fourier transformation.

Selective 1D DPGSE NOE data were collected using a spectral width of 14005.6 Hz and 32768 complex data points for a 1.17 s acquisition time with a 2 s recycle delay. A selective 120 msec Gaussian pulse was used to invert the target resonances in the PK940 methyl cluster to observe interligand transfer of NOEs to the TLM methyl groups.

## Results and Discussion:

Conflicting  $^1\text{H}$  NMR assignments have been reported for some of the TLM resonances in earlier literature (118), therefore the  $^1\text{H}$  and  $^{13}\text{C}$  NMR spectra for TLM were reassigned using values obtained from our  $^1\text{H}$  1D,  $^1\text{H}$ - $^1\text{H}$  COSY,  $^1\text{H}$ - $^{13}\text{C}$  HMQC and HMBC NMR data. These assignments agree with values presented in more recent literature (95). The methyl peaks of TLM at C6, C7, and C12 (**Figure 2.6**) are assigned to the resonances at 1.41 ppm, 1.50 ppm and 1.44 ppm, respectively. For the PK940 ligand, non-prochiral assignments of the singlet proton peaks at 0.714 ppm and 0.75 ppm are made to the geminal methyl groups at C9' and C10' and the doublet of doublets centered near 0.708 ppm is assigned to the C1' terminal methyl protons (**Figure 2.6**). The overlap of the PK940 C1' methyl resonance with the upfield C9'/C10' methyl singlet hinders the analysis of the standard 1D  $^1\text{H}$  and 2D NOESY spectra.



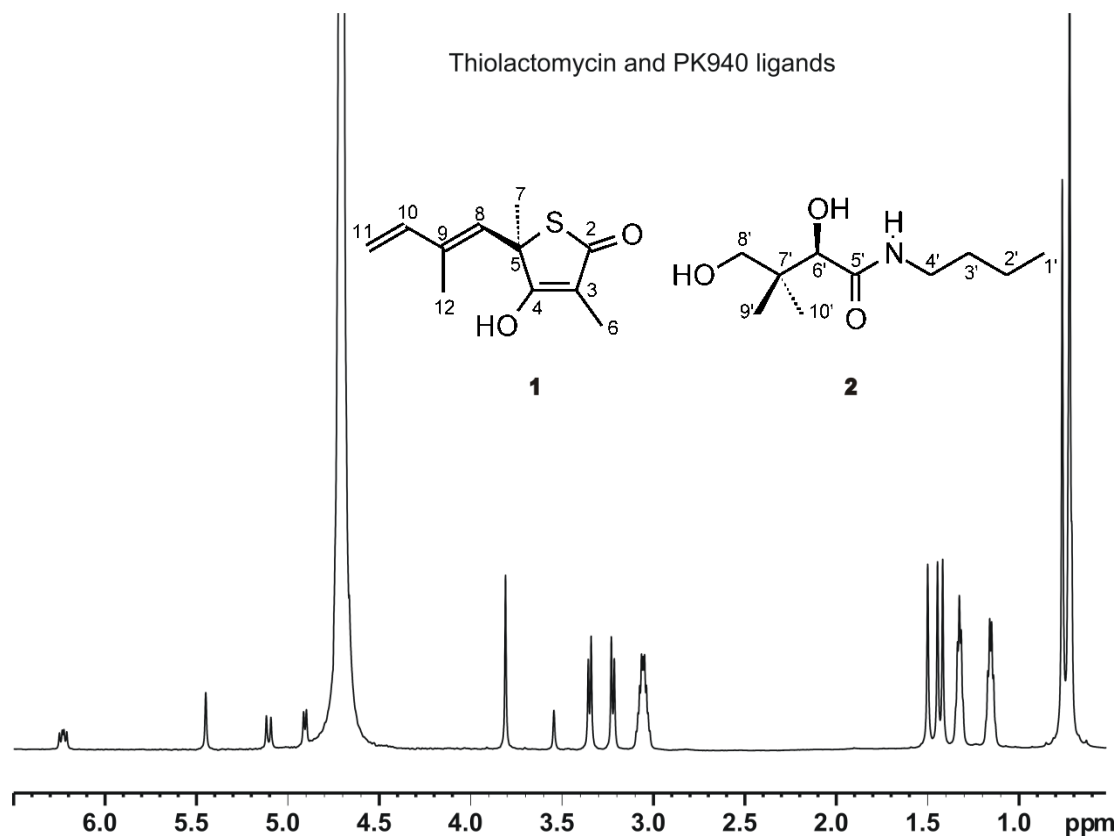


**Figure 2.6: <sup>1</sup>H NMR spectrum of TLM and PK940 in D<sub>2</sub>O at 700 MHz.** TLM (**1**) <sup>1</sup>H NMR (D<sub>2</sub>O) 6.23 (dd, 1H, H10), 5.45 (s, 1H, H8), 5.1 (d, 1H, H11, J = 18Hz), 4.9 (d, 1H, H11, J = 10.4 Hz), 4.7 (H<sub>2</sub>O), 1.50 (s, 3H, H7), 1.44 (s, 3H, H12), 1.41 (s, 3H, H6). The TLM methyls at position 6, 7 and 12 are at 1.41, 1.50 and 1.44 ppm respectively. PK940 (**2**) <sup>1</sup>H NMR (D<sub>2</sub>O) 3.81 (s, 1H, H6'), 3.35 (d, 1H, H8'), 3.22 (d, 1H, H8'), 3.06 (dd, 2H, H4'), 1.32 (dd, 2H, H3'), 1.15 (dd, 2H, H2'), 0.75 (s, 3H, prochiral H9'/H10'), 0.714 (s, 3H, prochiral H9'/H10'), 0.708 (dd, 3H, H1'). Stacked doublet of doublets (H1', 0.708 ppm) were resolved from geminal methyl peaks (H9' and H10', 0.714 and 0.75 ppm) after examining HMQC, HMBC data and DPGFSE line shapes.

After revisiting the assignments of TLM we performed a standard 2D NOE experiment similar to that performed in other interligand NOE NMR experiments (113). Close inspection of the 2D NOE spectra in **Figure 2.7** show apparent negative ILOE cross-peaks between the C6, C12, and C7 TLM methyl resonances at 1.41, 1.44 and 1.50 ppm, respectively and the PK940 methyl cluster peaks spanning 0.71-0.75 ppm. The cross peaks have chemical shifts equal to the other C2' and C3' NOE signals observed from the PK940 methylene groups at 1.15 and 1.32 ppm, respectively. Given the close proximity of the geminal C9' and C10' methyls, we expect that they should have similar NOEs to any point on TLM. Therefore, the presence of only one associated ILOE eliminates the geminal methyls as the interacting partners with TLM.

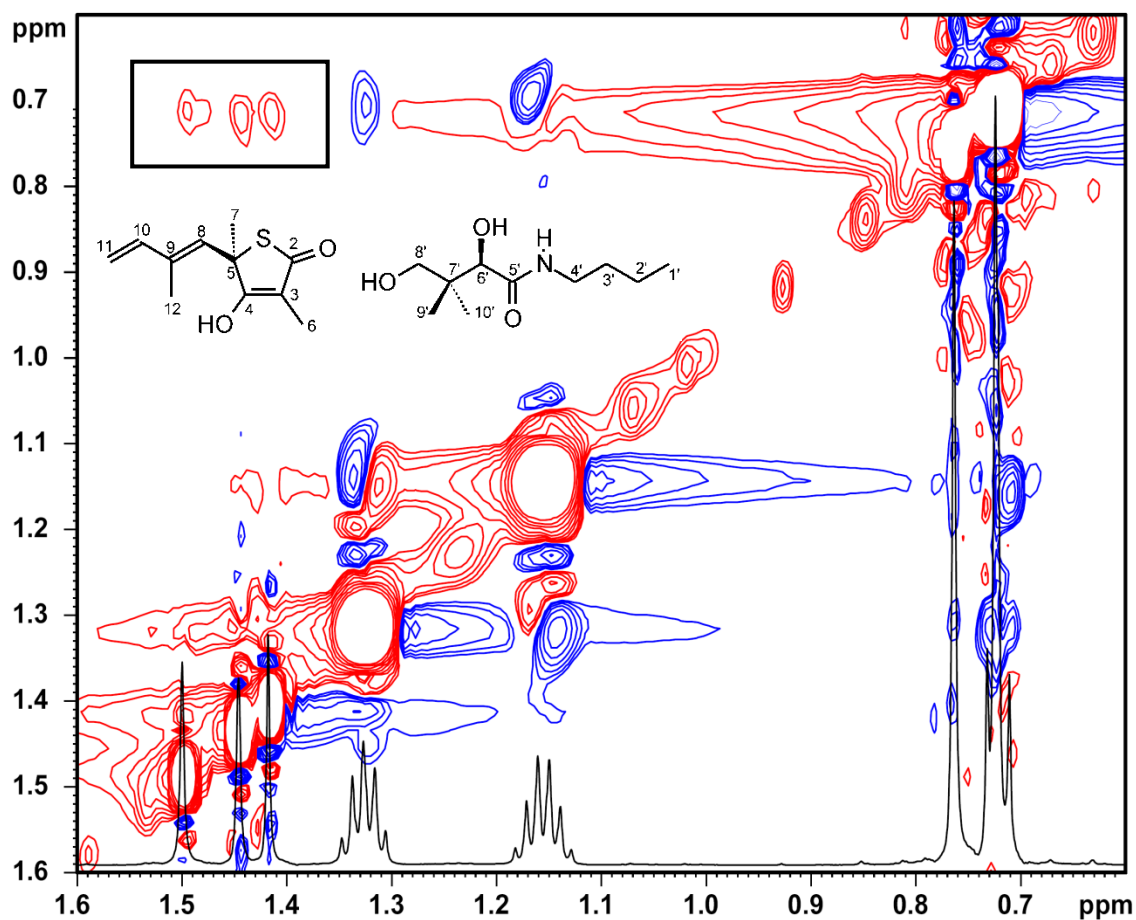


**Figure 2.7: 2D NOESY spectrum to detect ILOEs between TLM and PK940.**

The spectrum was recorded on a 700 MHz Brüker Avance instrument at a mixing time of 700 msec. Negative (red) interligand NOE cross peaks can be observed between the TLM methyls at 1.41, 1.44 and 1.50 ppm and the terminal PK940 methyl doublet. Positive (blue) intraligand NOE cross peaks can be seen between terminal PK940 methyl and C2' and C3' methylenes.

In our 2D experiments, we were able to observe interligand NOEs between TLM and the pantetheine analog (PK940) only at mixing times longer than 500 msec and were unable to detect ILOE signals at lower mixing times that are crucial for distance assessment. The lack of sensitivity and the inability to detect and differentiate signal in the presence of overlapping chemical shifts and high background noise have previously been reported to hinder ILOE detection involving small molecules (114). We thus acquired 1D NOE data using the DPGSE method, inverting the PK940 methyl cluster signal at ~0.75 ppm. Due to enhanced sensitivity, the 1D experiment (114, 115) allowed us to detect the ILOE signal even at very low mixing times (~100 msec) giving us very clean and easily interpretable spectra. Moreover, the acquisition times were greatly reduced for the 1D experiment which also improved the quality of the data given that the enzyme was not very stable over long periods of time in the experimental conditions. The 1D NOE experiment also indicated the presence of transient interligand NOEs between the three TLM methyls and the PK940 methyl cluster in the presence of the enzyme (**Figure 2.8**).

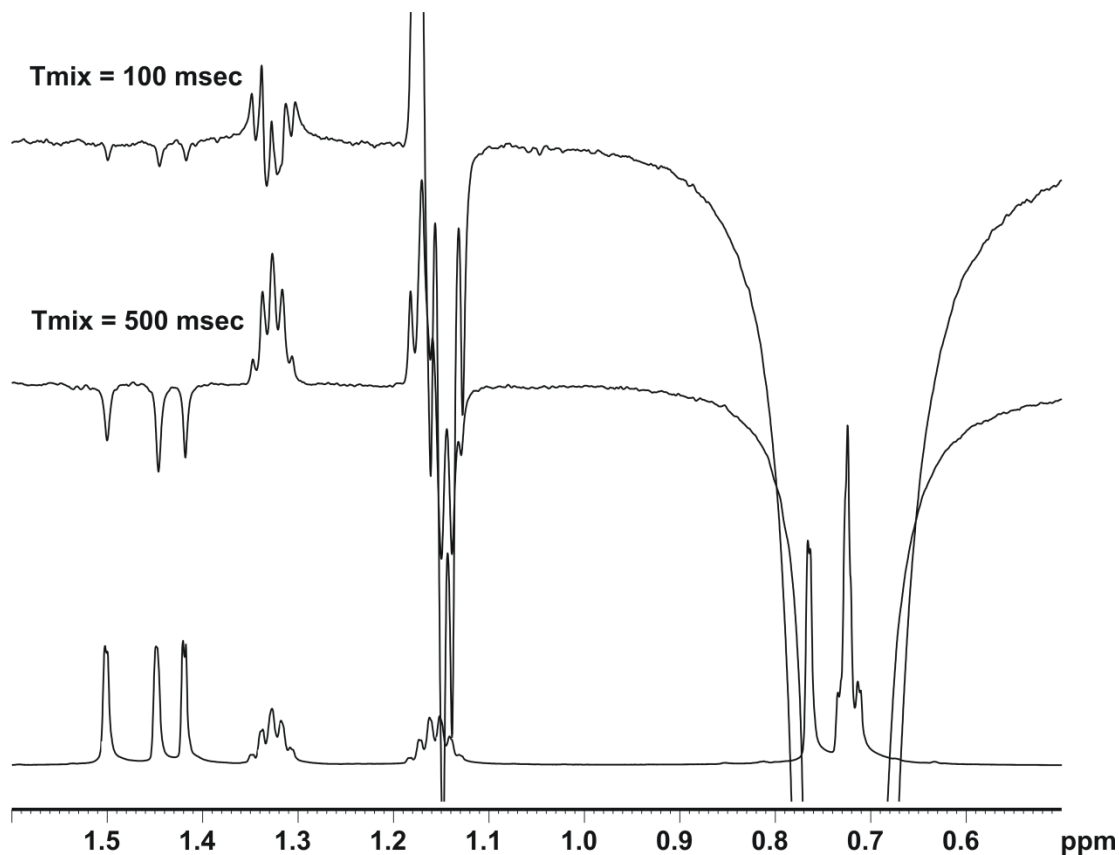


**Figure 2.8: Overlay of  $^1\text{H}$  NMR DPGSE 1D NOE spectra.** ILOE between TLM and PK940 in the presence of C171QKasA with mixing times of 100 and 500 msec. Negative interligand NOE's can be seen with the TLM methyl resonances upon inversion of the PK940 methyl cluster at  $\sim 0.75$  ppm with a 120 msec shaped Gaussian pulse. Anti-phase contributions are observed in the line shapes of the C2' and C3' methylene protons of PK940 at 1.15 ppm and 1.32 ppm due to possible strong coupling or Zero-Quantum artifact that were not removed by the DPGSE pulse sequences that were used (114). The spectra were recorded on a 700 MHz Brüker Avance instrument.

Moreover, the simultaneous selective inversion of the three TLM methyl groups allows us to specifically assign these ILOEs to interactions between the three TLM methyl groups and the terminal C1' methyl of PK940. NOE build up curves were obtained for the three TLM methyls over a range of mixing times (**Figure 2.9A**). The NOE intensities normalized with respect to the inverted peak intensity were plotted against the mixing time to obtain build ups that, to a large extent, canceled the effect of external relaxation at moderate mixing times (116) (**Figure 2.9B**). Using the distance between the TLM vinyl protons on C11 (1.85 Å) as a reference, calculated distances of 3.0 Å, 3.4 Å, 3.4 Å were obtained between the C1' PK940 methyl and TLM C12, C6 and C7 methyls, respectively. However, the intraligand NOEs build up mainly on a short T1 regime of the unbound ligand, while the interligand NOEs build up in the bound state with the long T1 regimes of the protein. Hence, the estimated distances can, at most, be considered as qualitative constraints.

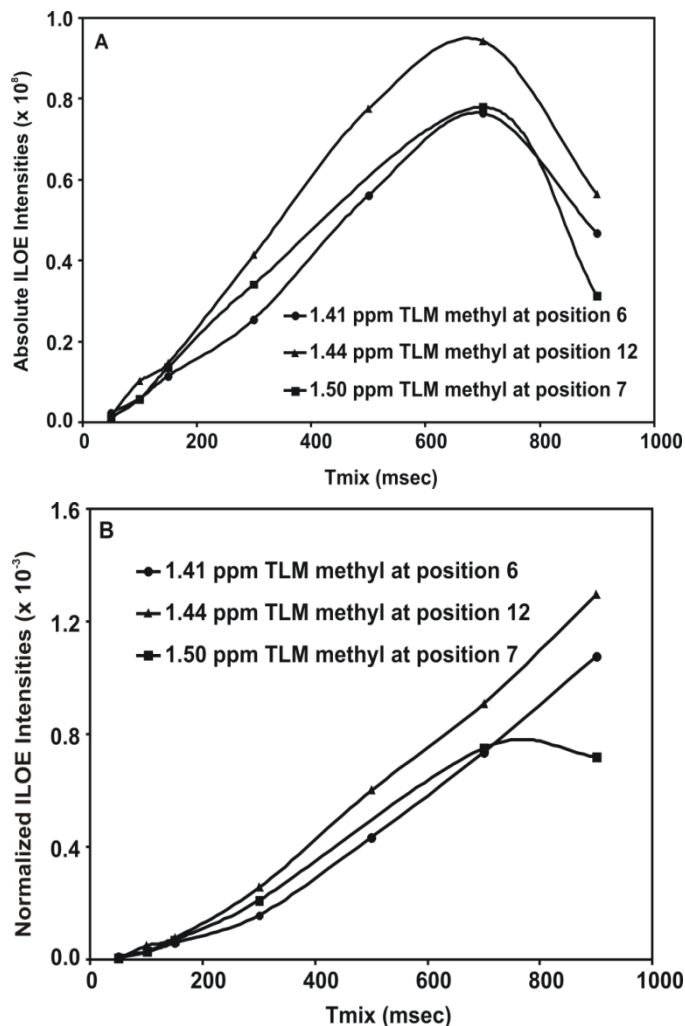


**Figure 2.9: NOE build up curves. A)** NOE build up curves for the TLM methyls C6, C7 and C12 upon inversion of the PK940 methyl cluster at  $\sim 0.75$  ppm are shown. The build-up rate for the TLM methyl 12 at 1.44 ppm (depicted as solid triangles) appear to be faster than the build-up's for 6 and 7 implying that methyl 12 may be closer the terminal PK940 C1' methyl. **B)** NOE build ups for TLM methyls 6, 7 and 12 normalized with respect to the inverted peak at  $\sim 0.75$  ppm show the same extended utility of the longer mixing times for estimating distances with the limitations mentioned in the text.

To refine the relative positions of the two ligands we attempted to invert the three TLM methyls individually to observe the interligand NOE with the terminal methyl of PK940. This turned out to be a challenging task for a number of reasons. Firstly, the chemical shifts of the three TLM methyls are very close, making individual inversion problematic. Use of a higher magnetic field (900 MHz) increased the separation of the three peaks sufficiently to provide selectivity in the absence of the enzyme. However, upon addition of enzyme, we observed a loss of selectivity, wherein inversion of all three methyls was observed upon inversion of any one methyl, especially at higher mixing times. This observation can be explained by proposing that the dipolar coupling between KasA and TLM provides a route for cross-relaxation between the KasA methyls / methylenes and TLM methyls by the spin diffusion mechanism (119). Attempts to target the PK940 methyl cluster at ~0.71 ppm and the singlet at 0.75 ppm exclusively on a 900 MHz field also resulted in a loss of selectivity that worsened at higher mixing times. Additionally, the expected line broadening due to modulation in the transverse relaxation time ( $T_2$ ) in the bound and the unbound state of the ligands could contribute to the observed loss of selectivity.

Various controls were performed to confirm that the observed signal was an interligand NOE and not a transferred NOE with the protein. Firstly, the experiments were repeated in the absence of the enzyme as a control. No ILOE was observed between the two ligands. Secondly, the bandwidth at ~0.75 ppm was irradiated in the presence of only TLM bound to the enzyme, with the result



that no signal was observed at ~1.45 ppm, whereas negative ILOEs were previously observed in the presence of PK940. Subsequently, the methyl bandwidth at ~1.45 ppm was irradiated in the presence of only PK940 bound to the enzyme, and as expected, no signal was observed at ~0.75 ppm. These negative controls confirmed the presence of interligand NOEs between TLM and PK940 with the terminal methyl of PK940 pointing toward the TLM methyls. Using this information we modeled PK940 into the active site of KasA using the X-ray structure of the TLM:C171Q KasA complex (69). In this model, PK940 occupies the putative KasA pantetheine binding pocket with the terminal methyl group of the analog oriented toward the bound TLM molecule (**Figure 2.10**). Thus our structural analysis suggested that elaboration of the TLM thiazole ring at either the 3 or the 4 position would result in an increase in affinity of the inhibitor for the enzyme.

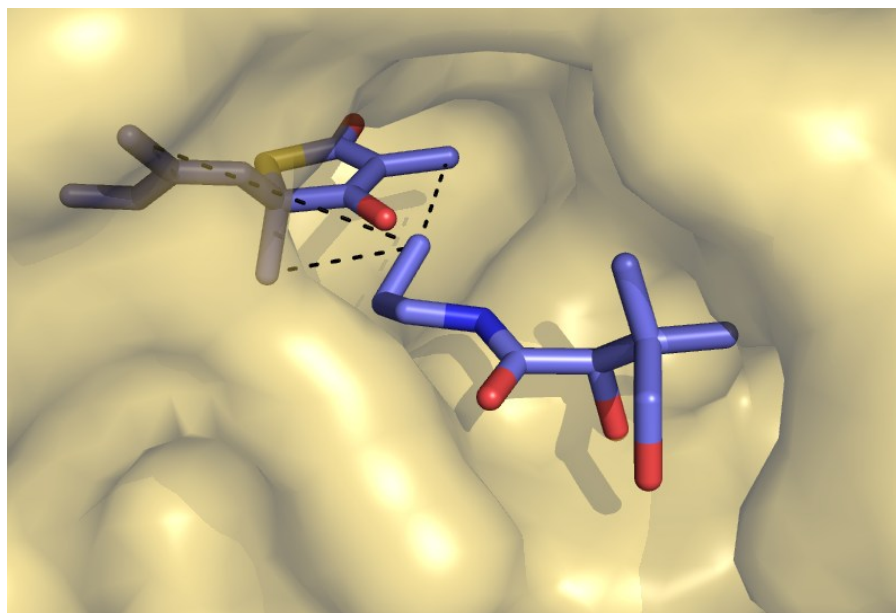


**Figure 2.10: Orientation of TLM and PK940 in the C171Q KasA active site.**

The figure was made using Pymol (120).

### **Conclusions:**

ILOE is a powerful tool to aid fragment based drug discovery. Standard 2D NOESY has traditionally been used towards this end. However, long experimental times, background noise issues and lack of sensitivity limit the application of this technique especially for time sensitive samples. Here, we have successfully been able to use the DPGSE pulse sequence to obtain NOEs between ligands bound to a protein. This technique enables rapid acquisition of cleaner NOE spectra over a wider range of mixing times. We anticipate extensive use of this method as an improvement on the standard 2D NOESY methods for

rapid and more efficient detection of interligand NOEs for guiding fragment based drug discovery. The NOEs and the subsequent orientations obtained from this method provide useful constraints for future modeling experiments by limiting the degrees of freedom. Also, they aid in lead optimization and guiding development of new analogs with potentially better binding affinities to the target.

In this study, we have used interligand NOEs between TLM and a pantetheine probe to map out the relative orientations of the two ligands when they are bound to KasA. Our data indicate that elaboration of either the 3 or 4 position of the TLM thiazole ring may be a promising approach to developing TLM analogues with improved affinity for KasA since substituents at these positions will occupy the pantetheine binding channel.

# Chapter 3

## *KasA Inhibition*

## Introduction:

### *Thiolactomycin as a lead:*

Thiolactomycin (TLM) is a natural product thiolactone first isolated from *Nocardia* sp., a bacterial strain isolated from a Japanese soil sample in 1981 (121). The antibacterial activity of TLM is known to result from an inhibition of fatty acid biosynthesis. TLM is a selective and reversible inhibitor of the KAS enzymes in the FASII pathway (112, 121, 122), but does not inhibit the mammalian FASI enzyme (123). TLM resistant *E. coli* strains contain mutations in the *fabB* KAS gene (124) and overproduction of FabB confers TLM resistance *in vivo* (125) suggesting that FabB is the major cellular target in *E. coli*.

TLM has a broad range of antibacterial activity, although with MIC values that are only in the range of 6-200 µg/ml (**Table 3.1**). Despite the relatively poor MIC values, TLM has activity in animal models of infection. TLM is rapidly absorbed in rats when administered both orally and by intramuscular injection, and it provides protection from both urinary tract and oral infections in animals infected with *Serratia marcescens* and *Klebsiella pneumoniae* despite the fact that the MIC values of TLM against these organisms are only ~100 µg/ml (107, 126). This is partly the result of the favorable *in vivo* properties of the molecule, which satisfies all of the criteria in Lipinski's "Rule of 5" (127), as well as the low toxicity and high bioavailability of the molecule.

<b>Table 3.1: MIC values of TLM against different bacterial strains.</b>	
<b>Organism</b>	<b>MIC (µg/ml)</b>
<i>M. tuberculosis</i>	25
<i>S. aureus</i>	25
<i>S. marcescens</i>	100
<i>K.pneumoniae</i>	100
<i>E. coli No9</i>	100
<i>E. coli 11</i>	25
<i>S. flexneri 2b T1</i>	6.3
<i>S. enterides T-1</i>	12.5
<i>S. typhi</i>	12.5
<i>S. paratyphi</i>	50

**Table 3.1: MIC (µg/ml) values for thiolactomycin against various bacteria.**  
(107, 126)

*Optimizing TLM:*

Based on kinetic and structural data, TLM is thought to be a competitive inhibitor of malonyl-AcpM (112, 128). MTB has three KAS enzyme KasA, KasB and FabH (KASI, II and III respectively). While, TLM inhibits KasB and FabH

weakly, it has been shown to bind preferentially to the acyl-enzyme intermediate for KasA with slow onset kinetics (128-130). Time dependent inhibition of TLM with acyl-KASI might be partly the reason for its *in vivo* activity (130). The KASI enzymes (FabB) from *S. marcescens* and *K. pneumonia* have a high sequence similarity to *ecFabB* suggesting a similar binding mode. Although not characterized yet, time dependent binding of TLM to *smFabB* and *kpFabB* might explain the *in vivo* efficacy against these organisms despite moderate MIC values.

Slow onset kinetics, characteristic of the interaction of TLM with the acyl enzyme, is of great significance as slow onset inhibitors have long residence times on their targets resulting in prolonged activity of the drug, even at low systemic concentrations. In fact several reviews (17, 131, 132) suggest that factoring in the lifetime of the drug-target complex, or the residence time of the drug on its target, can account for efficacy of small molecule drugs *in vivo*. While a time based inhibition can be observed due to various mechanisms, the binding of TLM to acyl-KasA has been shown to be a two-step process. The initial binding of TLM to acyl-KasA results in the formation of the E-I complex which is followed by a conformational change in the protein to form E\*-I. The increased energy barrier for dissociation of the inhibitor off the target results in longer residence times of the inhibitor on the target (**Figure 3.1**).



**Figure 3.1: Time based inhibition of acyl KasA.** A two-step binding model depicting the binding of TLM to acyl-KasA (130). The formation and breakdown of the initial complex is fast, while the isomerization is slow and determines the overall duration of drug-target interaction.

While comparing crystal structures does show tighter interactions between the ligand and the acyl enzyme mimic as compared to wild type KasA (**Figure 3.2**), it fails to implicate an obvious conformational change responsible for the slow onset kinetics.



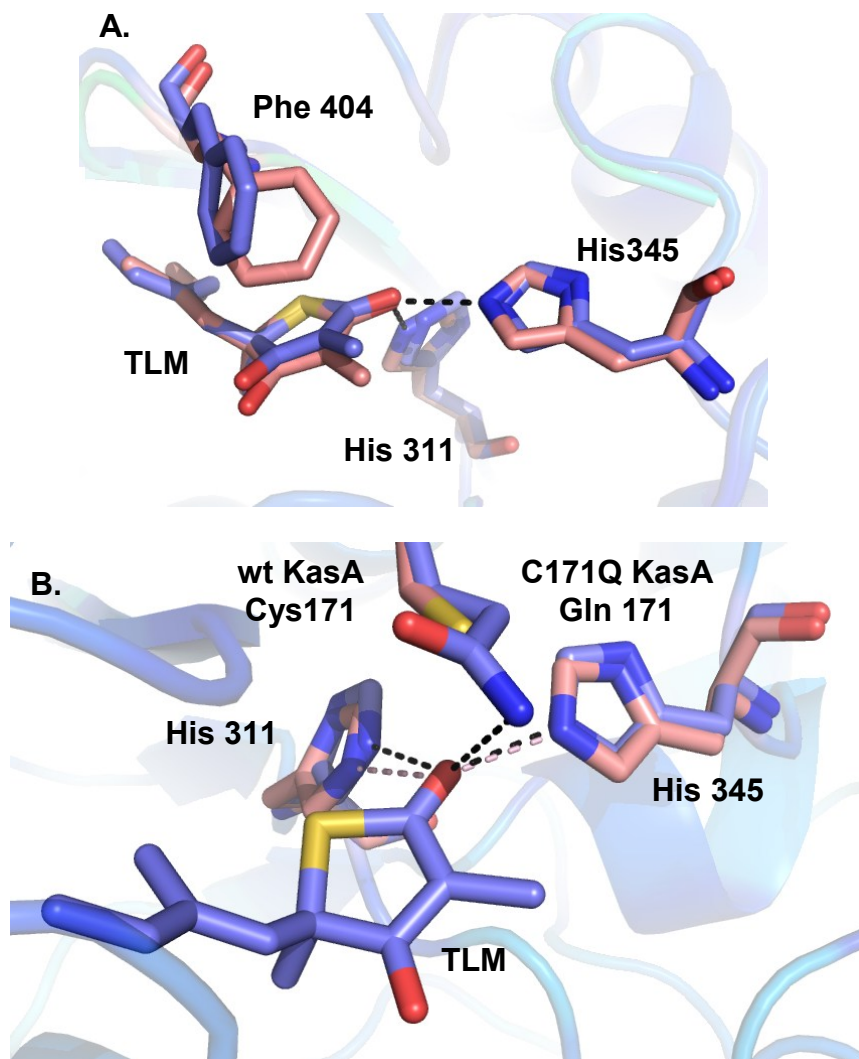


**Figure 3.2: Interactions between TLM with wild type and C171Q KasA. A.)** Increased edge to face interaction between Phe404 and the thiolactone ring in C171Q KasA (pink). **B.)** Hydrogen bonding interactions between the thiolactone ketone and His 311/His 345 are conserved in the two structures. In the acyl enzyme mimic (C171Q KasA (68, 98)) the thiolactone is further stabilized via hydrogen bonding with the side chain amide carbonyl of the Gln171. Gln side chain mimics the thioester formed upon acylation of the active site Cys in wild type KasA.

The tighter interaction between TLM and C171Q KasA can be explained by an increase in the edge to face interaction between Phe404 and the thiolactone ring (**Figure 3.2A**). Also, the shift in Phe404 is accompanied by movement of a flexible loop (residue 402-406) which increases solvent accessibility of the active site. Modeling studies have implicated Phe 404 as a key player in triggering the conformation change mediated by Met 144 and Met 277 in the neighboring monomer.

Since, slow onset inhibitors are believed to be more efficacious in an *in vivo* system, in optimizing TLM one must retain the slow-off kinetics such as to retain the *in vivo* efficacy. Various groups have worked on elaborating TLM to improve its potency against various pathogens (129, 133-136). However most of the previous synthetic efforts have primarily explored modifications to the 5 position of the TLM thiolactone nucleus primarily due to its synthetic accessibility. However, these studies have failed to improve the activity of TLM.

## **Materials and Methods:**

### *Materials:*

### *5R-TLM and analogs:*

It is widely accepted that only the 5R-TLM, the natural stereoisomer, binds to the KAS enzyme while the 5S-isomer is biologically inactive (135).

Enantiomerically pure 5R-TLM and analogs were synthesized in our lab using reported protocol (137, 138) by Dr. Gopal Bommineni. For the synthesis of TLM, chemicals were purchased from the commercial source and used as such.

### *Enzymes:*

Wild type and C171Q KasA was purified from *M. smegmatis* mc<sup>2</sup>155 strain as described in **Chapter 2**. Importantly, the protein was used within 1 week after preparation.

### *Direct binding fluorescence titrations:*

Binding of TLM and TLM analogs to wild type and C171Q KasA was quantified by monitoring changes to the intrinsic tryptophan fluorescence using a Quanta Master fluorimeter (Photon Technology International). The fluorophore was excited at 280 nm and the emission was monitored at 337 nm, with an excitation slit width of 4.0 nm and an emission slit width of 8.0 nm. Inhibitor solutions in DMSO or the storage buffer (50 mM Tris-HCl, 150 mM NaCl, 1 mM DTT, pH 8.5) were titrated into the enzyme in the same buffer. The concentration of enzyme in the direct binding measurements was 1  $\mu$ M. Titration curves were corrected for Inner filter effect (139) and the  $K_i$  values were calculated using the Morrison equation (Grafit 4.0).

## Results and Discussion:

### *Direct binding measurements and analysis:*

The binding of TLM to both wild type KasA and C171Q KasA (acyl-KasA mimic) has been characterized by a previous lab member (130). For comparing the exhibited time dependent inhibition of KasA, binding was quantified using a fluorescence decay assay. For these inhibitors, titration of the inhibitor into the enzyme results in a time dependent quenching of fluorescence after an instantaneous change as observed for rapid-off inhibitors (**Figure 3.4**). The rate of this slow quenching of the fluorescence ( $k_{obs}$ ) increased as a function of the concentration of the inhibitor. The decay curves (**Figure 3.5**) were fitted to a double exponential (**Equation 3.1**) to account for a background photo-bleaching ( $k_b$ ) (140).

**Equation 3.1:** 
$$y = Ae^{-k_{obs}t} + Be^{-k_b t}$$

The  $k_{obs}$  increased as a function of the inhibitor concentration and was fitted to **Equation 3.2**, to obtain the  $k_{off}$ . Since, the initial decrease in fluorescence corresponds to formation of the E-I complex, while the final stabilized fluorescence values (at 2000 sec) correspond to the formation of the E\*-I, we can obtain the  $K_i$  and  $K_i^{*app}$  by taking the difference of these values, corrected for dilution and the inner filter effect, from the initial tryptophan fluorescence. Subsequently, the  $k_{on}$  can be easily calculated using **Equation 3.3**.

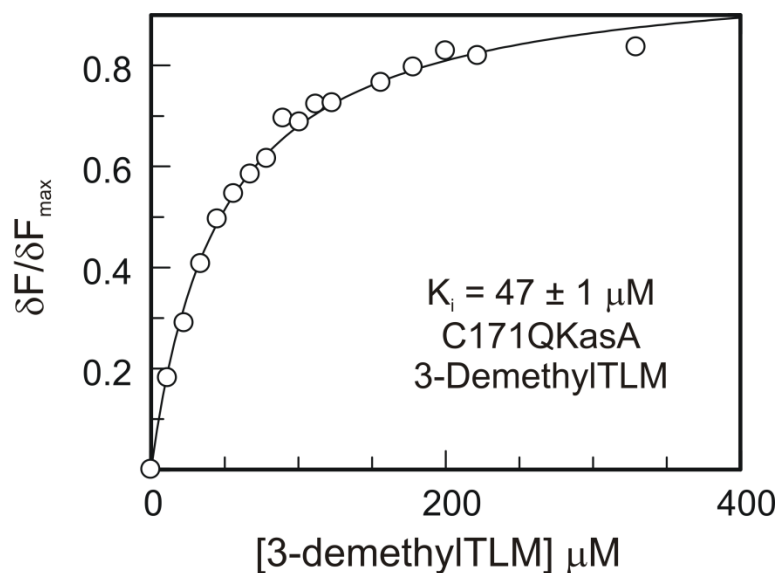
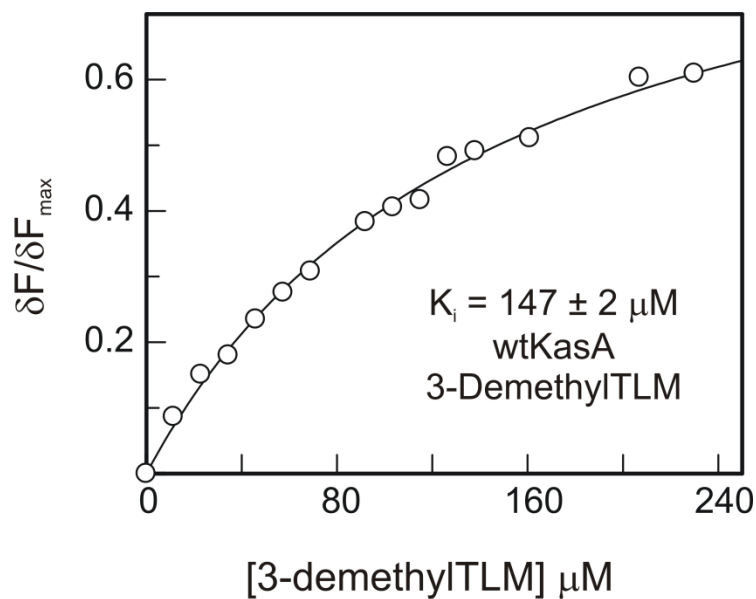
**Equation 3.2:**

$$k_{obs} = k_{off} \left[ \frac{1 + \frac{[I]}{K_i^{*app}}}{1 + \frac{[I]}{K_i^{app}}} \right]$$

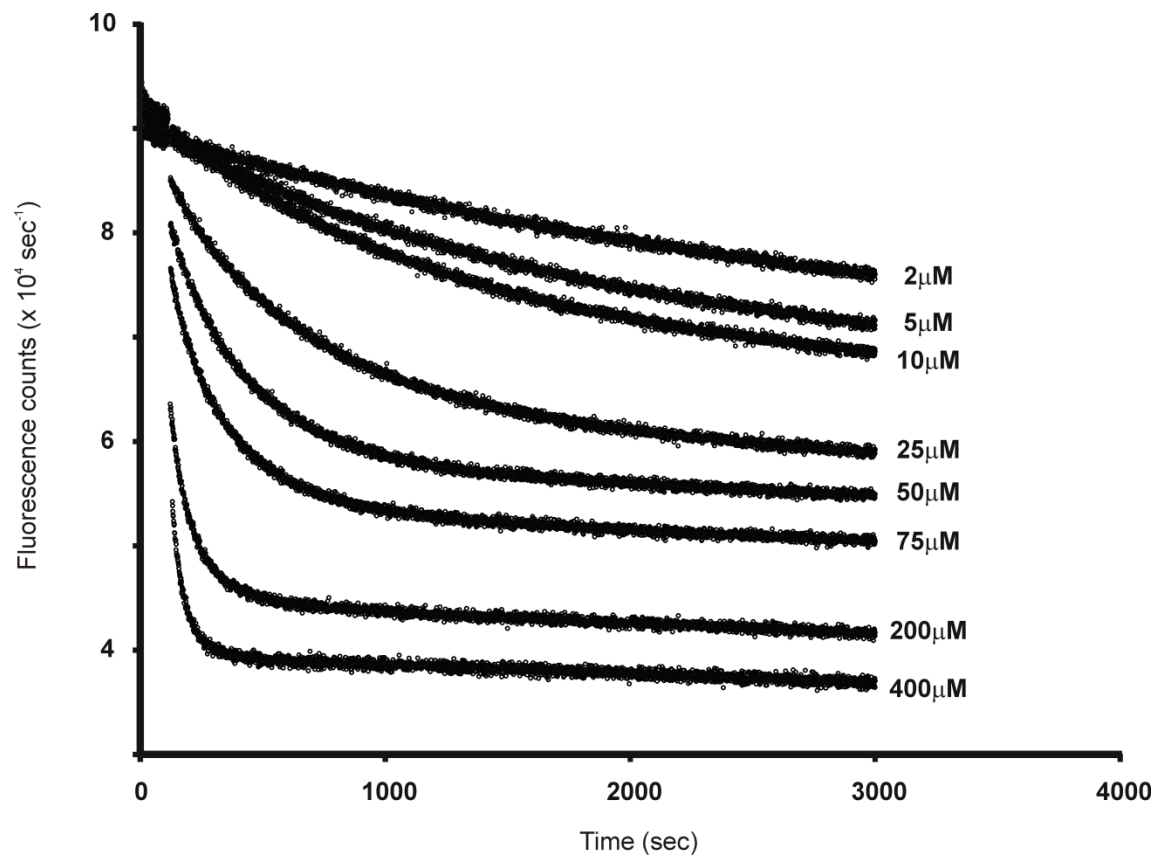
**Equation 3.3:**

$$K_i^* = \left[ \frac{K_i}{1 + \left( \frac{k_{on}}{k_{off}} \right)} \right]$$

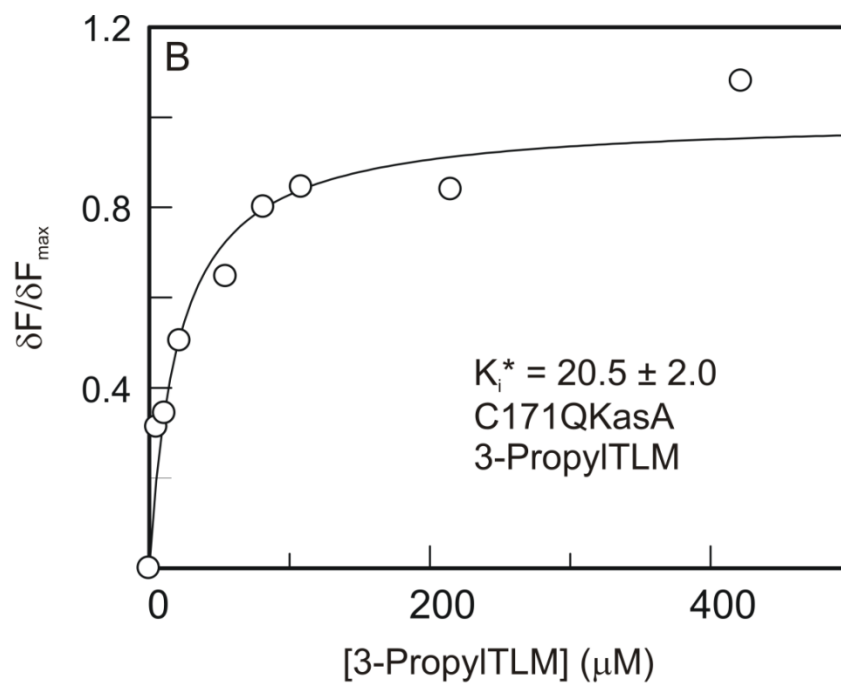
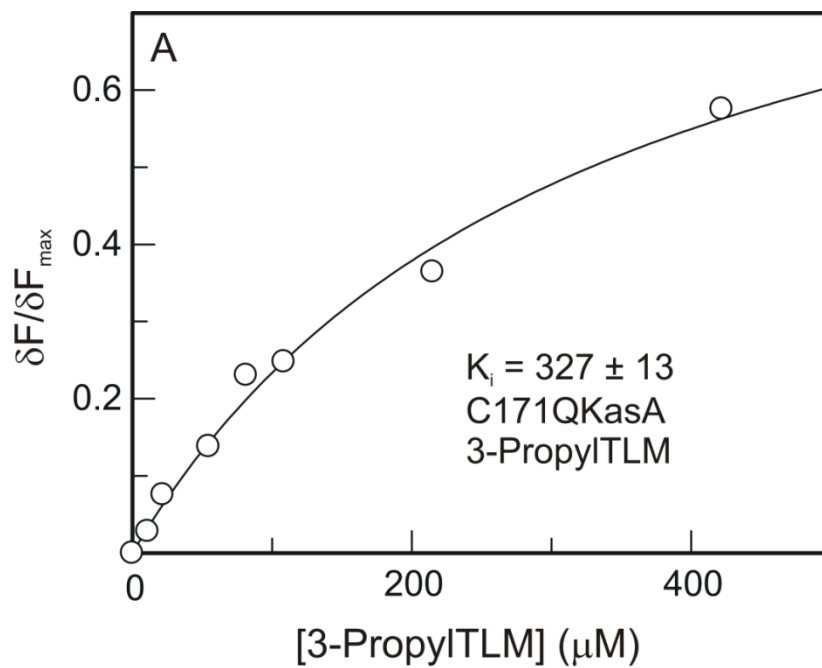
**Figure 3.4** describes the direct binding curves for a rapid reversible inhibitor (3-demethylTLM) with the free enzyme and the acyl-KasA mimic and **Figure 3.6** sheds light on the analysis for the slow onset inhibitor with C171Q KasA.



**Figure 3.4: The direct binding curves for 3-demethylTLM (Table 3.3):** The initial fast quenching of the intrinsic tryptophan fluorescence of free KasA and the acyl-KasA mimic were monitored as a function of the inhibitor concentration. The solid line is the best fit to the Morrison equation.



**Figure 3.5: Time dependent inhibition of C171Q KasA by 3-propylTLM (Table 3.3).**





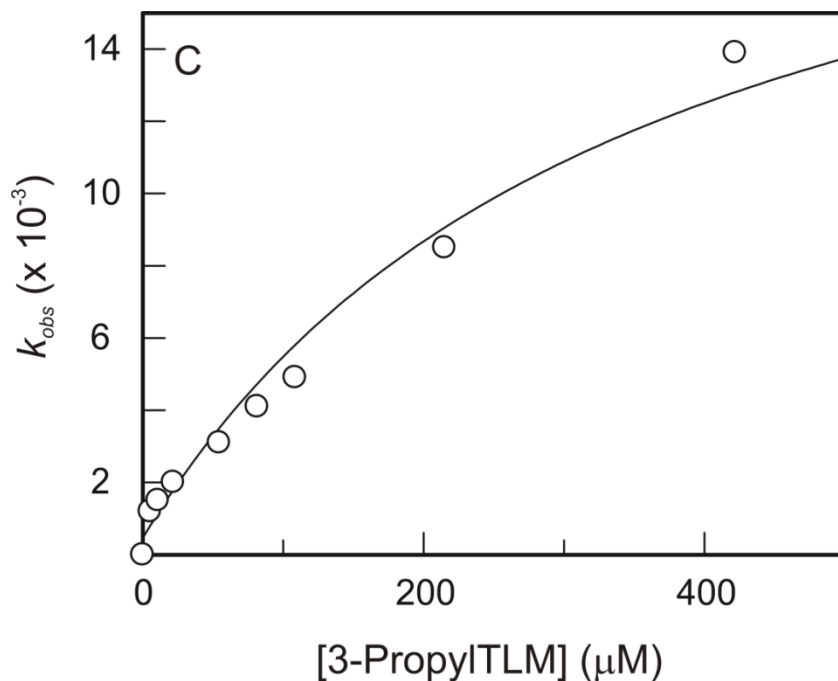


**Figure 3.6: Slow-onset kinetics of 3-propylTLM binding to C171Q KasA. A)**  $K_i$  for the EI complex between the ligand and the enzyme, **B)**  $K_i^*$  of the  $E^*I$  complex between 3-propylTLM and acyl-KasA mimic, **C)** Plot of  $k_{obs}$  as a function of the ligand concentration.

*Rational Inhibitor design:*

Based on our ILOE studies and structural analysis, we modeled PK940 into the active site of KasA using the X-ray structure of the TLM:C171Q KasA complex (69) (**Chapter 2**). In this model, PK940 occupies the pantetheine binding pocket in KasA with the terminal methyl group of the analog oriented towards TLM thiolactone. To corroborate our model, we linked the fragments and

docked the lead into the active site using DOCK6 (141, 142) (**Figure 3.7**, Cheng-Tsung Lai and Carlos Simmerling). Our docking data suggested that substituents at C3 position of TLM, with an appropriate linker, should be able to occupy the pantetheine binding pocket and enhance binding of the inhibitor.

The structural analysis suggested that elaboration of the TLM thiolactone core at either the C3 or the C4 position would result in an increase in affinity of the inhibitor for the enzyme. In order to optimize TLM, we synthesized and tested three sets of compounds with elaboration at these two positions of the thiolactone core.

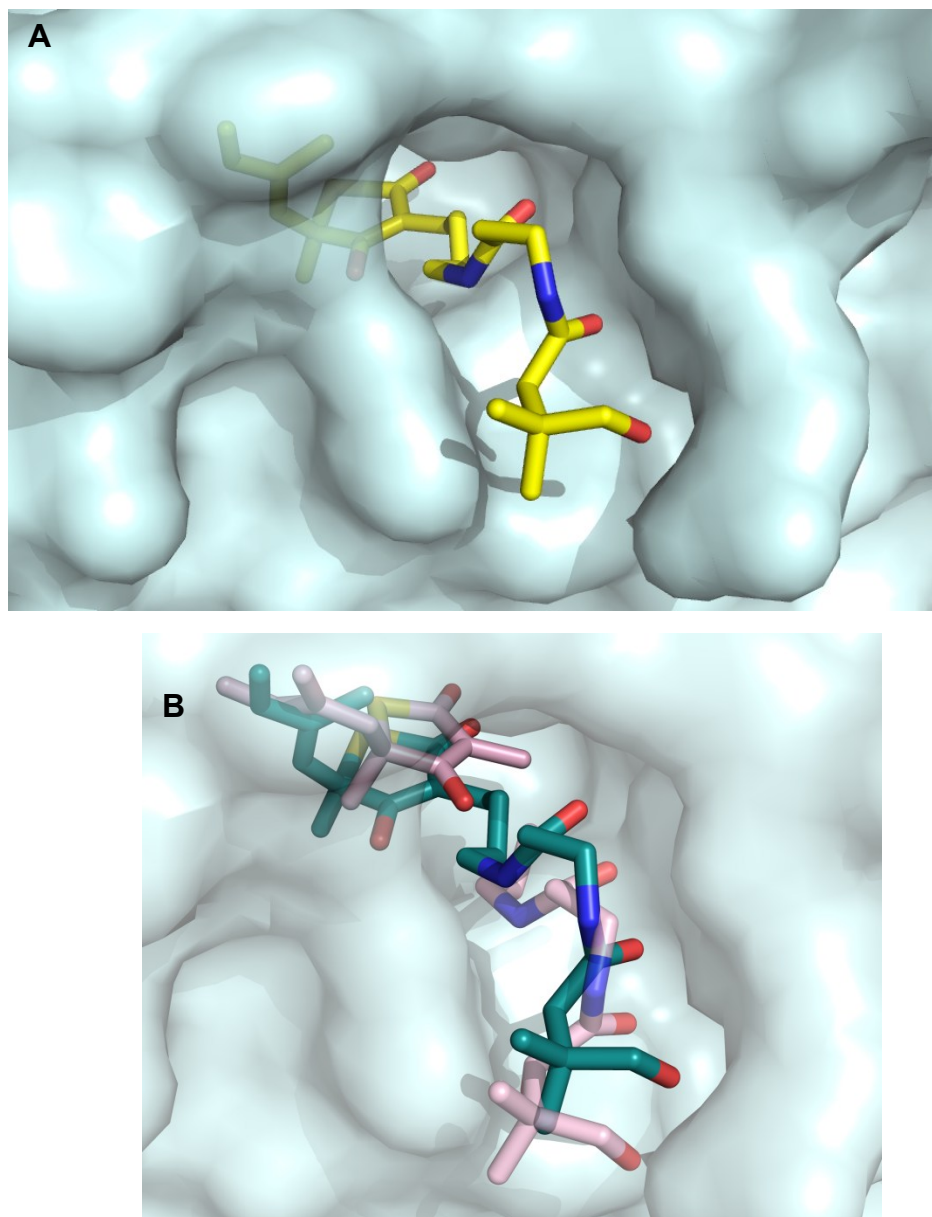


**Figure 3.7: Docked structure of the linked-fragment lead bound to KasA. A)** The linked-fragment compound docked into the KasA active site. **B)** Overlay of the docked structure with the model described in **Chapter 2**. The ligand conformations were calculated using the DOCK6 suite of dock programs wherein default parameters were used (141, 142). The substituent occupies the pantetheine binding pocket as shown by the ILOE data and structural analysis.

The first set of compounds (**Set A; TLM 21-24**) includes analogs with substituents at the C4 position (**Table 3.2**). Subsequently, we designed and tested **TLM 2-20 (Set B)** that have substituents at the C3 position with a variable linker length to allow the substituent to occupy the pantethene binding pocket. Moreover, as TLM is a thiomalonate isostere (**Figure 3.8**) (138), substituting a hydrogen bond donor/ acceptor at C3 would improve binding by interacting with the active site His (His311, His345) or Thr (Thr313, Thr315) residues via a hydrogen bond network involving water molecules (**Figure 3.9**) (138, 143). Therefore, we tested analogs **TLM 16-20** that have substitutions at C3 with a hydrogen bond acceptor at this position (**Table 3.3**).

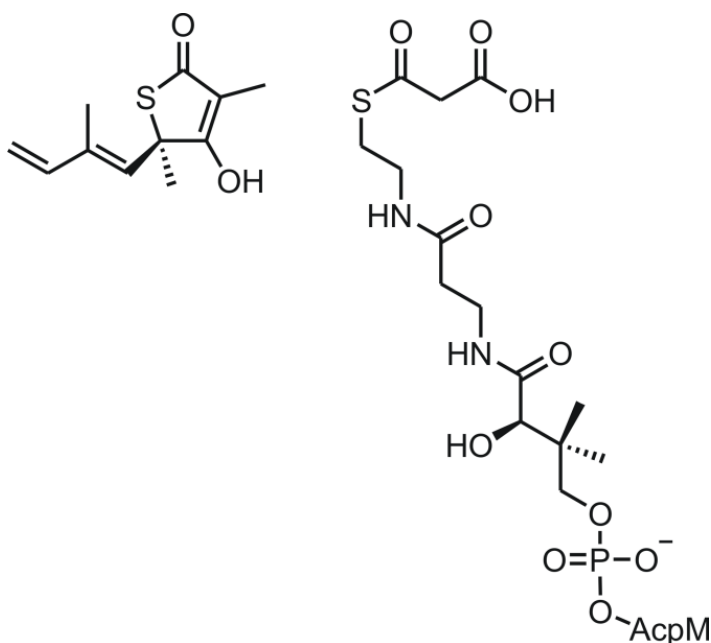


**Figure 3.8: TLM as an iso-stere of malonyl-AcpM.**

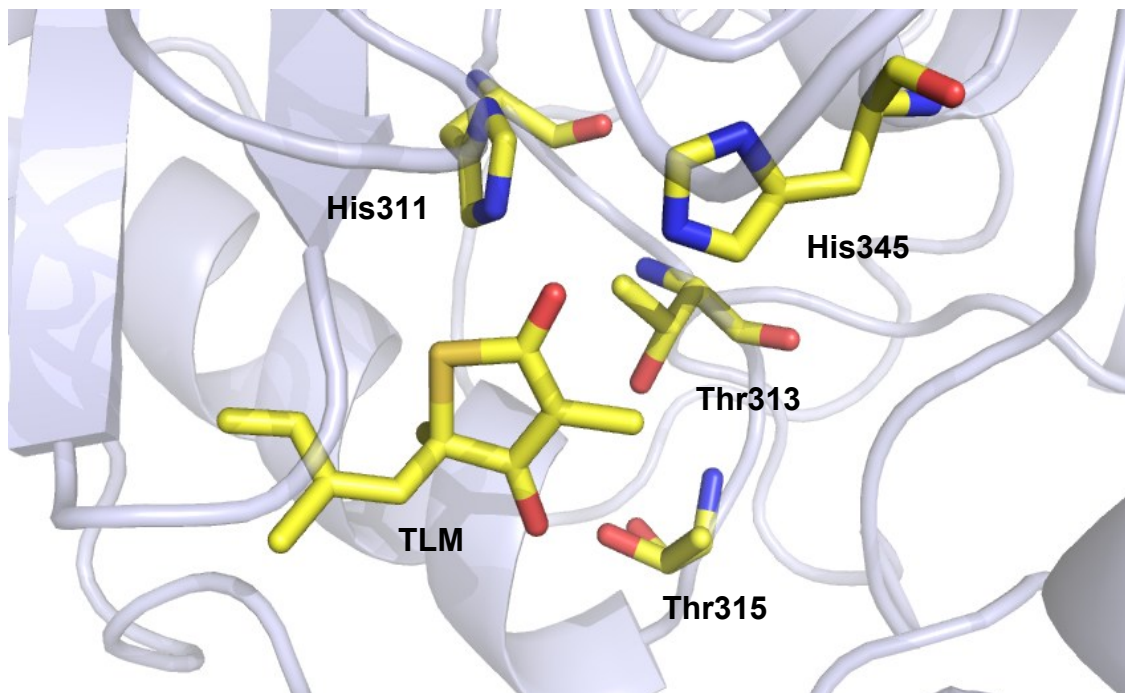


**Figure 3.9: Active site residues stabilizing a hydrogen bond donor/acceptor at C3.**

Apart from our ILOE experiments we have also utilized docking studies and crystallography to aid rational drug design. For instance, the crystal structure of TLM bound to C171Q KasA (pdb 2WGG(69)) delineates the acyl binding pocket via the binding of a PEG20 chain (**Figure 3.10**). This observation led us to design **TLM 25** where the palmitoyl acyl chain is predicted to occupy the acyl binding pocket.

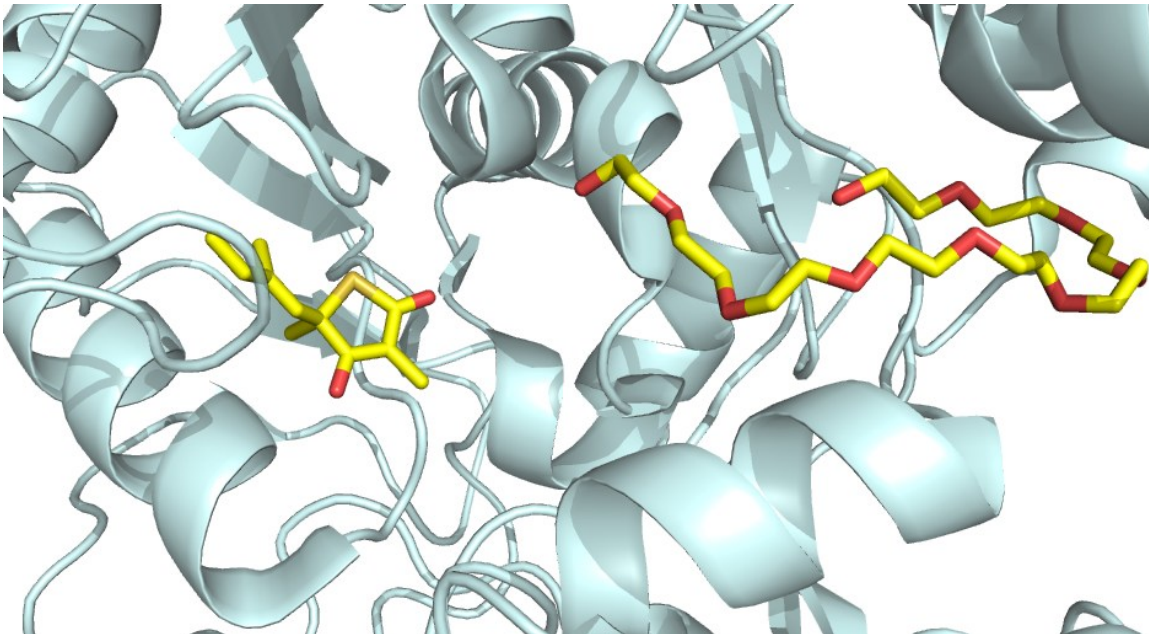


**Figure 3.10: Hydrophobic pocket in C171Q KasA occupied by an acyl chain.**

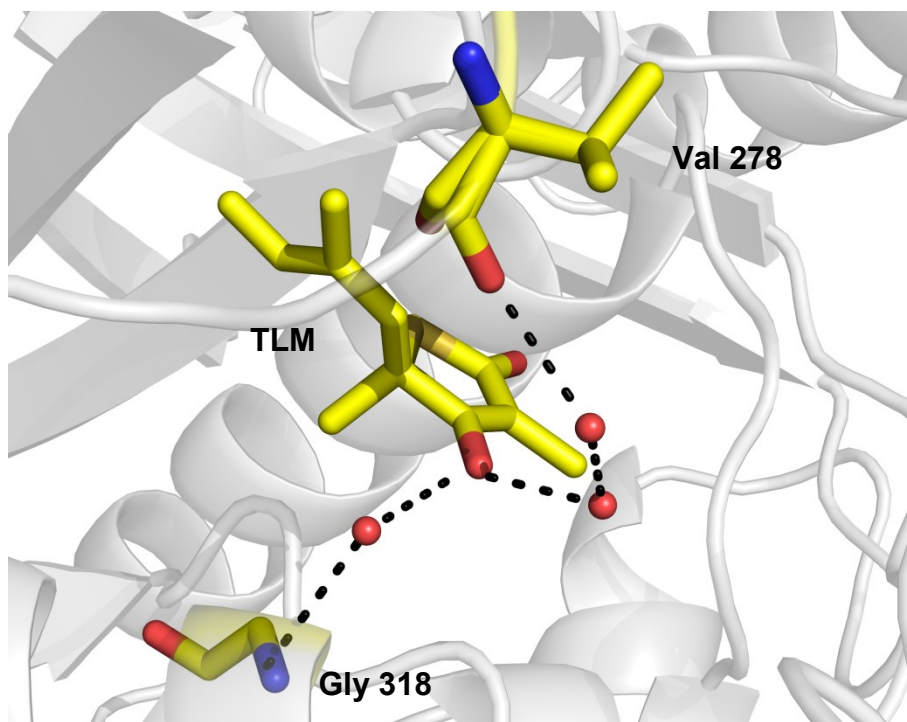
TLM occupies the malonyl-AcpM and a PEG20 binds to the acyl-AcpM binding pocket in C171Q KasA (69).

*Structure activity relationships:*

**SetA:** As noted by Price *et al.*, alkylating the C4 hydroxyl of the TLM core posed a challenge (138). Hence, for ease of synthesis we decided to synthesize C4 analogs of 3-demethylTLM (**TLM 2**) the binding of which to KasA was also characterized by us and is discussed subsequently. However, these inhibitors didn't show quenching of the tryptophan fluorescence implying either a different mode of binding or a lack of binding altogether. Hence, we used an NMR based waterLOGSY (144) assay to qualitatively assess binding. Competition

experiments were performed in the presence of saturating amounts of TLM. The C4 analogs that were designed and tested are presented in **Table 3.2**.

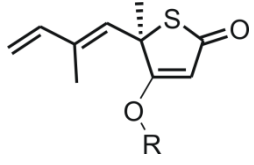
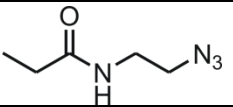
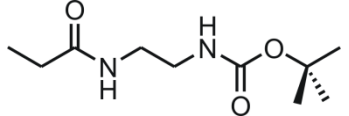
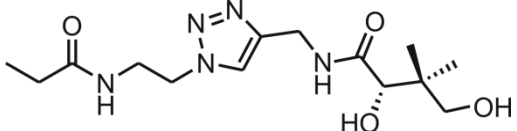
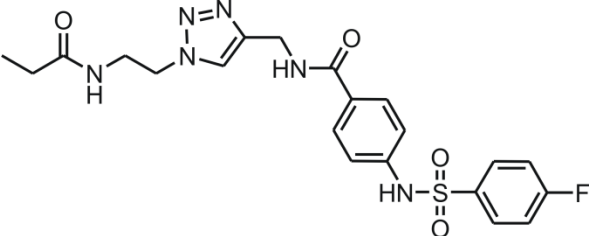
None of the C4 TLM analogs showed binding to KasA and also had a poor MIC against MTB H37Rv. The C4 hydroxyl of TLM is involved in a hydrogen bond network involving the carbonyl of Val 270 and the amide of Gly 305 of ecFabB (**Figure 3.11**) (112). These residues are conserved in KasA (Val 278 and Gly 318) and presumably are pivotal in the binding and stabilization of TLM to the active site. Moreover, the keto-enol tautomerism in TLM could play a role in stabilizing the TLM:KasA complex by increasing the partial negative charge on the thiolactone carbonyl. Alkylating the C4 hydroxyl would not only obviate tautomerism but also interrupt the hydrogen bond donor ability of the hydroxyl group deleteriously affecting stabilization of the enzyme inhibitor complex.



**Figure 3.11: Hydrogen bond network stabilizing the TLM:KasA complex.**



**Table 3.2: Binding parameters of C4 analogs of TLM to free enzyme and acyl-KasA mimic**

	Name	Binding affinity for KasA			MIC <sub>99</sub> MTB (µg/ml)
		K <sub>i</sub> (µM) wild type KasA	Slow Onset	K <sub>i</sub> (µM) C171Q KasA	
R =					
	<b>TLM21</b>	>226	ND	>130	>100
	<b>TLM22</b>	>226	ND	>130	>100
	<b>TLM23</b>	ND	ND	ND	>100
	<b>TLM24</b>	ND	ND	ND	100

**Table 3.2: C4 analogs of TLM (Set A; TLM 21-24).** Binding to the free enzyme and C171Q KasA was measured using a WaterLOGSY experiment. Competition experiments were carried out with the analogs in the presence of TLM.

ND: not determined

**Set B:** Our SAR data of the C3 analogs (**Table 3.4; TLM 2-4, TLM 11, 12, 16 and 17**) have yielded insights in optimizing time dependent inhibition of acyl-KasA. The lack of slow-off kinetics for **TLM 2** (3-demethyl TLM) suggests the requirement of the methyl group at the C3 of the thiolactone for time-dependent inhibition. Moreover, **TLM 3-4** and **TLM 11-12** suggest that the slow off characteristics are retained in the presence of a longer aliphatic chain. **TLM 3**, with an ethyl substituent at C3, has an approximately 4 fold weaker binding affinity than TLM to acyl-KasA with a  $K_i^*$  of 7  $\mu\text{M}$ . However, the **TLM 3:acyl-KasA** complex has a longer half-life (23 min) as compared to TLM (5 min) (130) and interestingly an improved  $\text{MIC}_{99}$  against *M. tuberculosis*. While with this compound we have slightly destabilized the **E\*I** complex, we have perhaps destabilized the transition state to a greater extent resulting in slower off rates. On the other hand, **TLM 4** has a propyl substituent which results in a slightly smaller half-life **TLM 4:acyl-KasA** complex (10 min) than **TLM 3**.

**TLM 16** and **17**, with an acetyl and a trifluoro-acetyl group, show a 10 fold improvement in binding to the free enzyme with a  $K_i$  of 25  $\mu\text{M}$  and 20  $\mu\text{M}$  respectively. These analogs also show tighter binding to C171QKasA compared to TLM with a  $K_i$  of 12  $\mu\text{M}$  and 8  $\mu\text{M}$  respectively. Importantly, these analogs also show stabilization of the **E\*I** complex with a  $K_i^*$  of 0.9  $\mu\text{M}$  and 0.46  $\mu\text{M}$  respectively as compared to 1.9  $\mu\text{M}$  for TLM. . The improved binding affinities are perhaps due to the stabilization of the carbonyl group by the active site Thr and His residues (**Figure 3.9**). However, we see faster on and off rates suggesting

that the transition state of the conformational change is stabilized. The faster  $k_{off}$  results in a smaller half-life (3 minutes) of the enzyme-inhibitor complex for both **TLM 16** and **17**. Moreover, time based inhibition of C171Q KasA by analogs **TLM 11** and **12** suggests that a longer aliphatic chain can be tolerated at the C3 position of the thiolactone.

Our extensive structural study coupled with medicinal chemistry has led to the development of TLM analogs with improved binding affinity to the free enzyme. In particular for **TLM 5-7** the  $K_i$  values are  $\sim 70 \mu\text{M}$ , which is a  $\sim 3$ -fold decrease compared to TLM ( $230 \mu\text{M}$ ). In addition, the improvement in affinity of **TLM 5-7** (C4 linker) compared to **TLM 8** and **TLM 10** (C2 linker) may indicate that the 4 carbon linker enables the substituent to dock into the pantetheine binding channel. This observation is consistent with the docked structure of the linked fragments and **TLM 9** (**Figure 3.12**).

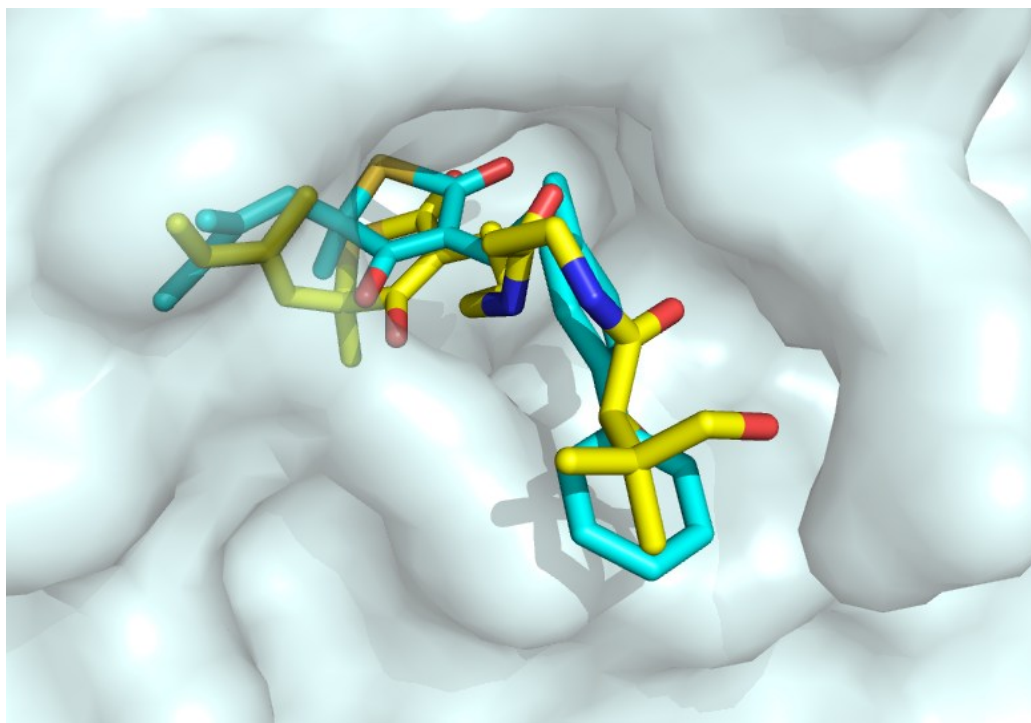


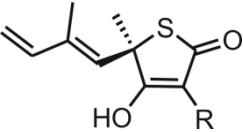
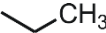

**Figure 3.12: Docked structures of TLM9 bound to KasA.** The ligand conformations were calculated using the DOCK6 suite of dock programs wherein default parameters were used (141, 142). The substituents occupy the pantetheine binding pocket as suggested by our ILOE and structural analysis.

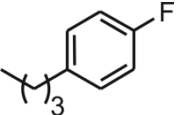
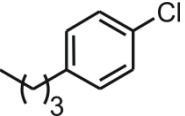
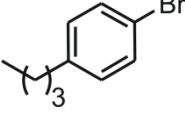
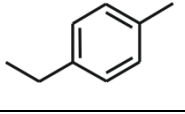
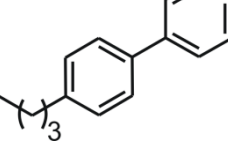
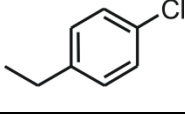
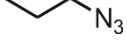
The docked structure of **TLM 9 (Figure 3.12)** shows how the biphenyl substituent fits very well into the pantetheine binding pocket. This might explain why **TLM 9** has the highest affinity for KasA with a  $K_i$  value of 10  $\mu\text{M}$  for the free enzyme which is 20 fold tighter than TLM. Apart from **TLM 9**, we have designed and synthesized a variety of compounds with biphenyl substituents, **TLM 15** and **TLM 27**, which also show an approximate 10 fold improvement in binding to the free enzyme compared to TLM with a  $K_i$  of 25  $\mu\text{M}$ . The  $K_i$  of these compounds for

C171Q KasA also shows a 20 fold improvement in the case of **TLM 27** (similar to **TLM 9**) and a 10 fold improvement for **TLM 15** compared to TLM. Our SAR data suggest that while bulkier substituents and longer aliphatic chains with a carbonyl group are tolerated at C3 (**TLM 18-20 and 25-27**), we observe a loss of time dependent kinetics.

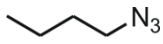
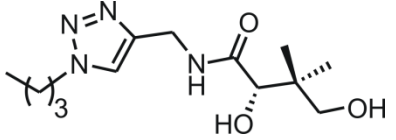
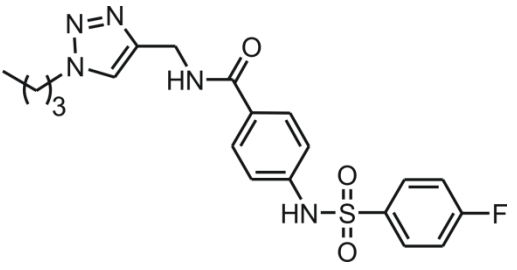
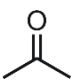
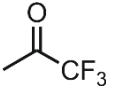
We have successfully been able to design and synthesize C3 and C4 analogs of TLM that show improved binding to the free enzyme and the acyl-KasA mimic. We have also been able to optimize the time dependent kinetics typical to binding of TLM to acyl-KasA mimic with **TLM 3** that has longest half-life of the drug target complex. Also, **TLM 3** shows an MIC<sub>99</sub> of < 7.8 µg/ml against MTB compared to TLM (13.2 µg/ml). Our analogs with aliphatic substituents at the C3 position (**TLM 3, 4, 11 and 12**) retain the MIC<sub>99</sub> against MTB as TLM. On the other hand our most potent inhibitors **TLM 9, 15, 17, 18 and 27** do not show improved MIC<sub>99</sub> values. This apparent lack of correlation between binding data and activity in whole cell assays can be attributed to multiple factors including breakdown of the inhibitors in the cell, uptake or efflux issues or presence of multiple targets (129, 138).

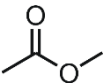
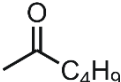
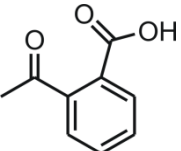
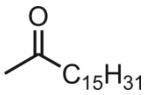
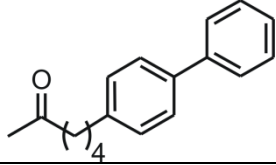
**Table 3.3: Binding parameters of C3 analogs of TLM to free enzyme and acyl-KasA mimic.**

	Name	Kinetic and Thermodynamic parameters with MTB KasA						MIC MTB (H37Rv) ( $\mu\text{g/ml}$ )
		$K_i$ ( $\mu\text{M}$ ) wild type KasA	Slow Onset	C171Q KasA		$k_{on}$ ( $\text{sec}^{-1}$ )	$k_{off}$ ( $\text{sec}^{-1}$ )	
R =				$K_i$ ( $\mu\text{M}$ )	$K_i^*$ ( $\mu\text{M}$ )			
-CH <sub>3</sub>	<b>TLM</b>	226 $\pm$ 9	Yes	175 $\pm$ 3	2 $\pm$ 0.3	0.206 $\pm$ 0.04	0.0022 $\pm$ 3 e <sup>-5</sup>	13.2
-H	<b>TLM2</b>	147 $\pm$ 2	No	47 $\pm$ 1	ND	ND	ND	>100
 CH <sub>3</sub>	<b>TLM3</b>	330 $\pm$ 4	Yes	357 $\pm$ 35	7.1 $\pm$ 1.3	0.026 $\pm$ 0.008	0.0005 $\pm$ 1 e <sup>-5</sup>	<7.8
 CH <sub>3</sub>	<b>TLM4</b>	233 $\pm$ 7	Yes	305 $\pm$ 8	16 $\pm$ 2	0.021 $\pm$ 0.004	0.0011 $\pm$ 2 e <sup>-5</sup>	12.5

	<b>TLM5</b>	71 ± 1	No	69 ± 2	ND	ND	ND	25
	<b>TLM6</b>	68 ± 1	No	77 ± 1	ND	ND	ND	25
	<b>TLM7</b>	71 ± 0.6	No	82 ± 2	ND	ND	ND	25
	<b>TLM8</b>	150 ± 2	No	93 ± 1.4	ND	ND	ND	25
	<b>TLM9</b>	11 ± 0.3	No	14 ± 0.2	ND	ND	ND	50
	<b>TLM10</b>	128 ± 4	No	>400	ND	ND	ND	25
	<b>TLM11</b>	233 ± 7	Yes	ND	ND	ND	ND	12.5



	<b>TLM12</b>	ND	Yes	ND	ND	ND	ND	ND
	<b>TLM14</b>	$274 \pm 5$	No	>400	ND	ND	ND	>100
	<b>TLM15</b>	$25 \pm 4$	No	$32 \pm 3$	ND	ND	ND	12.5
	<b>TLM16</b>	$25.5 \pm 0.5$	Yes	$8 \pm 0.8$	$0.9 \pm 0.2$	$0.035 \pm 0.01$	$0.0039 \pm 3 e^{-5}$	12.5
	<b>TLM17</b>	$22 \pm 2$	Yes	$12 \pm 0.6$	$0.46 \pm 0.05$	$0.145 \pm 0.03$	$0.0056 \pm 2 e^{-5}$	>100

	<b>TLM18</b>	$31 \pm 2$	No	$22 \pm 2$	ND	ND	ND	100
	<b>TLM19</b>	$66 \pm 2$	No	$65 \pm 1$	ND	ND	ND	12.5
	<b>TLM20</b>	$34 \pm 2$	No	$102 \pm 3$	ND	ND	ND	>100
	<b>TLM25</b>	$65 \pm 1$	No	$105 \pm 4$	ND	ND	ND	>100
	<b>TLM27</b>	$26 \pm 0.5$	No	$8 \pm 0.5$	ND	ND	ND	50

**Table 3.3: Binding parameters for C3 TLM analogs to free enzyme and the acyl-KasA mimic. ND: not determined**

*SAR of TLM analogs against other bacteria:*

TLM has broad spectrum antibacterial activity and *in vivo* efficacy against *K. pneumoniae* and *S. marcescens* (107, 108). In our attempts to optimize TLM as an antibacterial, we tested the MIC against different pathogens including *Y. pestis*, *F. tularensis*, *Burkholderia sp.* and *S. aureus*. All these bacteria utilize different KAS enzymes in the elongation step of their FASII pathway (**Table 3.4**). For instance, while *M. tuberculosis* and *Y. pestis* have both KASI and KASII, *S. aureus* and *B. pseudomallei* only have KASII.

<b>Table 3.4: KASI and KASII enzymes in various bacteria.</b>			
<b>Organism</b>	<b>Staining properties</b>	<b>KASI</b>	<b>KASII</b>
<i>Y. pestis</i>	Gram negative	+	+
<i>M. tuberculosis</i>	Gram positive (acid/ alcohol fast)	+	+
<i>S. aureus</i>	Gram positive	-	+
<i>B. pseudomallei</i>	Gram negative	-	+
<i>F. tularensis</i>	Gram negative	-	+

**Table 3.4: KASI and KASII enzymes in various bacteria.** KASI and KASII in *Mtb.* are referred to as KasA and KasB, in other bacteria they are usually referred to as FabB and FabF respectively.

<b>Table 3.5: MIC values of TLM analogs against a wide variety of bacterial strains</b>						
<b>Name</b>	<b>MIC (µg/ml)</b>					
	<i>F. tularensis</i>	<i>Y. pestis</i>	<i>B. thailandensis</i> Bt.38 (efflux <sup>-</sup> )	<i>B. pseudomallei</i> Bp82z66	<i>S.aureus</i>	
					RN4220 MSSA	BAA1762 MRSA
<b>TLM</b>	2.81	8.09		13.1	75	75
<b>TLM2</b>	123.9	250	148.3	155	150	100
<b>TLM3</b>	6.9	144.6	148.3	61	150	125
<b>TLM4</b>	25.8	250	250	>256	>200	>200
<b>TLM5</b>	3.153	250	250	>256	>64	75
<b>TLM6</b>	1.731	250	81.0	>256	64	50
<b>TLM7</b>	2.17	250	125.9	>256	32	50
<b>TLM8</b>	3.451	250	250	>256	>64	>100
<b>TLM9</b>	1.974	250	145.2	>256	16	25
<b>TLM10</b>	3.1	250	250	>256	64	100

<b>Table 3.5: MIC values of TLM analogs against a wide variety of bacterial strains</b>						
<b>Name</b>	<b>MIC (µg/ml)</b>					
	<i>F. tularensis</i>	<i>Y. pestis</i>	<i>B. thailandensis</i> Bt.38 (efflux <sup>-</sup> )	<i>B. pseudomallei</i> Bp82z66	<i>S.aureus</i>	
					RN4220 MSSA	BAA1762 MRSA
<b>TLM11</b>	23.5	250	250	>256	>64	>100
<b>TLM12</b>	15.3	250	250	>256	>64	>100
<b>TLM14</b>	250	250	250	>256	>64	>100
<b>TLM15</b>	250	250	250	>256	>64	>100
<b>TLM16</b>	8.8	>250	ND	154.6	64	32
<b>TLM17</b>	98.1	>250	ND	159.8	>64	64
<b>TLM18</b>	58.2	>250	ND	160.3	>64	>64
<b>TLM19</b>	1.8	>250	ND	171.4	16	32
<b>TLM20</b>	15.9	>250	ND	154.5	32	32
<b>TLM21</b>	39.1	>250	ND	>256	>64	>64

Table 3.5: MIC values of TLM analogs against a wide variety of bacterial strains						
Name	MIC (µg/ml)					
	<i>F. tularensis</i>	<i>Y. pestis</i>	<i>B. thailandensis</i> Bt.38 (efflux <sup>-</sup> )	<i>B. pseudomallei</i> Bp82z66	<i>S.aureus</i>	
					RN4220 MSSA	BAA1762 MRSA
<b>TLM22</b>	54.4	>250	ND	>256	>64	>64
<b>TLM23</b>	158.9	>250	ND	149.5	>64	>64
<b>TLM24</b>	>256	>250	ND	177.9	>64	>64
<b>TLM25</b>	3.9	>250	ND	1.4	0.5	1
<b>TLM26</b>	ND	ND	ND	ND	16	16
<b>TLM27</b>	0.21	>250	ND	4.6	0.5	2

**Table 3.5: MIC values of TLM analogs against a different bacterial strains.** (Susan Knudson, Jason Cummings, Richard Slayden, CSU). ND: Not determined.

Through extensive SAR we have been able to design compounds that show inhibition not only against MTB but also against a variety of Gram positive and negative bacteria. **TLM 9** shows a 5 fold improvement in the MIC against drug sensitive *S. aureus* (16 µg/ml) and a 3 fold improvement against MRSA (25 µg/ml) compared to TLM (75 µg/ml). **TLM 25** which has a palmitoyl group on C3, shows a 150 fold improvement in the MIC against drug sensitive *S. aureus* (0.5 µg/ml) and a 75 fold improvement in the MIC against MRSA (1 µg/ml) compared to TLM. **TLM 25** also showed a 9 fold improvement in MIC against *B. pseudomallei* (1.4µg/ml) compared to **TLM** (13.1 µg/ml).

**TLM 27**, with a biphenyl substituent with a carbonyl group, shows a 150 fold improvement in activity against *F. tularensis* with an MIC of 0.2 µg/ml and a 3 fold improvement against *B. pseudomallei* (13.1 µg/ml) as compared to TLM (2 µg/ml). Interestingly, none of the C4 analogs (**Set A**) showed potency in the whole cell assays suggesting the requirement a C4 hydroxyl for effective binding of the TLM and derivatives.

## Conclusions:

Using ILOE NMR spectroscopy, we have designed and subsequently synthesized TLM analogs that have improved binding to KasA. We have designed two sets of TLM analogs with substitutions at the C4 and the C3 position of the thiolactone core. C4 TLM analogs (**TLM 21 - 24**) do not show

binding to KasA or the acyl-KasA mimic. Interestingly, these analogs have poor whole cell activity against all Gram positive and negative bacterial strains tested. These data suggest the importance of the C4 hydroxyl in stabilizing the binding of TLM and analogs to KAS enzymes.

On the other hand elaboration at the C3 position affords analogs with potent inhibition against KasA and the acyl-KasA mimic. Our SAR analysis coupled with docking studies suggests that a 4 carbon linker (**TLM 5-7, 9**) enables the substituent to dock into the pantetheine binding pocket resulting in enhanced binding compared to analogs with a shorter 2 carbon linker (**TLM 8, 10**). By studying alkyl (**TLM 2-4, TLM 11, 12**) and short-chain acyl substituents (**TLM 16, 17**) at C3, we were able to optimize both the thermodynamics and the kinetics of binding of our analogs to the free enzyme and the acyl enzyme mimic. Aryl substituents at C3 with the longer 4 carbon linker also give us enhanced inhibition especially analogs with the biphenyl substituents (**TLM 9, 27**). Also, while bulkier groups and long chain acyl chains are tolerated at the C3 position, we lose slow onset inhibition. Apart from **TLM 3** where we see improved whole cell activity against MTB, many of analogs have very similar MIC values against MTB as TLM (**TLM 4, 11, 15, 16 and 19**). However, we don't see improved whole cell activity for some C3 analogs that show potency in the *in vitro* binding assay (**TLM 9, 17, 18, 20 and 27**).



Our analogs show improved MIC values against various other priority pathogens such as *B. pseudomallei*, *F. tularensis* and *S. aureus*. Interestingly, these bacteria have only one of the two elongating KAS enzymes (FabF). Though we have not characterized the binding of our analogs to the KAS enzymes from these bacteria, our data suggests that our analogs should have potent inhibition of these targets. Our SAR has laid the foundation for additional inhibitor discovery which is significant given the dearth of high affinity inhibitors for this important drug target.

# Chapter 4

*InhA – protein dynamics and ligand binding*

## Introduction:

### *Trans-2-enoyl-AcpM reductase:*

The last step of the FASII pathway which is catalyzed by the *trans-2-enoyl-ACP* reductase, involves the reduction of the double bond between C2 and C3 of the growing acyl chain (**Chapter 2, Figure 2.1**). This NADH dependent enzyme is encoded by the *fabI* gene and was first shown to be essential by Bergler *et al* (51). Enoyl-ACP reductases have been extensively studied in various organisms such as *E. coli* (47, 54, 145, 146), *M. tuberculosis* (147, 148), *S. aureus* (149) and *F. tularensis* (150). They are tetrameric  $\alpha/\beta$  proteins with a classical Rossmann fold and belong to the short-chain alcohol dehydrogenase/reductase (SDR) superfamily. They are characterized by a highly conserved Tyr-X6-Lys motif (53). The enzyme mechanism for InhA involves Tyr158 donating a proton to C2, and NADH donating a hydride to C3 of the enoyl substrate. The Tyr proton is replenished by a proton relay network through Lys 165, the ribose hydroxyls and a chain of four water molecules that communicate with solvent. Subsequently, the resulting enol undergoes tautomerization to yield the final product (**Figure 4.1**). Enoyl-ACP reductases from different bacterial species show a very high structural similarity apart from a mobile loop region commonly referred to as the substrate binding loop as it covers the active site (52).

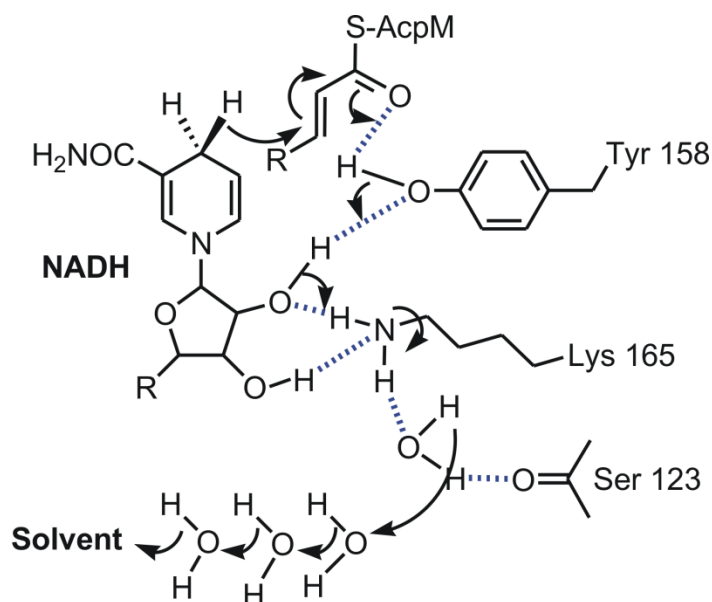


**Figure 4.1: The catalytic mechanism for the enoyl-AcpM reductase in MTB.**

*Inhibition by isoniazid and resistance:*

Isoniazid (INH) is a frontline drug for the treatment of tuberculosis. INH is a prodrug and is activated by KatG, the mycobacterial catalase-peroxidase, to form the INH-NAD adduct along with the NAD(H) cofactor (**Figure 4.2**) (151). This adduct is a slow onset inhibitor of InhA and has a complex mode of action (55, 57, 58, 152, 153) (**Chapter 1**). The INH-NAD adduct exhibits slow-onset inhibition to InhA with the ordering of the substrate binding loop providing the energy barrier for the slow step (**Chapter 1, Figure 1.5**). Since the predominant mechanism of resistance against isoniazid arises from mutations in KatG (151),

novel inhibitors that circumvent the activation could be promising candidates to combat INH resistance in Mtb (154)

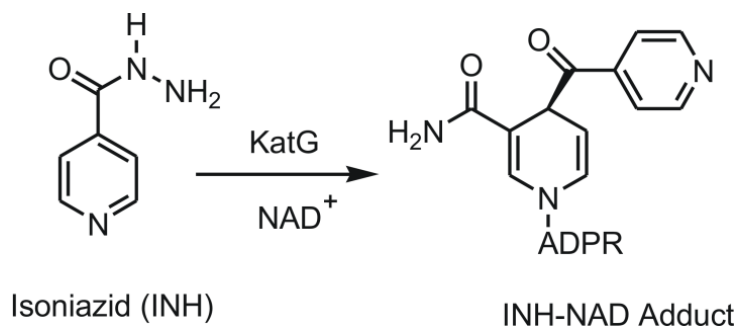


**Figure 4.2: Activation of Isoniazid by KatG.** The prodrug and the cofactor  $\text{NAD}^+$  are utilized by the catalase-peroxidase for the INH-NAD adduct.

*Lead optimization with triclosan:*

Triclosan (**Figure 4.3**), a broad spectrum antibiotic, has been shown to be a potent inhibitor of FabI enzymes from different organisms (60, 61). Triclosan binds to  $\text{ecFabI/NAD}^+$  binary complex with an overall  $K_i$  of 7 pM (61, 62) and shows slow onset kinetics similar to binding of the INH-NAD adduct to InhA (52, 59). Importantly, the triclosan based inhibitors designed in our lab are uncompetitive inhibitors of InhA with respect to the cofactor  $\text{NAD}^+$ .

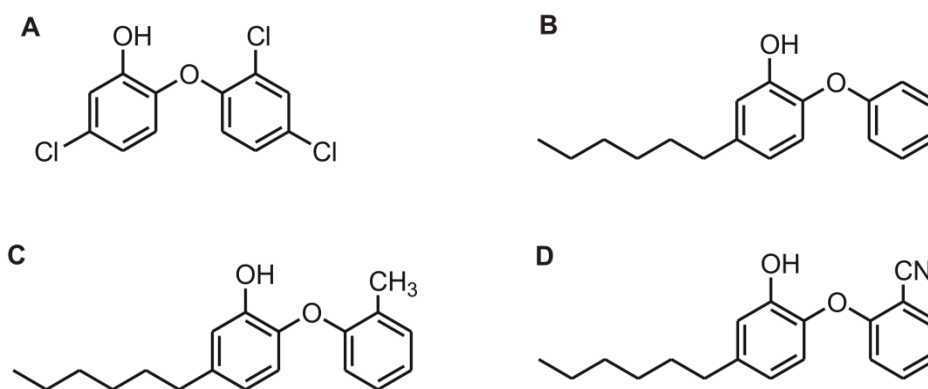


**Figure 4.3: Diphenyl ether lead and inhibitors. A)** triclosan, **B)** PT04 **C)** PT70 **D)** PT119.

While, triclosan is very effective against FabI enzymes from *E. coli*, *S. aureus* and *P. falciparum*, it shows a much weaker  $K_i$  (0.2  $\mu\text{M}$ ) and a modest  $\text{MIC}_{99}$  against *M. tuberculosis* (12.5  $\mu\text{g/ml}$  for H37<sub>Rv</sub>) (60, 155). InhA and ecFabI share a 46% sequence identity and a high degree of structural homology, presumably triclosan has a similar mode of binding with both the enzymes. Also, triclosan does not require activation by KatG and inhibits InhA directly (60, 149). Hence, it can provide a useful scaffold for development of novel inhibitors. Extensive structure-activity-relationship (SAR) studies based on triclosan have resulted in some very potent slow, tight binding inhibitors of InhA (**Figure 4.3**) (11, 59, 63).

Our rational drug design efforts based on the diphenyl ether scaffold have yielded nanomolar inhibitors of InhA with MIC values of 1-2  $\mu\text{g/ml}$  against both

drug sensitive and drug resistant strains of MTB (59). However, despite showing potent inhibition *in vitro* these inhibitors have limited *in vivo* efficacy, perhaps due to their low bioavailability (156-158). Therefore, there is interest in improving the “drug-like” characteristics of these inhibitors while optimizing their inhibition.

*Slow onset inhibition with diphenyl ethers:*

The efficacy of a drug, amongst other factors, requires the drug to be physically bound to its physiological target, with longer interactions resulting in greater efficacy both *in vitro* and *in vivo*. The lifetime of drug-target complex is controlled by kinetic constants, the association rate constant ( $k_{on}$ ) and more critically the dissociation rate constant ( $k_{off}$ ). Typically the lifetime of the drug on the target is described in terms of its residence time ( $1/k_{off}$ ), which is the time required for ~63% dissociation of the remaining drug-target complex (159). This results in the classification of drugs into two categories – rapid-off (transiently binding) and slow-off (slow binding) drugs. Slow binding inhibitors associate with and/or dissociate from the target enzymes slowly, thus leading to time dependent inhibition.

Various workers suggest that factoring in the lifetime of the drug-target complex, or the residence time of the drug on its target, can result in increased efficacy of a small molecule drug *in vivo* (17, 131, 132). Thus, in our SAR efforts we have been keen on optimizing not just the thermodynamic binding of the

inhibitor but also the residence times to result in greater efficacy. Hence, in order to design more potent inhibitors targeting InhA it is important to understand the mechanism of the time dependent inhibition.

*Mechanism of time dependent inhibition in InhA:*

X-ray crystallography and other structural techniques have been extensively utilized in the past by us and other workers to aid rational/ structure based drug design. FabI enzymes in particular have been extensively characterized from various organisms with an aim to target them for antibacterial drug discovery. Our studies based using the diphenyl ether motif have resulted in some very potent slow, tight binding inhibitors of InhA (11, 59, 63). Comparing the crystal structures of InhA bound to slow onset and rapid-off inhibitors implicate the “substrate binding loop” for the slow step in binding (59). The binding of the ligand is followed by a conformational change in the protein that provides the energy barrier for the ligand dissociation (**Figure 4.4**).



**Figure 4.4: The two step mechanism for time based inhibition of InhA.**



In InhA, part of the loop region (Leu 195-Ileu 200) gets ordered on binding to the INH/NAD adduct, while it stays disordered upon triclosan binding. Since, INH-NAD adduct is a slow, tight binding inhibitor of InhA, it is plausible that the slow step in binding is the loop ordering event. This hypothesis is corroborated by comparing crystal structures of InhA bound to other slow onset inhibitors to rapid off inhibitors, where we only see an ordered loop region in the former (59). **(Figure 4.5).**

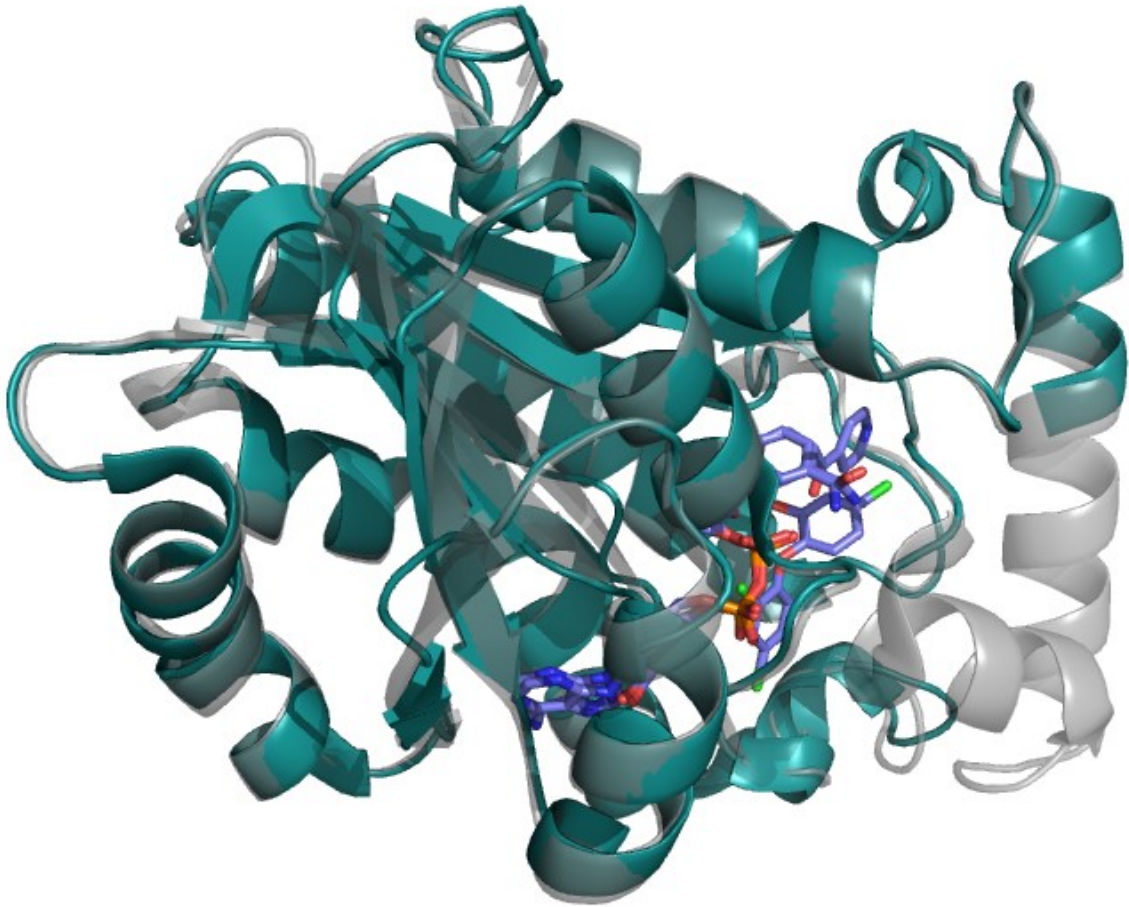


**Figure 4.5: Substrate binding loop and slow onset inhibition.** Overlay of crystal structures of InhA bound to INH-NAD adduct (slow onset, grey, PDB:1ZID) and triclosan/NAD<sup>+</sup> (rapid-off, teal, PDB:2B35). The substrate binding loop can be seen ordered in the INH-NAD adduct bound structure while is disordered in case of the triclosan/NAD ternary complex.

*Methods to study conformational dynamics in InhA:*

Traditionally, a variety of methods have been utilized to study conformational dynamics such as NMR, fluorescence, circular-dichroism, mass

spectrometry, infra-red and Raman spectroscopy (160, 161). We chose to use NMR and fluorescence in conjunction with site directed mutagenesis to understand the intricacies of loop dynamics in InhA and its effect on inhibitor kinetics.

*Site directed mutagenesis:*

Triclosan is a slow onset inhibitor for *ecFabI* while it is a rapid-off inhibitor for InhA. The sequence of the relatively long substrate binding loop in InhA is LAMSAIVGGALGEEA. Examining the primary sequence shows a high density of Gly residues in this region. The *ecFabI* loop is much shorter (LAASGI) and is composed of fewer Gly residues. Moreover, triclosan is a slow onset inhibitor of *ecFabI* and not of InhA. Since Gly residues are known to impart a high degree of flexibility to a protein chain (162), it is possible that by replacing the Gly residues with helix stabilizing residues (Ala) one can induce loop ordering upon binding of a previously rapid-off inhibitor. Moreover, replacing the InhA loop by the active site loop in *E.coli* could give us information on the dependence of binding kinetics on loop dynamics.

*Fluorescence spectroscopy:*

Fluorescence spectroscopy has been used extensively to study protein dynamics and function, with the vast majority of studies making use of the

naturally occurring fluorophores, Tyr and Trp (163, 164). However, there is interest in the incorporation of new fluorophores as they can offer site specific information and permit selective excitation and detection (165, 166). With the advent of bio-orthogonal protein labeling techniques, fluorescence based methods like FRET, and FRAP have gained extreme importance. The 21<sup>st</sup> pair aminoacyl t-RNA synthetase technique developed by Schultz et al (167), has been extended by Ryan Mehl et al (168) to incorporate various unnatural amino acid into a protein of interest. p-Cyanophenylalanine ( $F_{CN}$ ) has been developed as a robust probe to study protein dynamics and protein-protein interactions (169, 170). Apart from it being a fairly conservative substitution for aromatic amino acids,  $F_{CN}$  has been shown to have unique fluorescence properties. It can be selectively excited at 240 nm and has a emission maximum at 290 nm. The fluorescence quantum yield of  $F_{CN}$  is dictated by the hydrogen bonding interactions involving the cyano group. Moreover, it can be tolerated in both hydrophobic and hydrophilic environment making it a conserved substitution for Tyr, Trp and Phe (171).

#### *Nuclear Magnetic Resonance spectroscopy:*

While there are a wide variety of techniques that have traditionally been utilized for studying protein dynamics, most of these techniques require a reporter probe within the protein structure which might deleteriously perturb the dynamics. Nuclear magnetic resonance, replete in dynamic information, is indeed

a very convenient method to study protein structure, function and dynamics without creating a structural perturbation. To study ligand binding, one can label the protein of interest with  $^{15}\text{N}$  and use  $^{15}\text{N}/^1\text{H}$  HSQC to see differential changes in chemical shifts upon ligand binding (172-175).

NMR spectroscopy can help characterize the ensemble of conformations accessed by a macromolecule and the dynamics of their inter-conversion. The sensitivity of nuclear chemical shifts to the local environment makes NMR a useful tool to diagnose changes in molecular conformations. Changes in chemical shifts (chemical shift mapping) have been traditionally used for characterizing protein-protein and protein-ligand interactions that are of great interest in drug discovery programs. Previous workers have used  $^{15}\text{N}/^1\text{H}$  TROSY HSQC,  $^{13}\text{C}/^1\text{H}$  HMQC along with chemical shift mapping in conjunction with backbone assignments to get a detailed description of the conformational states of supra-molecular structures. These include a plethora of studies focusing on conformational changes in proteins upon ligand binding (172, 173, 176). Comparison of the  $^{15}\text{N}/^1\text{H}$  HSQC spectra of apo InhA and the drug bound ternary system could provide information on the conformational changes induced upon inhibitor binding.

However, the large size of InhA (120 kDa, homo-tetramer) could be prohibitive for the use of traditional NMR techniques. The advances in sample preparation and pulse sequences have allowed studies of large (177), previously

NMR inaccessible, proteins such as *E. coli* GroEL-GroES complex (900 kDa) (178), DHPR (120kDa) and DOXPR (174 kDa) (176), *S. aureus* DHN Aldolase (110 kDa) (179), *E. coli* Malate synthase G (82 kDa) (180) amongst many other examples. Hence, perdeuterating InhA and using transverse relaxation optimized spectroscopy (TROSY) techniques, we could surmount the problem of the large size of InhA.

Various other workers have used NMR to complement their understanding of protein dynamics upon inhibitor binding. Martin Vogtherr *et al.* have studied binding of various tight binding inhibitors (nM  $K_d$ ) to p38 kinase with residence times ranging from 5 minutes to 32 hours ( $k_{off} = 8.36 \times 10^{-6} \text{ sec}^{-1}$ ) (181, 182). Having seen a similar behavior in the case of InhA binding to the slow onset inhibitors, we believe conformational changes in InhA upon inhibitor binding would be amenable to studies using NMR spectroscopy. In support of this proposal, Dyson *et al* (183, 184) have extensively studied dynamics of the active site loop in metallo- $\beta$ -lactams and dihydrofolate reductase in the presence of tight binding inhibitors. Once we are able to assign the chemical shifts of the residues in the loop region,  $^1\text{H}/^{15}\text{N}$  heteroneuclear NOE experiments can be used to provide a qualitative idea of the mobility of the backbone in a sub-nanosecond time regime. Furthermore, studying the relaxation parameters of the residues in the loop region along with residues that are unaffected by ligand binding can help us understand changes in the backbone flexibility upon ligand binding. Hence,

we set out to understand the dynamics of the substrate binding loop upon binding of an inhibitor using NMR spectroscopy.

Since the biggest bottleneck in this project is the lack of backbone assignments, we intend to selectively  $^{15}\text{N}$  or  $^{13}\text{C}$  label specific amino acids (185) along with using kinetically similar loop-replacement mutants of InhA to assign peaks corresponding to the substrate binding loop.

## **Materials and Methods:**

### *Preparation of the InhA mutants:*

The mutations were introduced into InhA using Quikchange mutagenesis – G204A, G205A and G208A. The mutations were made in a stepwise manner, starting with G204A, followed by G204,205A InhA and finally G204,205,208A InhA

For replacing the InhA loop region with that of ecFabI, restriction sites for restriction enzyme NheI were engineered into the InhA loop by Quikchange mutagenesis. Primers corresponding to the ecFabI loop were designed with the same restriction sites at the two ends. The two loop primers were annealed by heating them at 95 °C and allowing them to slowly cool to room temperature. The annealed primers were then digested using NheI and ligated with the digested

vector using T4 DNA Ligase. However, we were unable to ligate the digested primers to the digested InhA vector, which we attribute to incomplete digestion of the InhA vector.

*Loop replacement experiments:*

NheI cut sites (G\*CTAGC) were engineered around the InhA loop region using Quikchange mutagenesis. The plasmid (pEt15) was then digested using NheI and the digestion was confirmed by running the digested samples on a 1.5% agarose gel. The complimentary *E. coli* loop fragments were annealed by heating them to 95 °C and cooling to room temperature. The double stranded loop fragment was digested using NheI and run on a 1.5% agarose gel. The digested vector and the digested *E. coli* loop fragments were extracted from the gel using the standard QIAquick purification kit (QIAGEN). The extracted DNA and the loop fragments were allowed to ligate with the digested *E. coli* loop primers in the presence of T4 DNA ligase. The plasmids were submitted for DNA sequencing but, the parent sequence (with the NheI cut sites) was obtained. It is clear from the gel that excision of the DNA is occurring. But since the ligation is not successful implies that probably only one of the restriction sites is cleaved by NheI and upon ligation the vector ligates back to give the parent sequence.

Alternatively, a one-step mutagenesis to mutate out the loop region in InhA and swap in the ecFabI loop was carried out. The primers encoding the



ecFabI loop were ordered and a single one step mutagenesis was carried out to replace the entire loop. The various primers obtained for carrying out the loop replacement are given in **Table 4.1**.

<b>Table 4.1: Quikchange primers for introducing mutations in InhA</b>	
Mutant	Primer
G204A InhA	Fwd : atg agt gcg atc gtc gcc ggt gcg ctc ggc gag
	Rev : ctc gcc gag cgc acc ggc gac gat cgc act cat
G204A, G205A	Fwd: atg agt gcg atc gtc gcc gct gcg ctc ggc gag gag
	Rev : ctc ctc gcc gag cgc agc ggc gac gat cgc act cat
G204A, G205A, G208A	Fwd : tcg ccg ctg cgc tcg ccg agg agg ccg gcg c
	Rev : gcg ccg gcc tcc tcg ggc agc gca gcg gcg a
C Terminal of the InhA loop (Nhe1)	Fwd : gct cgg cga gga ggc tag cgc cca gat cca gc
	Rev : gct gga tct ggg cgc tag cct cct cgc cga gc
N Terminal of the InhA loop (Nhe1)	Fwd : ccc tat ccg gac gct agc gat gag tgc gat c
	Rev : gat cgc act cat cgc tag cgt ccg gat agg g
ecFabI loop	Fwd : <b>gct agc act</b> ggc ggc ctc cgg tat <b>cgc tag c</b>
	Rev : <b>gct agc</b> gat acc gga ggc cgc cag <b>tgc tag c</b>
One step loop replacement	Fwd: cct atc cgg acg ctg gcg gcc tcc ggt atc ggc gcc cag atc Rev: gat ctg ggc gcc gat acc gga ggc cgc cag cgt ccg gat agg

**Table 4.1: The forward and the reverse primers for mutagenesis.**

*Purification of enzymes – InhA and mutants:*

The pET15b InhA vector was transformed into the *E. coli* BL21 DE3 pLysS competent cells. InhA and mutant over-expression was carried out by induction of cell expression with ~0.8 mM IPTG (isopropyl  $\beta$ -D thiogalactoside) around an  $A_{600}$  of 0.8 for 3 hrs at 25 °C. The cells were harvested by centrifugation at 4°C at 5000 rpm. The pellets were re-suspended in 30 mL binding buffer (0.5 M NaCl, 20 mM tris HCl and 5 mM imidazole, pH 7.9) and sonicated 5 times for 45 seconds, with a minimum time lag of 1 min between each round. The cell debris was pelleted down using a centrifuge (4 °C at 5000 rpm), and the supernatant was diluted by adding equal amounts of the binding buffer and filtered through a 0.45  $\mu$ m filter. The clear lysate was loaded onto a Ni-NTA His tag column which was washed with 40 mL Binding buffer and 20 mL wash buffer (60 mM imidazole, 0.5 mM NaCl, 20 mM tris-HCl, pH 7.9). The protein was eluted using a gradient mixer with binding buffer and elution buffer (1 M Imidazole, 0.5 mM NaCl, 20 mM tris-HCl, pH 7.9). The fractions containing the protein were transferred to a sephadex size exclusion column pre-equilibrated with the storage buffer (30 mM PIPES, 150 mM NaCl, 1 mM EDTA, pH 6.8). The resulting fractions were concentrated using 30 kDa MWCO centricon filters up to a concentration of about 300  $\mu$ M.

### *Synthesis of substrate:*

*Trans*-2-dodecenoyl-CoA (DDCoA) was synthesized from *trans*-2-dodecenoic acid using the mixed anhydride method as described previously (53, 186).

### *Enzyme kinetics:*

Kinetic parameters were determined at 25 °C in InhA storage buffer (30 mM PIPES, 150 mM NaCl, 1 mM EDTA, pH 6.8) as described previously (53).  $K_m$  and  $k_{cat}$  values were calculated by varying the concentration of DDCoA.

### *Inhibition of wild type and mutant InhA:*

Inhibition kinetic assays were performed as described previously (155) with *trans*-2-dodecenoyl CoA (DDCoA) and the wild type InhA and mutants. Reactions are initiated by the addition of the enzyme to solutions containing the inhibitor, substrate and 250  $\mu$ M NADH in the storage buffer.  $IC_{50}$  values were determined by varying the concentration of inhibitor. Further,  $IC_{50}$  assays were also carried out, with the PT04 inhibitor, as described in reference 3 in the presence of 1nm enzyme with substrate, 250  $\mu$ M NADH, 8% v/v glycerol and 0.1 mg/ml BSA. Data fitting was performed using Grafit 4.0 (Erithacus software Ltd.).

#### *Overexpression and purification of cyanophenylalanine incorporated InhA:*

Wild type InhA was cloned in a pBAD vector followed by replacing the codon for A201 with an amber codon (UAG) by Dr. Hao Lu. The modified InhA-pBAD was co-transformed with CyanoPhe-pDule in DH5 $\alpha$  *E.coli* cells. The protein was overexpressed and purified as described by R. Mehl *et al.* (187). F<sub>CN</sub>-InhA was purified in 100 mM NaH<sub>2</sub>PO<sub>4</sub>, 150 mM NaCl, pH 6.8 buffer and later exchanged into 100 mM NaH<sub>2</sub>PO<sub>4</sub> buffer with 150 mM NaF at pH 6.8.

#### *Fluorescence binding experiments with F<sub>CN</sub>-InhA:*

A PTI quanta master fluorimeter was used to perform emission scans of F<sub>CN</sub> in the absence and the presence of NAD, PT70 and PT04. The excitation wavelength was 240 nm with an excitation slit width of 4.0 nm and emission slit width of 8.0 nm. The final concentration of mutant InhA and NAD<sup>+</sup> were 1.8  $\mu$ M and 120  $\mu$ M respectively and that of the ligand (PT70/ PT04) was 10  $\mu$ M. An emission scan ranging from 250 – 400 nm was obtained at specific time intervals (5 minutes) and plotted using Origin.

#### *Over-expression and purification of <sup>15</sup>N/<sup>2</sup>H/<sup>13</sup>C labeled InhA:*

The wild type InhA gene was transformed to BL21(DE3) plysS cells and plated on M9 minimal media-agar plates (Glucose). A single colony was used to

inoculate 10 ml cultures in M9 (H<sub>2</sub>O) media. The cells were then acclimatized to an increasing concentration of D<sub>2</sub>O by successively inoculating 10 ml of M9 media in 10%, 25%, 50%, 75% and 99% D<sub>2</sub>O with 100µl of the preceding culture. Subsequently, the startup culture in 99% D<sub>2</sub>O was used to inoculate 1 liter M9-D<sub>2</sub>O media spiked with 8 ml appropriate 10x Bioexpress media. The cells were induced using 150 mg IPTG at an OD of ~1.0. Along with IPTG, 5 g glucose (<sup>12</sup>C/<sup>1</sup>H or <sup>13</sup>C/<sup>1</sup>H or <sup>13</sup>C/<sup>2</sup>H), 1 g <sup>15</sup>NH<sub>4</sub>Cl and 10 mg thiamine hydrochloride was also added to the cultures. The cells were harvested 24 hours post induction and the cell pellet stored at -20 °C. The 1 liter D<sub>2</sub>O culture, consisting of Na<sub>2</sub>HPO<sub>4</sub> (7.26 g), KH<sub>2</sub>PO<sub>4</sub> (3.0 g), NaCl (0.5 g), <sup>15</sup>NH<sub>4</sub>Cl (1.0 g), MgSO<sub>4</sub> (120.37 mg), vitamin B1 (10 mg), CaCl<sub>2</sub> (11.1 mg), glucose (<sup>12</sup>C/<sup>1</sup>H or <sup>13</sup>C/<sup>2</sup>H, 5 g), ampicillin (100 µg/ml) and chloramphenicol (30 µg/ml), was filtered using a 0.22 µm Millipore filter.

Subsequent to purification, the His<sub>6</sub> tag at the N terminus of InhA was cleaved using biotinylated thrombin at room temperature for 12 hours in 100 mM NaH<sub>2</sub>PO<sub>4</sub>, 150 mM NaCl, pH 7.0 buffer. The biotinylated thrombin was then removed by the addition of streptavidin beads and the flow through was subjected to size exclusion chromatography to exchange the protein into 30mM PIPES, 150mM NaCl, pH 6.8. The His<sub>6</sub> tag cleavage was confirmed by running a Western blot using an anti-His<sub>6</sub> antibody conjugated to alkaline phosphatase.

### *NMR spectroscopy:*

All NMR spectra were recorded on 900 MHz and 800 MHz spectrometers (Bruker, New York Structural Biology Centre) equipped with triple resonance cryoprobe heads. Unless specified, the spectra were acquire with total of 160 transients were recorded for 256 increments in  $t_1$  of the 2D [ $^{15}\text{N}/^1\text{H}$ ] TROSY-HSQC experiment and the temperature was maintained at 298 K. Subsequent experiments were done with a varying number of transients and different temperatures, the details of which have been mentioned in the results and discussion section of this chapter. The data were processed and visualized using the Bruker TOPSPIN 3.1 software.

2D-DOSY (Diffusion ordered spectroscopy) experiments were performed at 298 K on a 700 MHz Bruker Avance spectrometer at the Centre for Molecular Medicine at Stony Brook University. The values of  $\Delta$  and  $\delta$  were 99.9 msec and 7 msec respectively and the range of gradient strengths used was 0.674 – 32.03 G/cm. The experiments were performed in the presence of 0.05% dioxan for which the  $R_h$  is well known (188). The diffusion constant was calculated using **Equation 4.1** where  $\gamma$  is the gyromagnetic ratio of the nuclei being detected ( $^1\text{H}$ ),  $g$  is the gradient strength and  $\Delta$  and  $\delta$  are delays in the pulse sequence.

**Equation 4.1**      
$$I = k e^{-(\gamma g \delta)^2 D (\Delta - \frac{\delta}{3})}$$

TROSY based triple resonance experiments were conducted as described (189) and analyzed using the NMR pipe suite (190). The experimental details have been mentioned in the results section.

## Results and Discussion:

### *Kinetic studies of mutant InhA:*

$K_m$ ,  $k_{cat}$  studies of the triple Gly InhA mutant were carried out with a trans-2-dodecenoyl CoA substrate. The results are summarized in **Table 4.2**. The  $k_{cat} / K_m$  value of the mutant is similar to that of the wild type InhA which implies that the catalytic efficiency of the enzyme is not being affected by making the mutation. The ~5 fold reduction in  $K_m$  probably suggests a stronger substrate binding to triple Gly InhA as compared to wild type InhA. However, a similar reduction in  $k_{cat}$  suggests a perturbation in the rate limiting step after the substrate binding, which could be either the chemical step or product dissociation.

The loop-replacement mutant on the other hand had a higher  $K_m$  than the wild type InhA and a much lower  $k_{cat}$ . The higher  $K_m$  implies much weaker binding of the substrate to the enzyme. Also, the loss of turnover along with the ~ 18 fold decrease in the  $k_{cat} / K_m$  implies destabilization of the enzyme which was



expected as the mutation would result in a fairly drastic change in the enzyme structure.

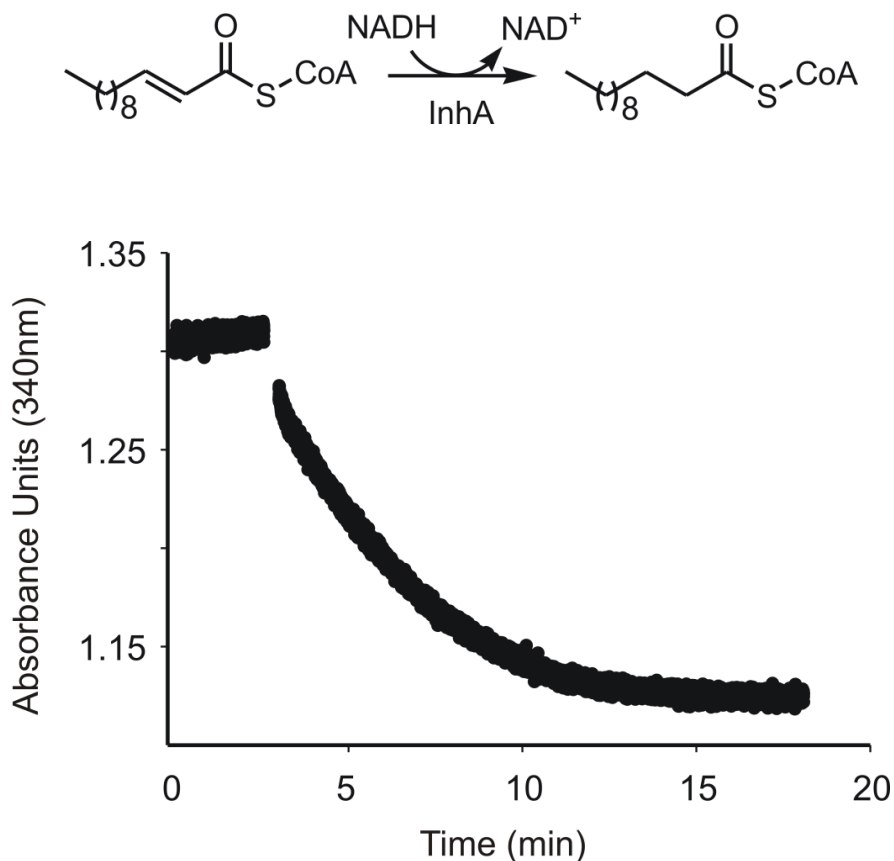


**Figure 4.6: The reaction catalyzed by InhA.** The reduction of the double bond is measured by monitoring a decrease in the NADH absorbance at 340 nm. The break in the curve represents the initiation of the reaction by the addition of the enzyme. The initial linear region of the curve was used to calculate the initial velocity for each concentration of the substrate and the initial velocities were fitted to a Michaelis-Menten equation to get the  $K_m$  and the  $k_{cat}$ .

<b>Table 4.2: Michaelis–Menten kinetic analysis of wild type InhA and mutants.</b>			
<b>Kinetic Parameters</b>	<b>Enzymes</b>		
	<b>Wild type InhA<sup>††</sup></b>	<b>Triple Gly InhA</b>	<b>Loop-replacement mutant</b>
<b><math>K_m</math> (<math>\mu\text{M}</math>)</b>	29	$6 \pm 2$	$43 \pm 5$
<b><math>k_{cat}</math> (<math>\text{min}^{-1}</math>)</b>	~250	$58 \pm 6$	$47 \pm 2$
<b><math>k_{cat}/K_m</math> (<math>\mu\text{M min}^{-1}</math>)</b>	8.4	$9.7 \pm 4$	$1.1 \pm 0.2$ ( $\sim 0.6$ ) <sup>‡</sup>

**Table 4.2: Kinetic parameters for wild type InhA and mutants.** <sup>††</sup>As reported by Sullivan et al (59) and reproduced as controls. <sup>‡</sup> Experimental repeat

We observe a 5 fold decrease in both the  $K_m$  and the  $k_{cat}$  implying that perhaps while the substrate binds more strongly to the enzyme, the catalytic efficiency isn't affected. The reduction in the  $k_{cat}$  suggests a perturbation of the rate limiting step following substrate binding. In case of the loop-replacement mutant, the drastic loss in activity was perplexing. We were cognizant of the fact that by replacing the longer InhA loop with a much shorted ecFabI loop we could have deleteriously affected the structural integrity of the enzyme. Therefore, we carried out UV Circular Dichroism measurements to see if the overall secondary

structure of the mutant was maintained in comparison to wild type InhA (**Figure 4.7**).

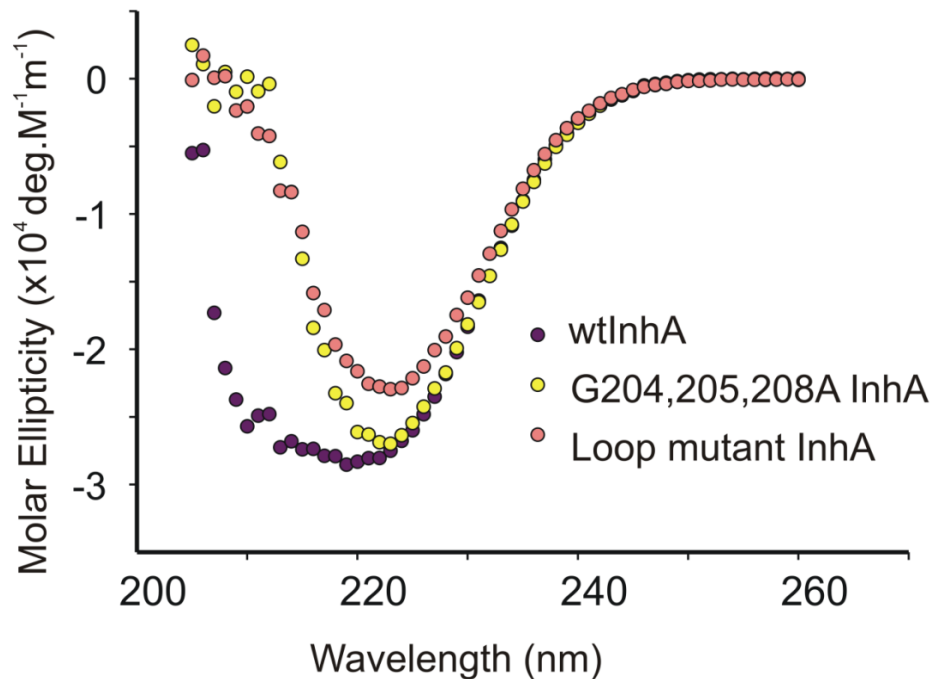


**Figure 4.7: UV-CD scans for wild type InhA and mutants.** The circular dichroism spectra were acquired on an Applied Photophysics Chirascan CD spectrometer. The proteins samples were in the 30 mM PIPES storage buffer (**Materials and Methods**). The final protein concentrations for far-UV CD experiments were 10  $\mu$ M. Spectra were recorded from 200 to 260 nm at 1 nm intervals in a quartz cuvette of 0.1 cm path length at 25°C. The signal was normalized with respect to the concentration of the protein.

In **Figure 4.7**, the CD spectra for the triple Gly mutant and wild type InhA look very similar especially around 220 nm. There are considerable differences at

lower wavelengths implying a slight difference in the secondary structure between the triple Gly mutant and the wild type enzyme. However, the loop-replacement mutant has a significantly smaller amount of secondary structure than wild type InhA which likely explains the sub-optimal kinetic parameters of the loop-replacement mutant.

*Inhibition studies with the InhA mutants:*

The inhibition assays were performed with inhibitors PT04 (**Figure 4.3B**) and triclosan and substrate *trans*-2-dodecenoylCoA. (59)

<b>Table 4.3 : IC<sub>50</sub> measurements for PT04 and triclosan with wild type InhA and mutants.</b>				
<b>Compound</b>	<b>IC<sub>50</sub> values (nM)</b>			
	<b>Wild type InhA<sup>a</sup></b>	<b>G204,205A InhA<sup>b</sup></b>	<b>G204,205,208A InhA</b>	<b>Loop- replacement mutant InhA<sup>c</sup></b>
<b>PT04</b>	11±1	19.8 ± 3	30.1 ± 9 <sup>b</sup> 36.4 ± 11 <sup>a</sup>	n.d
<b>Triclosan</b>	1000 ± 100	-	153.4 ± 37 <sup>b</sup>	n.d

**Table 4.3: IC<sub>50</sub> data for PT04 and triclosan for wild type InhA and mutants.**

The enzyme concentration was <sup>a</sup>1 nM or <sup>b</sup>~ 70 nM.

The IC<sub>50</sub> values for the inhibition of wild type and mutant InhA by triclosan and PT04 are given in **Table 4.3**. The Gly to Ala mutations in the loop do not have an effect on the inhibition of the enzyme by PT04. While triclosan shows a 6 fold improvement in inhibition of the triple Gly mutant than wild type InhA, it does not show slow onset kinetics as was tested by Dr. Nina Liu. This perhaps suggests that the flexibility imparted to the loop region by the glycine residues does not play a major role in the loop dynamics that cause the slow-off rates.

Unfortunately, the loop-replacement mutant lost activity upon addition of DMSO. Alternative conditions, with different solvents for dissolving the ligands and lower concentration of DMSO, were used such that the loop-replacement mutant remained active under all conditions. However, we observed a loss of activity of the mutant in all the cases. Hence, inhibition studies could not be carried out for the loop-replacement mutant.

*Fluorescence studies with F<sub>CN</sub>-InhA:*

The A201F<sub>CN</sub>InhA studies were initiated by Dr. Hao Lu. In his preliminary studies, he didn't observe any FRET between F<sub>CN</sub> and the protein Trp residues upon binding of the drug. However, this experiment was performed in the presence of 150 mM NaCl buffer. P. Marek *et al* (191) and H. Taşkent-Sezgin *et al* (171) have demonstrated that the F<sub>CN</sub> fluorescence is quenched drastically in the presence of chloride ions. Consequently, the A201F<sub>CN</sub>InhA was exchanged into a 100 mM NaH<sub>2</sub>PO<sub>4</sub> (pH 6.8) buffer, and the FRET experiments were repeated with the objective of observing a FRET signal between F<sub>CN</sub> and the intrinsic Trp fluorescence of the protein. The data were corrected for inner filter effect and dilution effects and are plotted in **Figure 4.10**.

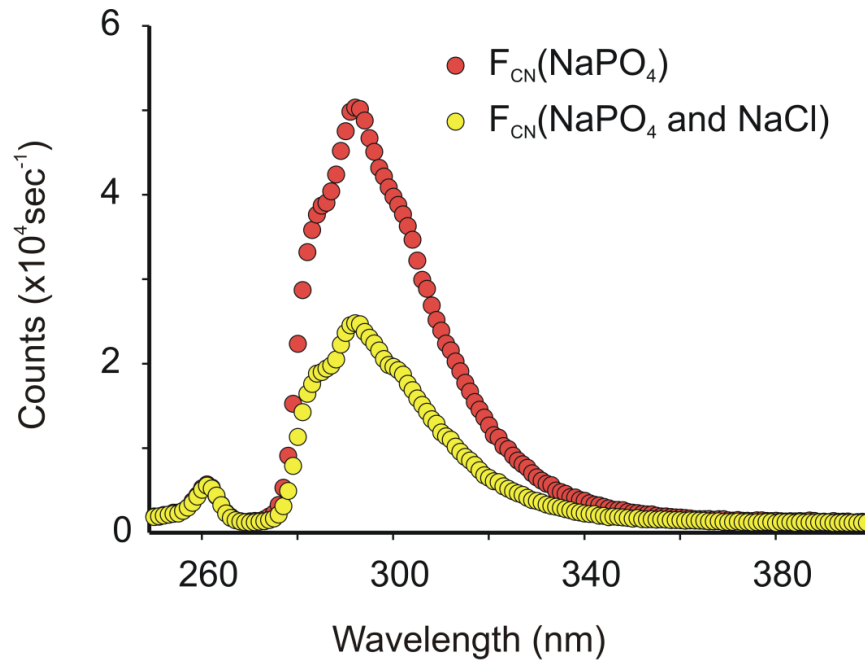


Figure 4.8: Quenching of F<sub>CN</sub> fluorescence by chloride ions.

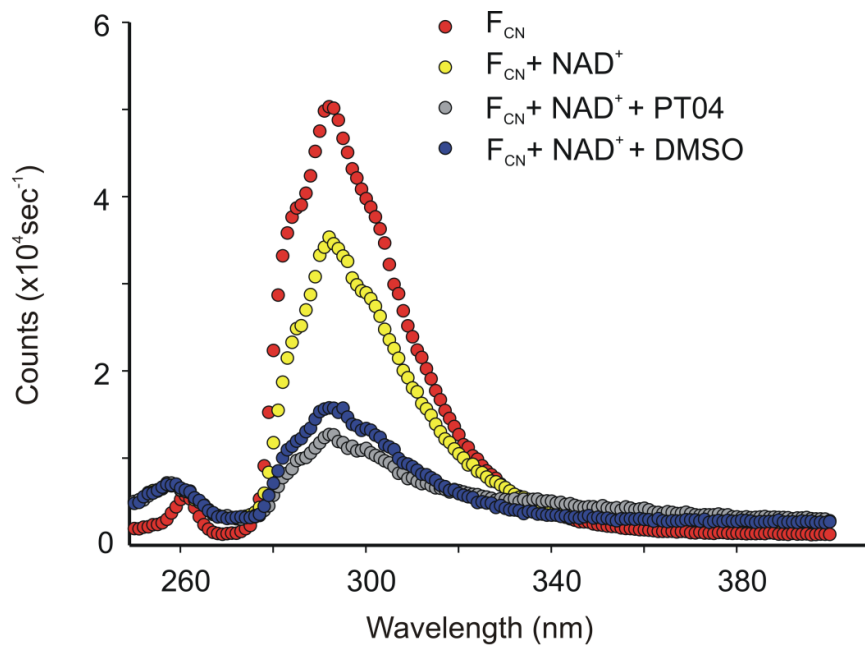
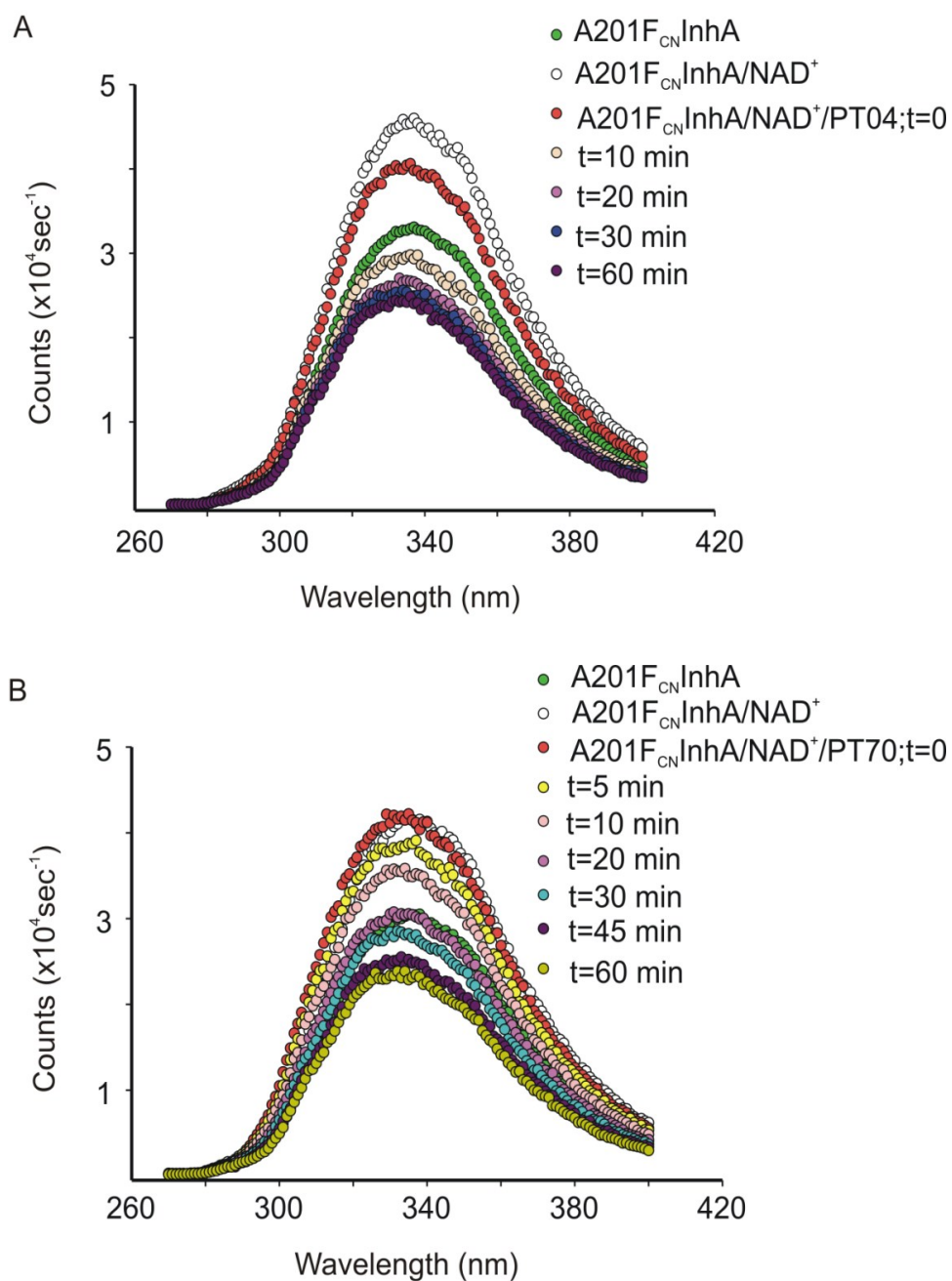


Figure 4.9: Quenching of F<sub>CN</sub> fluorescence by NAD<sup>+</sup> and DMSO.



**Figure 4.10: Emission scans of A201F<sub>CN</sub>InhA upon binding to inhibitors. A)** NAD<sup>+</sup>/PT04 and **B)** NAD<sup>+</sup>/PT70. The excitation was carried out at 240nm and the emission spectrum was scanned from 270nm to 400nm. The data were collected at 5 min intervals.



**Figure 4.8** and **4.9** show the quenching of  $F_{\text{CN}}$  fluorescence by chloride ions and  $\text{NAD}^+$  and DMSO respectively. Despite these efforts, similar results were obtained where a time dependent decrease in the Trp fluorescence was observed upon adding the inhibitor. However, a similar response was observed for both the inhibitors, PT70 (slow-off) and PT04 (rapid-off). InhA has four Trp residues in one monomer which results in a very large Trp emission at about 340 nm making it difficult to observe the weaker fluorescence signal of  $F_{\text{CN}}$  at 290 nm. In addition, we did not observe a reduction in the fluorescence at 340 nm and an increase in the  $F_{\text{CN}}$  emission at 290 nm suggesting a lack of a FRET between the  $F_{\text{CN}}$  and Trp residues.

#### *Protein dynamics – NMR and SAXS:*

The large size of InhA (120 kDa, tetramer), hinders dynamic studies using traditional NMR techniques. This challenge was overcome by perdeuterating the protein and using various transverse relaxation optimized spectroscopy (TROSY) methods that have dramatically increased the size of biomolecules that can be studied using NMR (177, 178). After optimizing the yields of the protein upon growing in labeled media, we performed an HSQC experiment with the apo and the holo ( $\text{NAD}^+$ ) protein. However, as shown in **Figure 4.11** (blue), we observe significant aggregation of resonances in the center of the spectra implying that either the protein is unfolded or that the resonances are exchange broadened. Since, the enzyme was confirmed to be active prior to doing the NMR, perhaps

the protein is flexible and can assume various conformations resulting in a lack of dispersion. Also, this would make it impossible to make comparisons between the bound and the unbound forms of the protein.

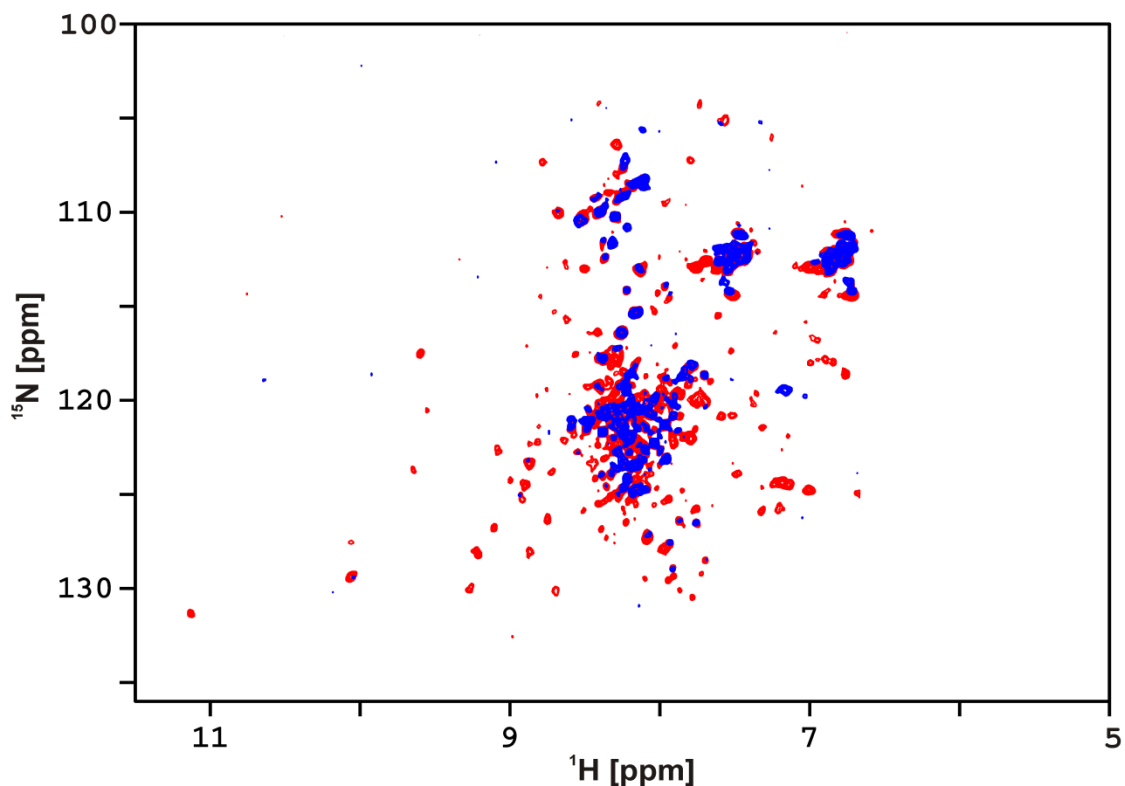


**Figure 4.11:**  $^{15}\text{N}/^1\text{H}$  HSQC of wild type InhA and inhibitor bound InhA.  $^{15}\text{N}/^1\text{H}$  HSQC (800 MHz, 25 °C) of U- $^{15}\text{N}/^2\text{H}$  wild type InhA (~0.4 mM) bound to  $\text{NAD}^+$  (~1.2 mM) (Blue) and  $^{15}\text{N}/^1\text{H}$  HSQC of U- $^{15}\text{N}/^2\text{H}$  wild type InhA (~0.4 mM) bound to PT70 (~0.5 mM) and  $\text{NAD}^+$  (~1.2 mM) (Red).

Interestingly, addition of saturating amounts of an inhibitor (PT70) resulted in much greater dispersion and what appeared to be predominantly a single conformer (**Figure 4.11; red**). This suggests that in presence of the ligand the

enzyme is trapped in a more restricted conformational space or that the enzyme has become smaller in size. We were able to identify approximately 220 cross peaks (of 290 amino acids) suggesting that we were perhaps looking at a single conformation.

Intrigued by the drastic increase in the dispersion we were curious if the protein undergoes a transition to a smaller oligomeric state. Subsequently, we set out to measure the radius of hydration ( $R_h$ ) using a  $^1\text{H}$  detect DOSY experiment which essentially is looking at the rate of translational diffusion. Using the slopes from the plots shown in **Figure 4.12**, we calculated a diffusion constant ( $D$ ) for the inhibited protein of  $7.8 \times 10^{-7} \text{ cm}^2/\text{sec}$  for the apo protein and  $11.09 \times 10^{-7} \text{ cm}^2/\text{sec}$ . These data suggest that InhA becomes more compact upon inhibitor binding.

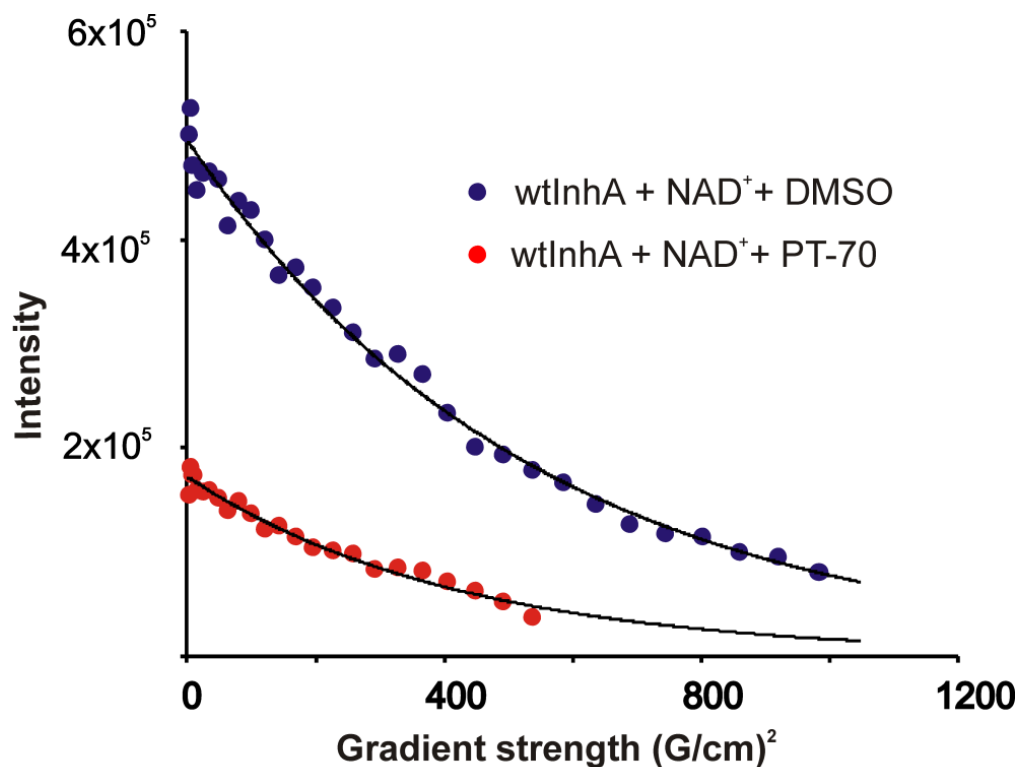


**Figure 4.12: Analysis of the <sup>1</sup>H detect DOSY spectra.** The peak intensity of the methyl region (~0.5 ppm) plotted as function of an increasing gradient strength. The diffusion experiments were performed at 25 °C on a 700 MHz magnet with 0.2 mM unlabeled wild type InhA, 0.4 mM PT70 and 1.2 mM NAD<sup>+</sup>. The same concentrations were used for the apo protein although DMSO was added instead of the inhibitor.

**Equation 4.2:** 
$$R_h^{protein} = \frac{D^{ref}}{D^{protein}} * R_h^{ref}$$

Using **Equation 4.2** (192) and a dioxan standard ( $R_h = 2.12 \text{ \AA}$  (193)) we calculated a  $R_h$  of  $42 \text{ \AA}$  for holo InhA and  $35 \text{ \AA}$  for the PT70 bound ternary complex implying a reduction in size of the protein upon inhibitor binding. Wilkins *et al* (193) reported an empirical relationship between the radius of hydration and the number of amino acids ( $N_o$ ) in a perfectly globular protein (**Equation 4.3**).

**Equation 4.3:** 
$$R_h = (4.75 \pm 1.11)N_o^{0.29 \pm 0.02}$$

Using this relationship, we calculated a ratio of 2:1 for the molecular weights (number of amino acids) for apo InhA and InhA bound to PT70. Since, InhA is believed to be a tetramer in solution (194), these data imply a tetramer to dimer transition upon binding of the inhibitor. Tonge *et al* (194) suggested a change in the shape of InhA upon inhibitor binding based on sedimentation velocity experiments but were unable to conclusively show a tetramer to dimer transition.

To corroborate our DOSY data, we used small angle X-ray scattering (SAXS) in collaboration with Bowu Luan and Prof. Daniel Raleigh. While SAXS experiments suggested a decrease in the radius of gyration ( $R_g$ ) by  $\sim 2 \text{ \AA}$ , we failed to see a change in the oligomeric state of the protein upon binding to the ligand (**Figure 4.13**). In **Figure 4.13A**, the scattering curves overlay well below a  $q$  value of  $0.2 \text{ \AA}^{-1}$  indicating that the protein size does not change drastically between the three samples. The Guinier analysis of these samples shows a

slight reduction in  $R_g$  by  $\sim 2 \text{ \AA}$  (**Table 4.4**). The differences in the region between  $0.2\text{-}0.4 \text{ \AA}^{-1}$  (region of medium resolution) can be used to monitor slight changes in the conformation upon binding of the inhibitors (195). The pair distance distribution function ( $P(r)$ ) describes the distance distribution of any given pair of electrons in the molecule. **Figure 4.13B** also shows a very slight reduction in the  $P(r)$  maxima suggesting that there is no tetramer-dimer equilibrium upon ligand binding.

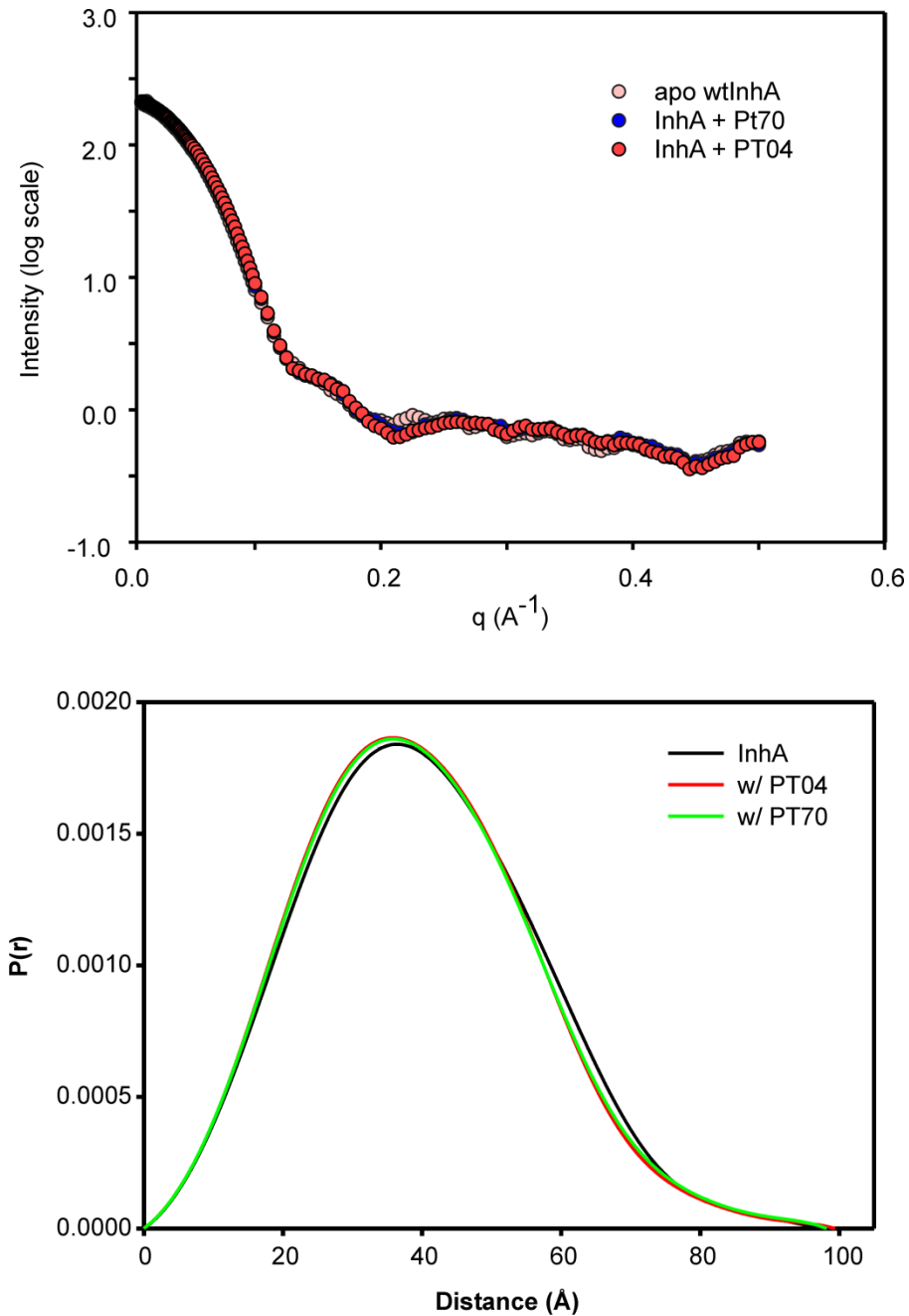


**Figure 4.13: SAXS data of wild type InhA and InhA bound to the inhibitors.**

**A)** Scattering curve (intensity versus scattering angle) for apo InhA and InhA bound to PT04 and PT70 **B)** The pair distribution function,  $P(r)$ , calculated from the scattering curve.

Analyzing the scattering data of InhA bound to the two ligands, as expected, SAXS as a technique lacks the resolution to discriminate local conformational changes though it does shed light on global changes in shape and size. Moreover, the fact that the scattering plots are not a perfect Gaussian suggests that the protein is not perfectly globular resulting in the molecular weights obtained from the empirical analysis (**Equation 4.3**) being biased and not appropriate for this system.

<b>Table 4.4: R<sub>g</sub> measurements</b>	
<b>Sample</b>	<b>R<sub>g</sub> (Å)</b>
<b>Apo InhA (NAD<sup>+</sup>,DMSO)</b>	31.9 ± 1.1
<b>InhA + NAD<sup>+</sup> + PT70</b>	29.5±1.6
<b>InhA + NAD<sup>+</sup> + PT04</b>	29.6±0.4

**Table 4.4: Radius of gyration calculated from the Guinier analysis.**

Having observed good dispersion in the <sup>15</sup>N/<sup>1</sup>HHSQC spectra, we were interested in seeing if we could observe subtle differential changes in the NMR spectra of wild type InhA bound to a slow-off inhibitor versus a rapid-reversible inhibitor such as triclosan or PT04. <sup>15</sup>N/<sup>1</sup>H TROSY-HSQC experiments were conducted in the presence of these two inhibitors (PT70 and PT04) and the representative data are shown in **Figure 4.14**.



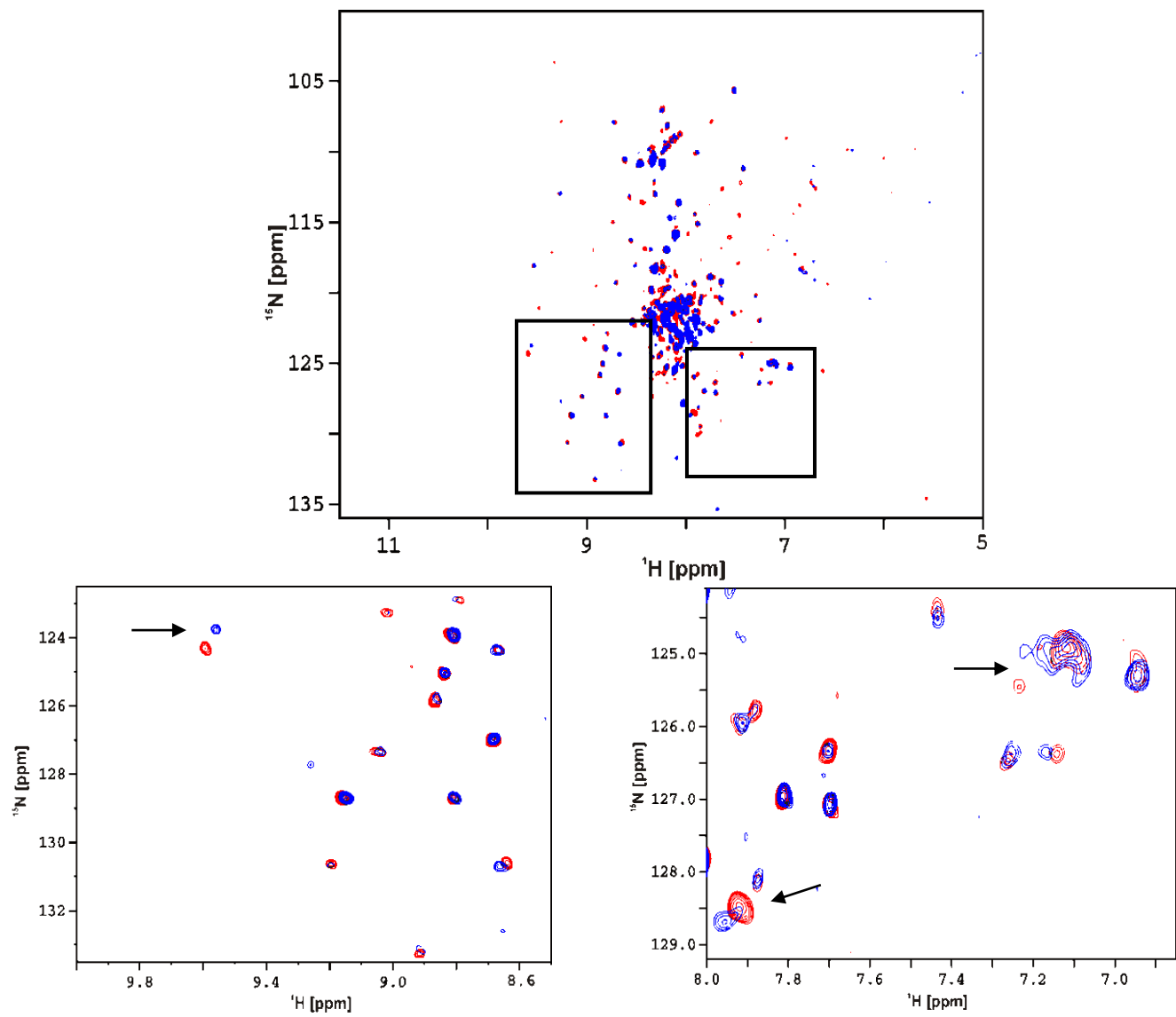


**Figure 4.14: Overlay of the  $^{15}\text{N}/^1\text{H}$  TROSY HSQC spectra.** Overlay of the  $^{15}\text{N}/^1\text{H}$  TROSY HSQC (800 MHz, 25 °C) spectra of wild type InhA bound to  $\text{NAD}^+$ / PT70 (blue) with  $\text{NAD}^+$ /PT04 (red). The arrows depict changes in the backbone amide chemical shifts upon binding to a slow-off (PT70) versus a rapid-off (PT04) inhibitor.

Having established that we can observe differences in the TROSY-HSQC spectra for the two classes of inhibitors, we set out to optimize conditions in order to obtain spectra that would be more conducive to performing assignments of the backbone amides. One of the main problems we faced was the overlap of resonances in the middle of the spectrum.

Therefore, we decided to vary the temperature and acquire the TROSY-HSQC in an attempt to reduce the aggregation of resonances. NMR spectra were acquired as a function of temperatures varying from 25 °C to 40 °C in increments of 5 °C. We were able to observe improvement in the dispersion of the resonances and a reduction in the clustering as a function of the temperature with the best spectra at 40 °C (**Figure 4.15**). The spectra were acquired with 80 transients per increment with 2048 complex points in the direct dimension and 256 real points in  $^{15}\text{N}$ . While raising the temperature to 40 °C and reducing the protein concentration to ~0.2 mM gave us a well dispersed set of peaks, the protein was not stable at such a high temperature and precipitated out by the end of the experiment.

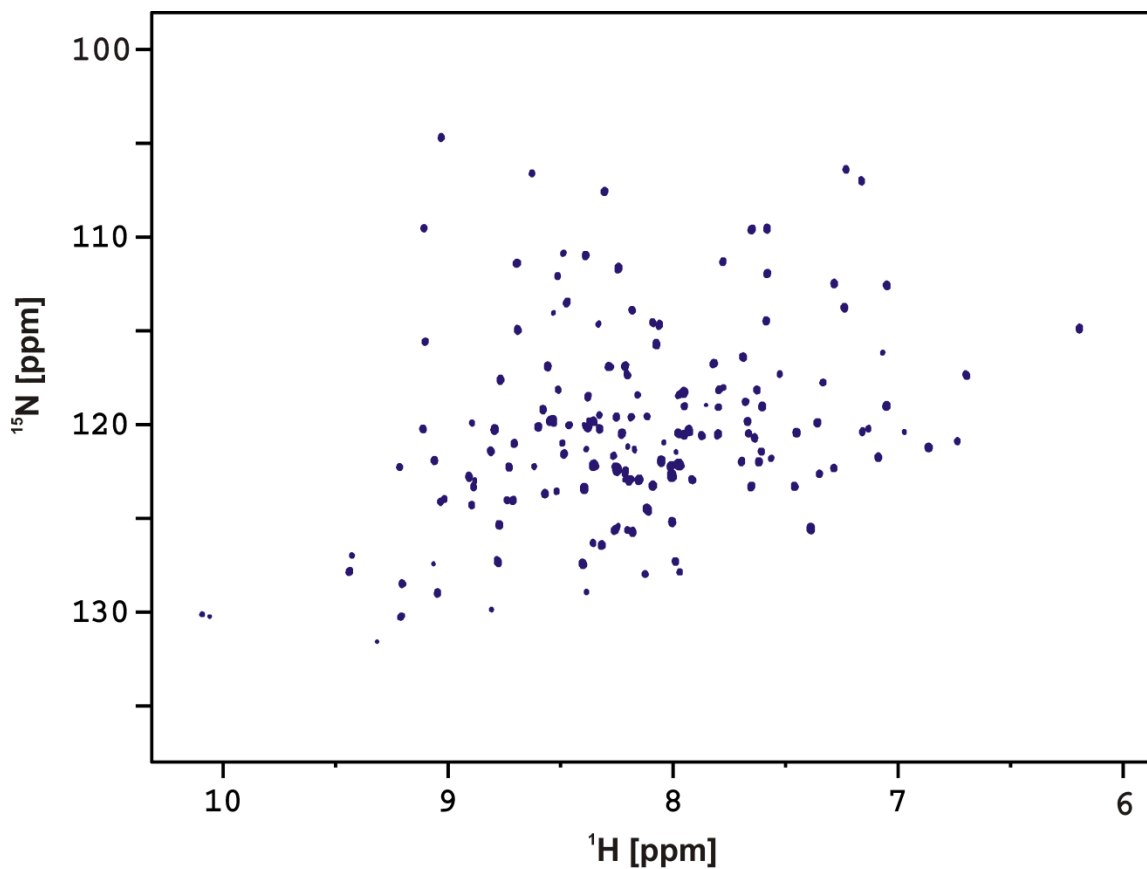


**Figure 4.15:**  $^{15}\text{N}/^1\text{H}$  TROSY-HSQC of InhA bound to PT70 at 40 °C.  $^{15}\text{N}/^1\text{H}$  TROSY-HSQC of  $^{15}\text{N}/^2\text{H}$  labeled wild type InhA (0.2 mM, 30 mM PIPES, 150 mM NaCl, pH 6.8, 700 MHz, 40 °C) in the presence of 0.4 mM PT70 and 1.2 mM  $\text{NAD}^+$ .

To get an idea of the sensitivity, we performed a trHNCO experiment with 16 transients in the direct dimension per  $(t_1, t_2)$  increment. The data was acquired with 64 real ( $^{15}\text{N}$ ), 60 real ( $^{13}\text{C}$ ) and 1024 complex ( $^1\text{H}$ ) points. However, the experiment did not yield a good spectrum (50 cross peaks; 17 % coverage) with

the mobile regions giving very strong resonances that make it difficult to observe the signal from the less mobile regions of the protein.

Therefore, we decided to cleave the His<sub>6</sub> tag from the N terminus of the protein which we know to be mobile from our X-ray studies. Cleaving the flexible tag led to a well dispersed spectrum at lower temperatures such as 30 °C where the protein is much more stable (**Figure 4.16**) and allowed data collection with just 8 transients per <sup>15</sup>N increment.

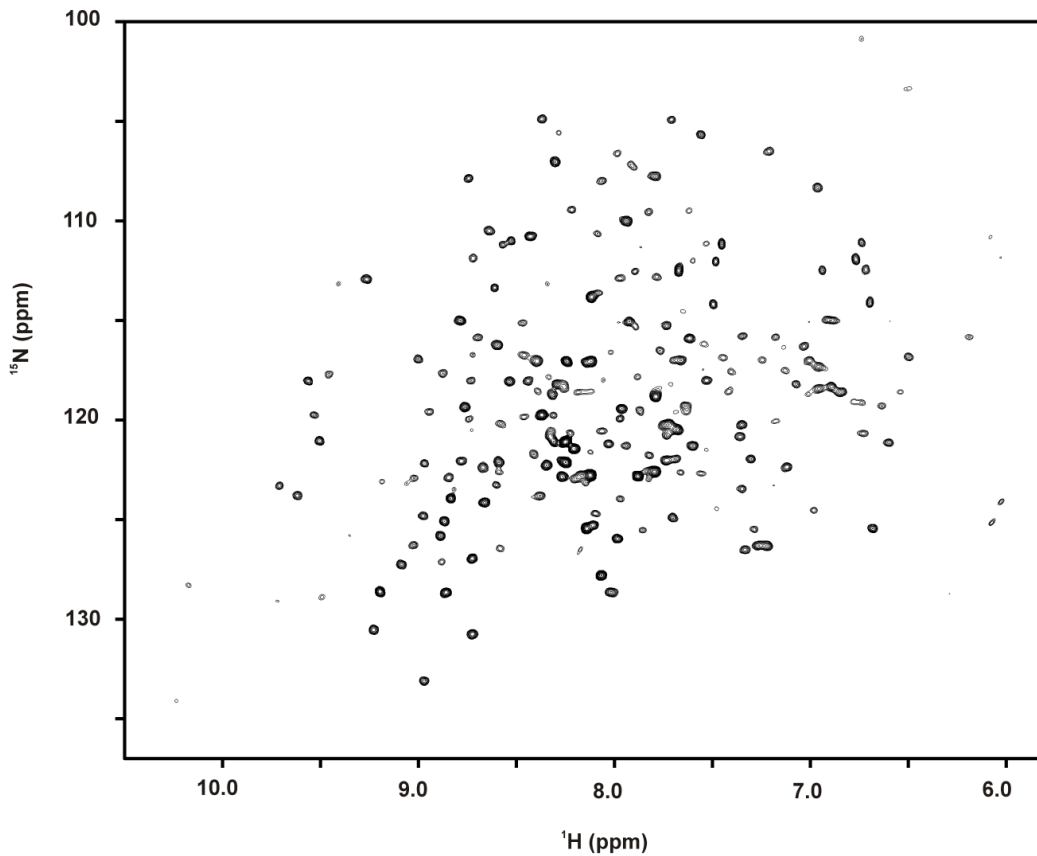


**Figure 4.16:** <sup>15</sup>N/<sup>1</sup>H TROSY-HSQC spectrum of (-) His<sub>6</sub> InhA bound to PT70.

<sup>15</sup>N/<sup>1</sup>H TROSY-HSQC of <sup>15</sup>N/<sup>2</sup>H labeled wild type InhA without the His<sub>6</sub> tag (0.15

mM, 30 mM PIPES, 150 mM NaCl, pH 6.8, 900 MHz, 30 °C) in the presence of 0.4 mM PT70 and 1.2 mM NAD<sup>+</sup>.

Presently, we are working towards acquiring the HNCO, HNCA and HNcoCA spectra to assign the backbone amides in the TROSY-HSQC. In order to improve the lack of sensitivity in these multidimensional experiments due to the low concentrations of the protein, we have used 33% non-uniform sampling (196). Sampling the signal at nonuniform intervals in the indirect dimensions, allows data to be collected at long evolution times (affording high resolution) without sampling at Nyquist intervals resulting in shorter acquisition times. The complete frequency domain spectrum is then constructed using non-Fourier methods of analysis. We have been successful in obtaining HNCO and HNCA data with the (-)His<sub>6</sub> InhA bound to PT70 and are in process of acquiring the HNcoCA spectra.

### **Conclusions:**

While this project is still in progress, we have been able to set up the system and optimize conditions to allow acquisition of multidimensional NMR spectra. InhA is a 120 kDa protein and hence not amenable to traditional NMR methods. The problem of fast relaxation of magnetization was overcome by perdeuterating the protein and using transverse relaxation optimized spectroscopy (TROSY) based techniques. Using diffusion measurements and

small angle X-ray scattering (SAXS) we were able to conclude that while InhA undergoes compaction upon binding to diphenyl ether inhibitors, it retains its tetrameric state. There has been considerable speculation about the oligomeric state of InhA upon binding its inhibitors (INH-NAD adduct), in attempts to understand their mode of action (194).

Moreover, we have also been able to optimize our system to allow quick acquisition of  $^{15}\text{N}/^1\text{H}$  TROSY-HSQC spectra. However, the lack of sensitivity in the 3D experiments is quite disheartening. While use of NUS greatly helps reduce acquisition time and increase S/N, it might be worthwhile to look at constructs where either InhA is monomeric or where the flexible regions (other than the His<sub>6</sub> tag) have been mutated out. Other ways of overcoming the problem of sensitivity is to use selective labeling methods, where the methyl groups of Ileu, Leu, Val (ILV labeling) or Ala are  $^{13}\text{C}$  labeled. Methyl TROSY experiments provide sensitivity enhancement due to cancellation of intra-methyl  $^1\text{H}-^1\text{H}$  and  $^1\text{H}-^{13}\text{C}$  dipole-dipole relaxation mechanisms (185, 197).

# Chapter 5

*Target quantitation and turnover*



## **Introduction:**

### *Attrition in the drug discovery pipeline:*

Drug development relies heavily on understanding the mechanism of action of enzyme inhibitors. The drug discovery pipeline faces various bottlenecks including not just target and hit identification but also lead optimization and the size of the medicinal chemistry effort that can be mounted (16, 198). However, a major source of attrition during the development of new drugs comes from a severe disconnect between *in vitro* performance and *in vivo* efficacy.

Traditionally, early phases of drug discovery have focused on optimizing target affinity and selectivity of lead candidates. However, it is important to consider the difference between drug behavior in a closed *in vitro* system and an open *in vivo* system. Typically *in vitro* measurements are performed in closed-systems where the target, substrate and the drug are in equilibrium. Whole cell assays including MIC (minimum inhibitory concentration) measurements can be considered closed systems as the activity is measured at fixed concentrations of the drug. *In vivo* systems on the other hand, can have not only fluctuating drug

concentrations but also varying amounts of the substrate or the target under native conditions or upon drug administration (17, 132). Therefore, if the drug and the target are not in equilibrium, thermodynamic equilibrium constants will be poor predictors of *in vivo* activity. In fact several reviews (17, 131, 132) suggest that factoring in the lifetime of the drug-target complex, or the residence time of the drug on its target, can improve the prediction of *in vivo* drug efficacy.

*Drug-target lifetime and pharmacology:*

Previous work in the field of drug design has very elegantly demonstrated the interplay of the pharmacokinetics of a drug and the lifetime of the drug-target complex in determining *in vivo* efficacy (17, 131, 132, 199). If we consider a case where the drug concentration reaches maximum systemic exposure in a short while after being administered after which the drug level diminishes as the drug is distributed to the tissues, metabolized and eliminated from the body. Over this time course the fractional occupancy of the drug target will be the main factor in determining the efficacy (17, 200). The key factors in determining target occupancy are the cellular concentrations of the target and drug, and the lifetime of the drug-target complex. Previously, Tober, C. *et al* have demonstrated a correlation between the half-life of the drug-target complex (residence time) and delayed onset of cell growth upon compound wash-out (*in vitro*) as indicative of *in vivo* efficacy (201, 202). However, the effects of the target residence time may be undermined by protein turnover typically observed in rapidly growing bacteria

(132). Ideally, if the drug has a long residence time on a target that has a slow turnover, the pharmacological efficacy can be sustained even at dwindling systemic concentrations of the drug due to significant target occupancy.

*Post antibiotic effect – target turnover:*

A delayed regrowth of the surviving bacteria after a limited exposure to the antibiotic, the post-antibiotic effect (PAE), is considered to be an important aspect of pharmacodynamics (203). The PAE phenomenon has several potential mechanisms including recovery after reversible damage to cell structures, persistence of the drug in cell or the target (residence times) and/or the need to synthesize new enzyme before growth (203). PAEs can be caused by any one of these factors, but it is likely that the observed delay in regrowth can be multifactorial. For instance, aminoglycosides interfere with protein synthesis by binding to the ribosomal subunits. Hence, the PAE observed in this case could be because of the time required to re-synthesize the ribosome or for the drug to dissociate and diffuse out of the cell (204, 205). On the other hand, while macrolides have a similar mode of action as aminoglycosides, the PAE from this class of antibiotics is believed to be representative of the time taken for the re-synthesis of the target rather than the dissociation of the drug-target complex (201, 203, 206).

In conclusion, the absolute target levels and the turnover rate of the drug target can have dramatic effects on the observed pharmacological effects of the

slow-binding inhibitor as these factors impact the level of target engagement. Also, the drug concentration inside the cellular compartment is an important factor that remains poorly predicted in current literature. This study focuses on the use of a mass spectrometry based method to determine the absolute levels of the target inside a cell, their rates of turnover and the effects of drugs upon these parameters.

*Mass spectrometry – target quantitation and turnover:*

Mass spectrometry has been extensively used in proteomics for identification of proteins and their post translation modifications, facilitating the identification of proteins associated with many cell states and protein complexes (207). While identifying proteins and their modifications has helped us understand cellular processes and function, the traditional methods used lack quantitative information. Hence, there has been a shift in focus from qualitative studies to quantitatively analyzing the amount of protein and modified protein expression levels in a cell (208). In the past 2-dimensional electrophoresis has been commonly used to compare two cellular states. However, this technique is useful only for proteins that are abundant in whole cell lysates and fails to provide quantitative information on proteins that are present in low stoichiometric abundance.

While more recent techniques such as metabolic labeling (SILAC) and post-harvest labeling (ICAT/iTRAQ) have high sensitivity and are very useful for quantitative studies, they have limitations such as lack of high throughput and a requirement of enrichment (207). SILAC metabolic labeling (stable isotope labeling in culture) is performed by comparing two protein samples in which one is labeled with heavy isotopes (one or more amino acids). This could be achieved by growing cells in the presence of a labeled anabolite (209) or a labeled amino acid. However, this technique can have limited applicability in analyzing whole tissue samples. ICAT (isotope codes affinity tag) targets cysteine containing peptides by reagents containing reactive sulfhydryl groups. However, this technique completely ignores cysteine free proteins. Other methods, such as the use of serine protease-catalyzed attack of  $^{18}\text{O}$  water in the digestion step have been shown to be useful for quantitative proteomics (210, 211). The choice of the labeling technique used obviously varies from one case to the other. For instance, universal  $^{15}\text{N}$ -labeling requires an *a priori* knowledge of the peptide sequence as both the backbone and the side chain nitrogens are labeled adding an additional layer of complexity to the data analysis.

In a seminal paper by Barr *et al* (212), the authors measured the amount of apo-lipoprotein A1 by comparing native peptides generated by proteolysis to deuterium labeled peptides using LC-MS. A similar technique was used by Lindall *et al* (213) to quantify the amount of rhodopsin in trypsinized membrane preparations using a directed LC-MS/MS experiment. Subsequently, Gerber *et al*

(208) have taken this technique a step forward by quantifying the amount of phosphorylated protein in whole cell lysate separated by SDS PAGE. The strategy, termed AQUA or absolute quantitation, uses synthetic peptides containing stable isotopes as a standard for absolute quantitation for native peptides generated by proteolysis. As a proof of principle, we have used this technique to quantify the concentration and the turnover of three targets from the fatty acid biosynthesis pathway in *E. coli* (**Chapter 1**) and examined the effect of drug treatment on these parameters.

## **Materials and Methods:**

### *Materials:*

*E. coli* cell lines BL21(DE3) pLysS was obtained from Invitrogen and *E. coli* MG1655 was a gift from Krithika Venkataraman (Prof. Wali Karzai, Stony Brook University). Cell growth media (LB and M9) and chemicals were obtained from commercial vendors.  $^{15}\text{NH}_4\text{Cl}$  was from Cambridge Isotopes Ltd. Trypsin gold was obtained from Promega Inc. and the peptides ( $^{13}\text{C}$  and  $^{15}\text{N}$  labeled C terminal amino acid, AQUA ultimate) from Thermo Fisher Inc.

<b>Table 5.1: Peptides used for quantitation and turnover.</b>	
ecFabI	Peptide 1: FDGFVHSIGFAPGDQLDGDYVNAV[*R] Peptide 2: VNAISAGPI[*R]
ecFabB	VGLIAGSGGGSP [*R]
ecFabF	TIFGEAAS [*R]

**Table 5.1: Peptides from FASII enzymes used as M.S standards.** The C terminal Arginine is  $^{13}\text{C}$  and  $^{15}\text{N}$  labeled resulting in 10 Da shift in molecular weight of the parent peptide as compared to native peptide.

*Sample preparation:*

The cells were grown to log phase ( $\text{O.D}_{600} = 0.8$ ) and lysed in 10 mls of 100 mM  $\text{NH}_4\text{HCO}_3$  (1 mM PMSF) and the cell debris was pelleted by centrifuging at 13,000 rpm for 20 min. The total protein concentration in the cell lysate was measured using a Bradford assay. The cell lysate was diluted to ~0.5 mg/ml and

200  $\mu\text{l}$  of this solution ( $\sim 100 \mu\text{g}$ ) was used for precipitation using methanol, chloroform, water. Briefly, four volumes of methanol were added to the diluted cell lysate. This was followed by the addition of one volume of chloroform followed by the addition of 3 volumes of doubly deionized water. The mixture was vortexed at each stage and centrifuged at the end for 2 min. The aqueous layer was removed followed by the addition of four volumes of methanol. The solution was then centrifuged and the protein pellet was dried under nitrogen. Subsequently, the pellet was re-suspended in 8 M urea followed by dilution to 0.8 M urea using 100 mM  $\text{NH}_4\text{HCO}_3$ . Trypsin digestion was performed overnight using 4  $\mu\text{g}$  of Trypsin (gold). Subsequently, the reaction was quenched with 1% acetic acid and the samples were concentrated using a speedvac.

*Cell cultures and growth conditions:*

**Quantitation experiments:** BL21(DE3)pLysS cells were grown to log phase ( $\text{O.D}_{600}$  0.8) in LB media at 37 °C by shaking at 250 rpm. The cells were pelleted and processed as described above. For experiments of target quantitation in the presence of drug, the cells were diluted 1:200 in fresh LB media and grown to mid log phase ( $\text{O.D}_{600}$  0.6). The inhibitors were administered at 2X MIC (MIC for triclosan is 0.25  $\mu\text{g}/\text{ml}$  (214), thiolactomycin is 100  $\mu\text{g}/\text{ml}$  (215)) and samples were taken at 2 and 6 hrs post treatment. The cells were re-suspended in 10 mls of 100 mM  $\text{NH}_4\text{HCO}_3$  and processed as described previously. The proteolyzed samples were quantitated by LC MS/MS at the Stony



Brook proteomics facility. For each sample, cell counting was performed using serial dilutions in PBS. Measurement of bacterial cell volumes under different conditions was carried out with a Multisizer 3 Coulter counter fitted with a 100- $\mu$ m aperture tube. The measurement was made in the range of 2 through 100 femtoliters (216).

**Turnover experiments:** A single colony of *E. coli* K-12 MG1655 cells was used to inoculate a 10 ml LB start-up culture. The culture was incubated at 37 °C with constant shaking at 250 rpm. Subsequently, 10 mls of M9 media (unlabeled M9 salts, 0.5% glucose, MEM vitamins, vitamin B1, MgSO<sub>4</sub> and CaCl<sub>2</sub>) were inoculated with 100  $\mu$ l of the startup culture. This 10 ml culture of M9-acclimatized *E. coli* was transferred to a 1liter culture of unlabeled M9 media (<sup>14</sup>NH<sub>4</sub>Cl). The culture was grown to OD<sub>600</sub> of ~ 0.2 and the cells were harvested. Subsequently, the cells were washed twice with Hank's balanced salt solution and the cells were then suspended in 1 L of labeled M9 media (<sup>15</sup>NH<sub>4</sub>Cl). As part of the chase, 100 ml aliquots of the culture were taken every 20 min and pelleted. Serial dilutions in PBS were performed to measure the cell count of the different samples and the OD<sub>600</sub> was also measured to ensure that the log phase of growth was being monitored.

The cells in each of the aliquots were pelleted and re-suspended in 10 ml of 100 mM NH<sub>4</sub>HCO<sub>3</sub>. The re-suspended cells were lysed by sonication using a sonic dismembrator (Fisher scientific, model 100). The cell debris was pelleted

and a Bradford analysis was performed with the supernatant to measure the total protein concentration. The lysate was diluted to 0.5 mg/ml and 200  $\mu$ l (100  $\mu$ g) of this sample was used for processing. The samples were processed as described previously and quantitated by LC MS/MS.

*Mass spectrometry:*

**MudPIT:** The samples were analyzed using a modification of the multidimensional protein identification technology method (217). Samples were pressure bomb loaded onto a column which was packed with 3 cm of strong cation exchange (Partisphere SCX, 5  $\mu$ m) matrix (Whatman) and 3 cm C18 matrix (Magic, Michrom Bioresources, 5  $\mu$ m). Following sample loading, the column was washed for 10 min with Buffer A (2% acetonitrile (ACN), 0.1% formic acid) at ~200-300 nL/min. The MudPIT column was connected to a C18 separation column (100  $\mu$ m) which was pulled using a P-2000 CO<sub>2</sub> laser puller (Sutter Instruments, Novato, CA) to a 5  $\mu$ m i.d. tip and packed with 10 cm of 5  $\mu$ m Magic C18 material (Agilent, Santa Clara, CA) using a pressure bomb and subsequently equilibrated in buffer A. The dual column construct was placed in line with a Thermo Surveyor MS pump. The HPLC pump flow was manually split so the flow at the end of the column was 500 nL/min. The HPLC separation was provided by a 13 step, three component gradient. Each step consisted of the following, in sequence: 5 min wash with 100 % Buffer A; 5 min wash with a fixed percentage of Buffer C (0.5 M CH<sub>3</sub>COONH<sub>4</sub>, in Buffer A); 10min wash with 100%

Buffer A; 60 min gradient of 0% to 40% Buffer B (90% ACN, 0.1% FA); 30 min wash, 100 % Buffer A. The 13 steps varied the fixed Buffer C from 0 to 100 %. The application of a 1.8 kV distal voltage electrosprayed the eluted peptides directly into a Thermo Fisher Scientific LTQ XL ion trap mass spectrometer equipped with a nanoLC electrospray ionization source. Full masses (MS/MS) spectra were recorded on the peptides over a 400-2000 m/z range, followed by five tandem mass (MS/MS) events sequentially generated in a data-dependent manner on the first, second, third, fourth and fifth most intense ions selected from the full MS spectrum (at 35% collision energy). Mass spectrometer scan functions and HPLC solvent gradients were controlled by the Xcalibur data system (ThermoFinnigan, San Jose, CA). MS/MS spectra were extracted from the RAW file with Readw.exe (<http://sourceforge.net/projects/sashimi>). The resulting mzXML file contains all the data for all MS/MS spectra and can be read by the subsequent analysis software. The MS/MS data were analyzed with Inspect (Tanner et al., 2005) against an *E. coli* database with trypsin restrictions and optional modifications: +15.9994 on Met and +57.0214 on Cys. Only peptides with at least a p-value of 0.01 were analyzed further.

**1D (TSQ)** : Samples were adjusted to 120  $\mu$ l with water and separated on a Dionex Ultimate 3000 (Sunnyvale, CA) HPLC system. Samples were spiked with 1 pmole of the isotopic peptides and 12  $\mu$ l was injected onto a Luna C<sub>18</sub> column (50 x 2 mm) from Phenomenex (Torrence, CA). A linear gradient using buffer A, 2 % acetonitrile (ACN) and 0.1 % formic acid (FA) and buffer B, 80 %

ACN and 0.1 % FA was used. The gradient started with 2 % B and increased to 30% B in 20 min, then increased to 80% B for 5 min. The column was equilibrated with initial conditions for 10 min at a flow rate of 200  $\mu$ l/min and then the HPLC was coupled to the ESI source of a Thermo-Fisher TSQ Quantum Access triple quadrupole mass spectrometer (San Jose, CA). The mass spectrometer was operated in the positive ion mode with the high voltage set to 4.0 kV, sheath gas pressure at 40 (arbitrary units), capillary temperature of 350 °C. The collision cell was operated at 1.5 mTorr Argon and the collision energy was set to 20 volts. Transitions for each peptide were monitored at a 100 ms dwell time during the course of the experiment. Quantitative analysis was performed in the multiple-reaction monitoring mode, and the transitions monitored were  $m/z$  569.5>684.3 for FabB,  $m/z$  481.4>747.5 for FabF and  $m/z$  504.4>610.4 (**Figure 5.1**).

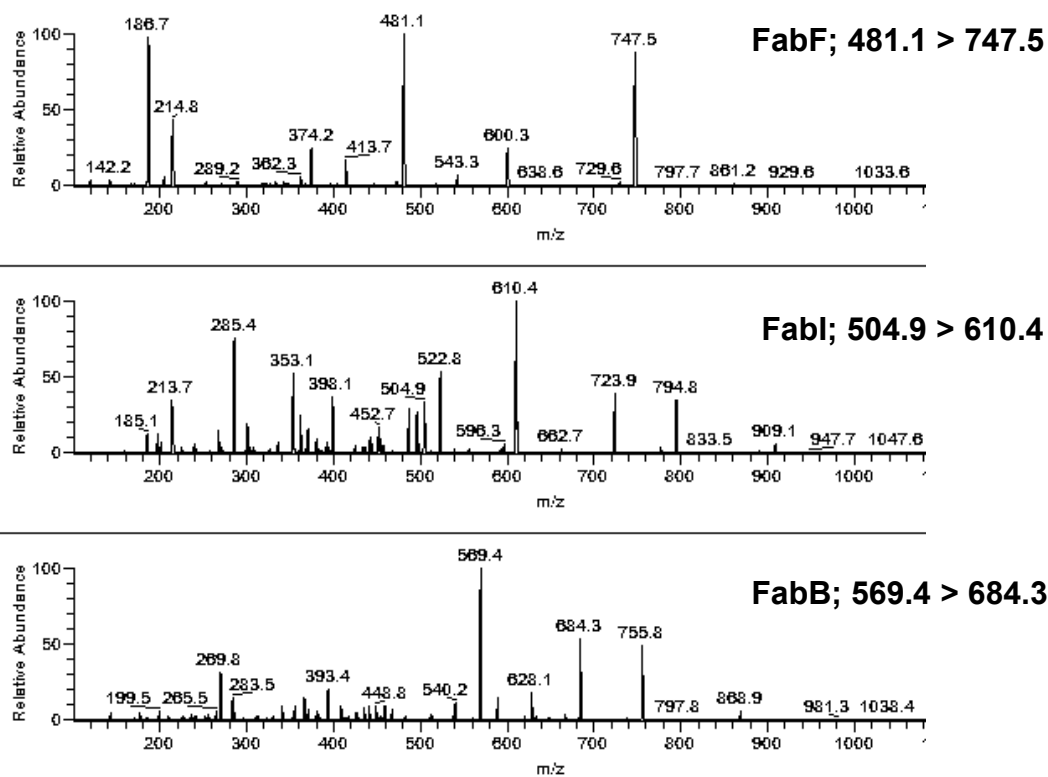


**Figure 5.1: MRM transitions for *ecFabX*.** Transitions monitored in the multiple-reaction monitoring (MRM) mode transitions for the FabX quantitation.

*Turnover experiments:*

The setup for the turnover experiments was the same as previously described for quantitation experiments with the following modifications. Samples were spiked with 1 pmole of the isotopic peptides and 10  $\mu$ l was injected onto a Luna C<sub>18</sub> column (50 x 2 mm). A linear gradient using buffer A, 2 % ACN and 0.1

% FA and buffer B, 98 % ACN and 0.1 % FA was used. The MRM transitions monitors for the various peptides (<sup>14</sup>N, internal standard and <sup>15</sup>N) are shown in **Table 5.2**. Curve fitting and regression was performed using Origin 8.6 and Sigma Plot 10.0. The plots were made using Corel Draw 12.

<b>Table 5.2: MRM details for the turnover experiments.</b>				
<b>Peptide</b>	<b>Calculated parent m/z</b>	<b>Observed parent m/z</b>	<b>Calculated fragment m/z</b>	<b>Observed fragment m/z</b>
FabB	564.3123	564.5	674.3	674.3
FabB(IS)	569.3164	569.5	684.3	684.3
FabB(N <sup>15</sup> )	572.2886	<b>572.5</b>	685.3	<b>685.3</b>
FabI	499.2934	499.4	600.3	600.4
FabI (IS)	504.2975	504.4	610.4	610.4
FabI (N <sup>15</sup> )	506.2726	<b>506.4</b>	609.3	<b>609.4</b>
FabF	476.2486	476.4	737.3	737.3
FabF (IS)	481.2528	481.4	747.4	747.5
FabF (N <sup>15</sup> )	482.2308	<b>482.4</b>	747.3	<b>747.5</b>

## **Table 5.2: Details of the MRM analysis for the turnover experiments.**

### **Results and Discussion:**

#### *Target quantitation:*

Peptides from different targets were identified based on their elution profile and signal intensity, by analyzing tryptic digests of the purified protein (*ecFabI*, *ecFabB* and *ecFabF*). Subsequently, a MudPIT analysis of the cell lysate was carried out to look at the peptides in the context of the native proteome. Different protocols for processing the lysate were assessed to get the best signal to noise. Gerber et al (208) used in-gel tryptic digests of the cell lysate separated on an SDS PAGE gel to quantify target levels. However, following a similar protocol, we were not able to identify peptides from the target proteins in the cell lysate. Also, in order to obviate the losses one might expect during extraction of digested peptides from the gel pieces, we decided to process the lysate instead of running a gel. Initial attempts included digesting the cell lysate directly after removing the cell debris. While this approach allowed us to identify a wide variety of peptides, there was considerable noise from background proteins and peptides. This led us to develop the protocol that is described in the **Materials and Methods** in which we precipitated the total protein and digested the re-suspended protein pellet.

Using a MudPIT analysis on the processed cell lysate, we were able to identify 1428 different proteins with 12 peptides from ecFabI (42.7% coverage), 14 peptides from ecFabB (51.7% coverage) and 17 peptides from ecFabF (56.4% coverage). In the MudPIT data, we looked at the elution profiles and the signal intensities for the different peptides from the targets to identify the best peptide for protein quantitation (**Table 5.1**). Subsequently, the peptides were subjected to an MS/MRM analysis to confirm that these peptides could be potentially used for quantitation.

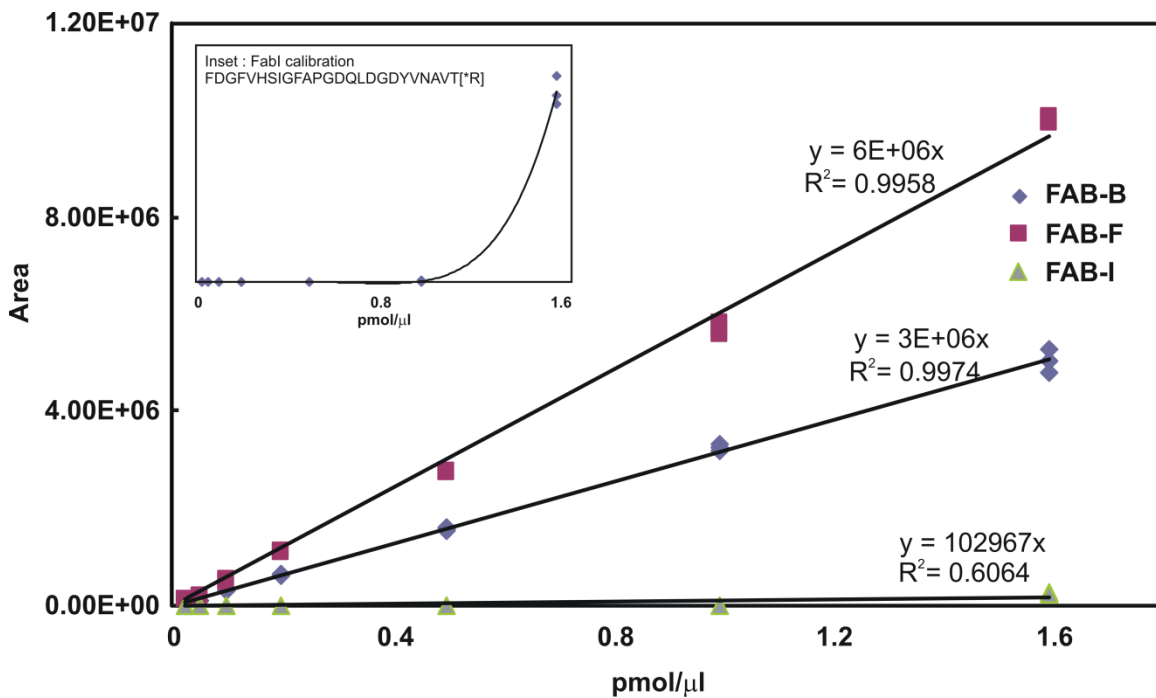


**Figure 5.2: Calibration curves for AQUA standard for ecFabX quantitation.**

10 μl of standard peptides (0.0125 – 1.6 pmol/μl) were injected and the area of the peak was monitored as a function of the concentration.



We were successfully able to quantify *ecFabB* and *ecFabF* using a calibration curve shown in **Figure 5.2**. However, peptide 1 that was used to quantify *ecFabI* showed a non-linear calibration curve up to a concentration of 1.6 pmol/ $\mu$ l (**Figure 5.2, inset**). While this prevented the accurate quantitation of *ecFabI* using this standard, the concentration of *ecFabI* was qualitatively assessed by comparing the peak intensities of the peptide to that of the standard. The results from these preliminary experiments are given in **Table 5.3**. The concentrations were calculated using a volume of 2 femtoliters for *E. coli* (218).

<b>Table 5.3: Target concentrations and copy-number per cfu.</b>		
<b>Protein</b>	<b>Copies/ cfu</b>	<b>Concentration (<math>\mu</math>M)</b>
<i>ecFabB</i>	731 $\pm$ 15	0.6 $\pm$ 0.01
<i>ecFabF</i>	855 $\pm$ 14	0.7 $\pm$ 0.01
<i>ecFabI</i>	1505 $\pm$ 446	1.2 $\pm$ 0.3

**Table 5.3: Target concentrations and copy-number per cfu.** Copy-number and concentrations of *ecFabX* enzymes present per cfu in *E. coli*. The concentrations were calculated using a cell volume of 2 femtoliters (218).

Subsequently, we revisited the MudPIT data to search for other peptides that could be used to quantify *ecFabI*. We identified peptide 2 that had promising

elution profile and S/N. Additional calibration curves were obtained on the TSQ with the new ecFabI peptide and the ecFabB/F peptides (**Figure 5.3**). Peptide 2 showed a linear response in the calibration curve along with the other peptides. We also used these set of samples for ecFabI quantitation using the new peptide 2 and perform the ecFabB and ecFabF quantitation in duplicate. Having a complete set of standards helped us quantify all three targets in *E. coli* in its log phase of growth. The results were reproducible and gave micromolar amounts of proteins in the growing cells (**Table 5.4**).

<b>Table 5.4: Target concentrations and copy-number per cfu.</b>		
<b>Protein</b>	<b>Copies/ cfu</b>	<b>Concentration (<math>\mu\text{M}</math>)</b>
ecFabB	1427 $\pm$ 135	1.2 $\pm$ 0.1
ecFabF	1389 $\pm$ 242	1.1 $\pm$ 0.2
ecFabI	1033 $\pm$ 86	0.9 $\pm$ 0.07

**Table 5.4: Copy-number/cfu and concentrations of ecFabX enzymes.** The concentrations were calculated using a cell volume of 2 femtoliters (218)

We have successfully been able to quantify the amount of target FASII proteins present in *E. coli* during log phase growth. In the growth phase of *E. coli*, cultured in rich media, the target levels in the cell are around 1  $\mu\text{M}$  for all the

three FASII proteins. Church *et al* (219) used 2D gel electrophoresis and isoelectric focusing to quantify protein levels in the cell. They suggested ~ 440 copies of FabI in *E. coli* K-12 which could give a concentration of 0.4  $\mu\text{M}$  assuming a cell volume of 2 femtoliters. The estimation was done in minimal media (glucose-MOPS) which explains the lower abundance estimated by the authors. Recently Frishman *et al.* (220) used the exponentially modified protein abundance index (emPAI) approach to quantify proteins at the level of a proteome. They reported target levels of 12500 and 14300 copies per cell for ecFabI and ecFabB while 1280 copies per cell of ecFabF which would yield give a concentration of 10  $\mu\text{M}$ , 12  $\mu\text{M}$  and 1  $\mu\text{M}$  respectively. Though the target copy-number suggested by our analysis are different than the ones reported for ecFabI and ecFabB, we are confident of the accuracy of our method in light of the probabilistic nature of the emPAI approach and differences in experimental set up. Moreover, the concentrations we report in this analysis are in the micromolar range as is proposed in the different studies.

Subsequently, we examined the effect on target levels in a cell upon administering an inhibitor for that target. We chose triclosan and thiolactomycin (TLM) that target ecFabI (214, 221) and ecFabB/F (215), respectively, to examine their effects on the target levels. The samples were prepared as described in the **Materials and Methods** section where the cells were exposed to 2X MIC concentrations of the inhibitors. It is important to note that triclosan and TLM are both slow-onset inhibitors of ecFabI and the acylated form of

ecFabB (**Chapter 1**) with a residence time of approximately 83 minutes (62) and 2 minutes (68) respectively.

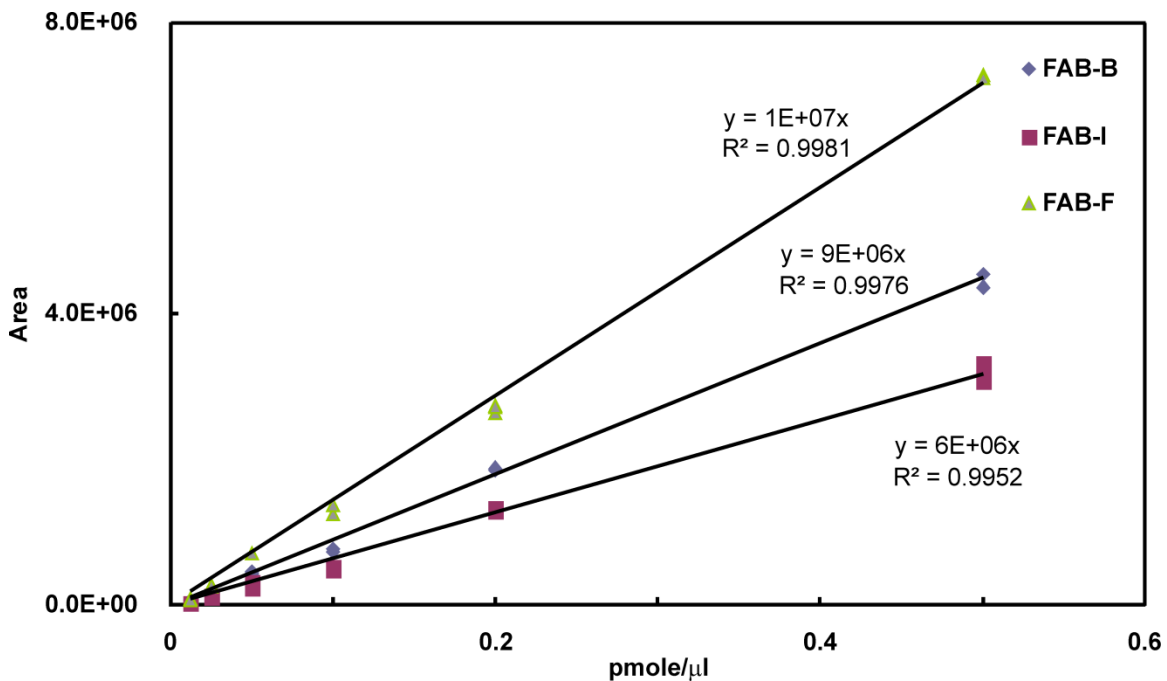


**Figure 5.3: Calibration curves for the new AQUA standards.** 10 μl of standard peptides (0.0125 – 0.5 pmol/μl) were injected and the area of the peak was monitored as a function of the concentration.

The results for the effect of triclosan on ecFabI are shown in **Table 5.5** and depicted in **Figure 5.4**. Triclosan was dissolved in DMSO and the results were compared to cells grown when only the solvent was administered. We observed a 5 fold increase in the ecFabI copy-number 2 hours post treatment, while 6 hours post treatment the copy-number returns to an approximate steady state. However, we also see 4 and 7 fold increase in FabF and FabB

respectively. The levels for all three enzymes return to steady state values 6 hours post induction.

<b>Table 5.5: Changes in copy-number per cfu of ecFabX post treatment with triclosan.</b>						
<b>Sample</b>	<b>Copies/cfu</b>					
	<b>ecFabB</b>		<b>ecFabF</b>		<b>ecFabI</b>	
	2hr	6hr	2hr	6hr	2hr	6hr
<b>DMSO</b>	2599 ±	6421 ±	2400 ±	4017 ±	1923 ±	3508 ±
	630	1505	679	977	356	831
<b>Triclosan</b>	16968±	16715 ±	8956 ±	8969 ±	7678 ±	8248 ±
	5622	5143	1186	2447	2548	2293

**Table 5.5: Changes in copy-number/cfu of ecFabX after treatment with triclosan.**

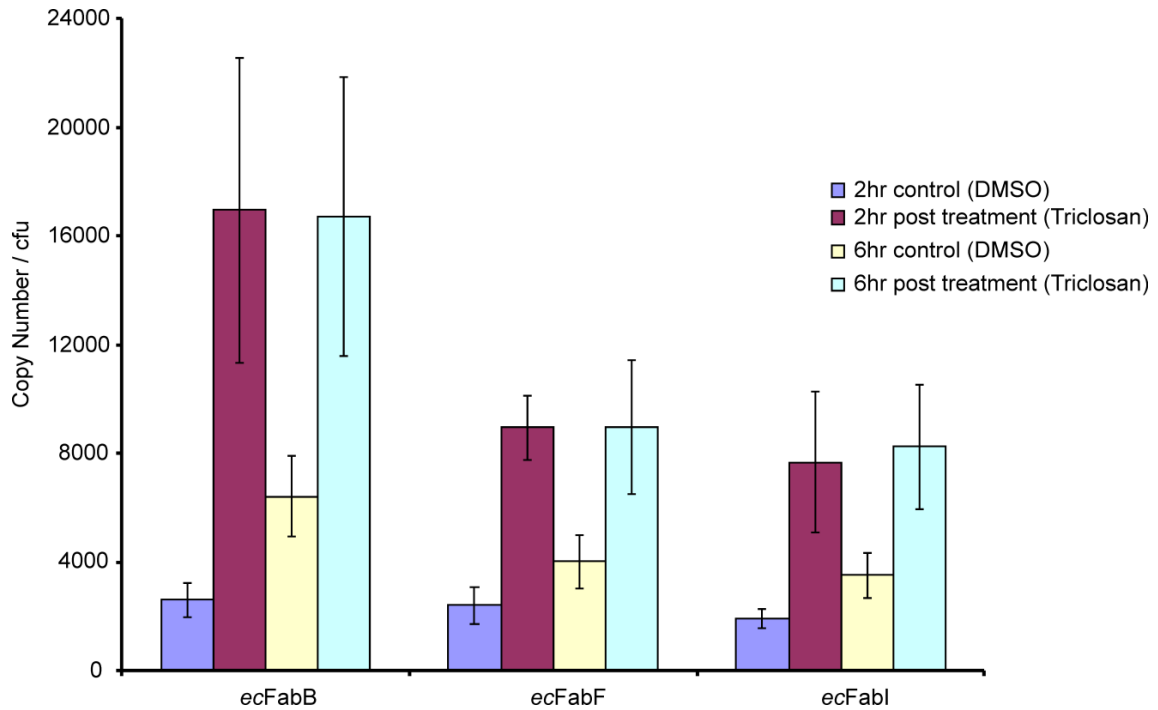


**Figure 5.4: Changes in copy-number/cfu in ecFabX upon treatment with triclosan.**

We also measured the target levels in the cells upon administering TLM. We were able to see a 35 fold increase in the copy-number of ecFabB and a 20 fold increase in the levels of FabF and FabI which may correlate to ecFabB being the primary cellular target of TLM.

<b>Table 5.6: Changes in copy-number/cfu of ecFabX post treatment with TLM</b>						
<b>Sample</b>	<b>Copies/cfu</b>					
	<b>ecFabB</b>		<b>ecFabF</b>		<b>ecFabI</b>	
	2hr	6hr	2hr	6hr	2hr	6hr
<b>Untreated</b>	1427± 134	2030 ± 762	1033 ± 86	1008 ± 412	1388 ± 242	1216 ± 343
<b>TLM</b>	49348 ± 4547	6233 ± 917	20575 ± 6973	5017 ± 778	29874 ± 4040	5788 ± 850

**Table 5.6: Changes in copy-number/cfu of ecFabX post treatment with TLM.**

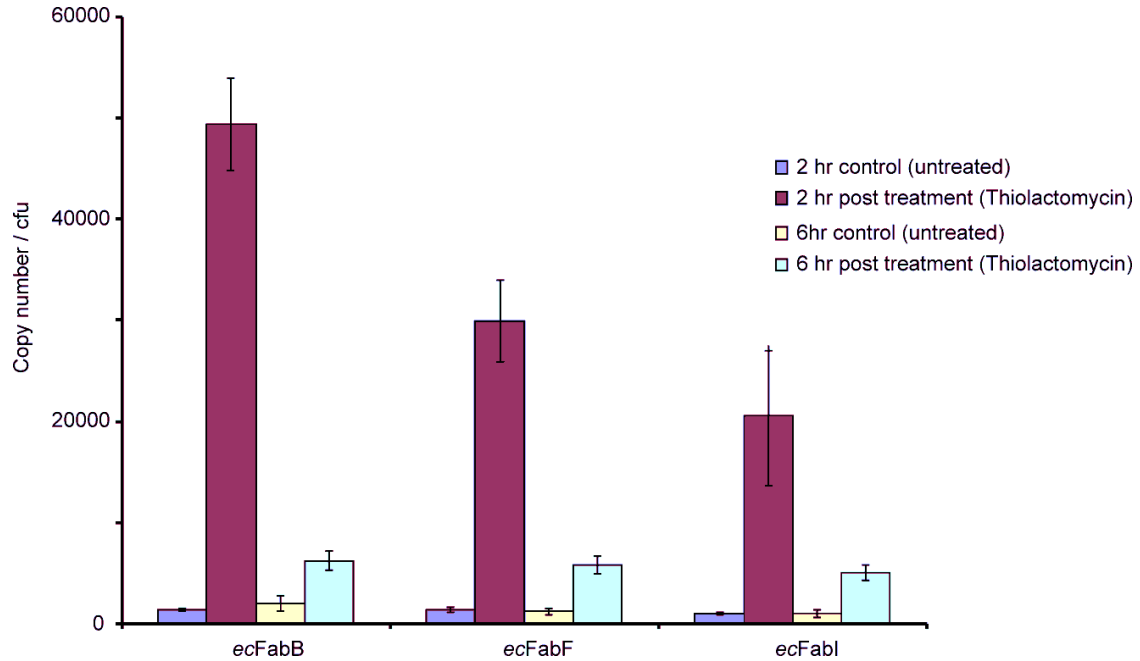


**Figure 5.5: Changes in copy-number/cfu in ecFabX upon treatment with TLM.**

It is very important to note that these numbers are copy-number per cfu and not concentrations. Upon administering an inhibitor that inhibits fatty acid biosynthesis, it is quite plausible that we have induced a change in the cell morphology and/or volume. Okazaki *et al* (102) have demonstrated morphological changes and cell elongation in *E. coli* upon treatment with TLM. Hence, in order to comment on the changes in the concentration of the target levels, it is exceptionally important to be able to measure the volume of the cell. Therefore, in an independent set of experiments we measured the volume of the cells with or without treatment with the drug (triclosan and TLM) as described in the **Materials and Methods**. The data was corrected for the periplasmic volume of *E. coli* which is about 20 to 40% of the total cell volume (222). The volumes do



not change drastically upon the addition of triclosan implying that the changes in the copy-number represents changes in protein concentration.

<b>Table 5.7: Bacterial cytosolic volume at different time points.</b>		
<b>Sample Name</b>	<b>Volume (femtoliters)</b>	
	<b>2 hour</b>	<b>6 hour</b>
Untreated	2.8±0.1	2.9±0.1
Thiolactomycin (2X MIC)	4.1±0.2	2.9±0.1
DMSO	2.8±0.1	2.9±0.1
Triclosan (2XMIC)	2.8±0.1	2.9±0.1

**Table 5.7: The cytosolic volume of *E.coli* cell.**

Interestingly, the bacterial volume increases ~1.5 fold after 2 hours of treatment with TLM while the original bacterial volume is restored 6 hours post treatment. This implies that we observe a ~23 fold increase in the copy-number of *ecFabB* and a ~13 fold increase in the levels of *ecFabF* and *ecFabI* which may relate to *ecFabB* being the primary intracellular target.

Changes in target levels can be seen upon administering drugs corresponding to the targets. Interestingly, we see accumulation of all three FASII targets, though to different extent, irrespective of the antibiotic being used. Bandow *et al* (223) in a recent pulse-chase study in *B. subtilis* observed induction

of various targets that are not believed to be targeted by the administered antibiotic. This observation can be explained by the fact that in *B. subtilis*, FabI and FabF proteins are found in the same operon. In *E. coli* the situation is more complicated as the FASII proteins are not in the same operon. However, the different enzymes could possibly be under the control of the same regulon or perhaps have a more complex interconnected regulatory mechanism that results in a simultaneous regulation of the targets in question. Lewis, K. and other workers examining protein transcription of different genes upon administering antibiotics have seen induction or repression of overlapping genes (224, 225). Our data begs the question whether the accumulation is due to an induction of gene expression for the target or a slower degradation due to stabilization of the target to proteolysis due to inhibitor binding (226).

*Target turnover:*

**Protein Degradation:** The  $^{14}\text{N}/^{15}\text{N}$  pulse-chase experiment allows us to measure the rate of protein degradation by monitoring the decrease in the  $^{14}\text{N}$  protein as a function of time. If  $\alpha$  is the level of incorporation of  $^{14}\text{N}$  in a protein and  $I_H(t_0)$  and  $I_L(t_0)$  are MS peak intensities of  $^{15}\text{N}$  peptide and  $^{14}\text{N}$  peptide a protein at time  $t = 0$ , then,

**Equation 5.1**      
$$\alpha = \frac{I_L(t_0)}{I_L(t_0) + I_H(t_0)}$$

In our case, a 100% incorporation of  $^{14}\text{N}$  in the beginning results in  $\alpha = 1$ . This value should be the same for all the proteins monitored provided the cells attained a steady state during the first phase. If,  $I_H(t)$  and  $I_L(t)$  are the peak intensities from the peptides at any time  $t$  ( $t > 0$ ) and the  $f$  is the fraction of protein (labeled + unlabeled) at time  $t_0$  that remains after time  $t$ , the ratio of  $^{14}\text{N}$  protein to the total protein can be written as (227) :

$$\frac{\text{Unlabeled protein at time } t}{\text{total protein at time } t} = \frac{f \cdot \alpha \cdot p(t_0)}{p(t)} = \frac{I_L(t)}{I_L(t) + I_H(t)}$$

**Equation 5.2** 
$$f = \frac{1}{\alpha} \cdot \frac{P(t)}{p(t_0)} \cdot \frac{I_L(t)}{I_L(t) + I_H(t)}$$

Where,  $p$  is the total amount of the intracellular target. In our analysis instead of using the peak intensities, we have normalized the data to the cell count of the sample to get the amount of protein per cfu. This way we can obviate the reduction in the  $^{14}\text{N}$  protein signal due to cell-growth mediated dilution. In a condition where the cells are in a steady state, i.e. there is no net synthesis or degradation of protein [ $p(t_0) = p(t)$ ],  $f$  can be calculated using

**Equation 5.3** 
$$f = \frac{1}{\alpha} \cdot \frac{I_L(t)}{I_L(t) + I_H(t)}$$

Then the function 'f' can be fitted to an exponential decay curve ( $e^{-kt}$ ) to get the rate of degradation (227) (**Figure 5.6** and **Table 5.8**).

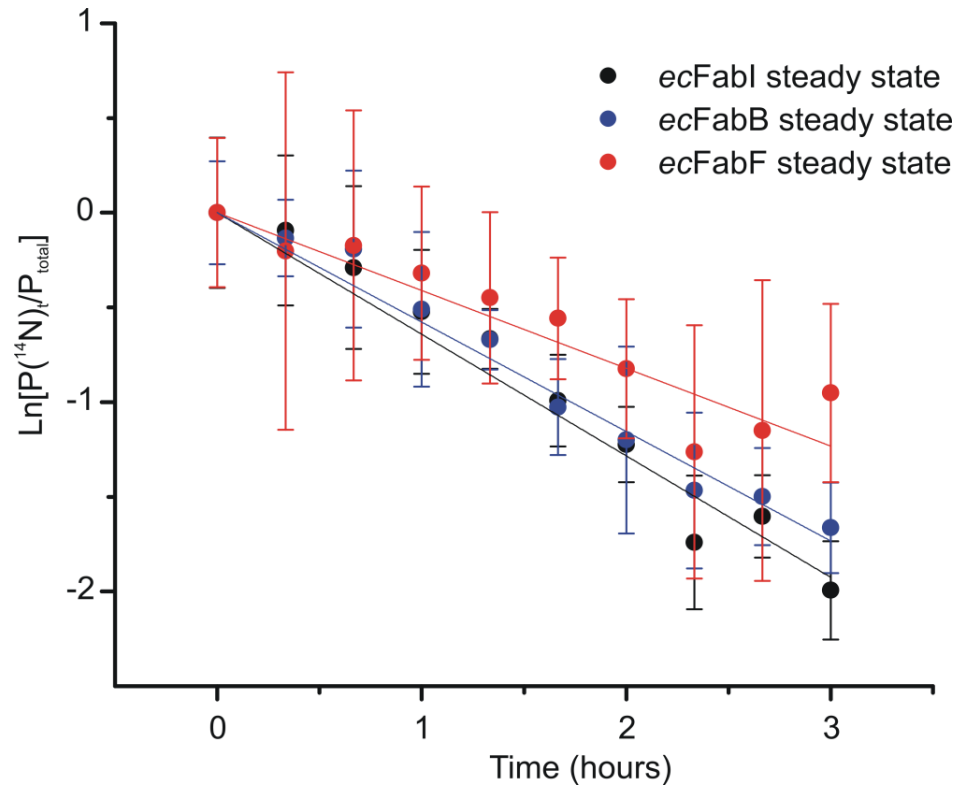


**Figure 5.6: Degradation of ecFabX using the steady state assumption.**  $\text{Ln}(f)$  (Equation 5.3) is plotted as a function of time. The solid line is the best fit of the data including the errors that were weighted using a direct weighting method. ecFabF data has higher errors than the other two enzymes due to an isobaric interference from the standard described subsequently.

Table 5.8: Rates of degradation of FabX using the steady state assumption.				
Target	$k_{deg}$ Steady state assumption	Adj. $R^2$	$T_{1/2}$ (hours)	$T_{1/2}$ (min)
ecFabI	$0.64 \pm 0.03$	0.98	1.08	64.96
ecFabB	$0.58 \pm 0.02$	0.99	1.19	71.69
ecFabF	$0.41 \pm 0.03$	0.95	1.69	101.41

**Table 5.8: Rates of degradation of FabX (steady state assumption).** The protein half-lives obtained are reported.

However, for fast growing organisms, such as bacteria, where the levels of intracellular protein change dynamically with time, the steady state assumption does not hold accord (227). Since, the AQUA methodology gives a direct measure of the  $^{14}\text{N}$  intracellular protein concentration, the fraction of protein at time  $t_0$  that remains after time  $t$  ( $f$ ) can be estimated directly.

**Equation 5.4** 
$$f_{AQUA} = \frac{P_L(t)}{P_L(t_0)}$$

For each of the data set, the Spearman's rank correlation ( $R_s$ ) was used to access the correlation between the fraction 'f' and time. As can be seen from **Table 5.9**, that these two parameters are anti-correlated with negative  $R_s$  values and P values  $<0.05$  rejecting the null hypothesis implying a statistical significance of these observations. Hence, the data was analyzed using the non-steady state assumption and is reported in **Figure 5.7** and **Table 5.10**.

<b>Table 5.9: Changes in target levels as a function of time.</b>		
<b>Target</b>	<b><math>R_s</math> Ln[<math>P_t/P_{t_0}</math>] versus time</b>	<b>P value</b>
<b>ecFabI</b>	-0.77	0.03
<b>ecFabB</b>	-0.77	0.02
<b>ecFabF</b>	-0.68	0.02

**Table 5.9: Anti-correlation of protein abundance/cfu as a function of time.**

The spearman's correlation and the standard deviation in  $\text{Ln}[P(t)/P(t_0)]$  across time are reported along with the statistical significance (P value, double tailed) of this correlation.

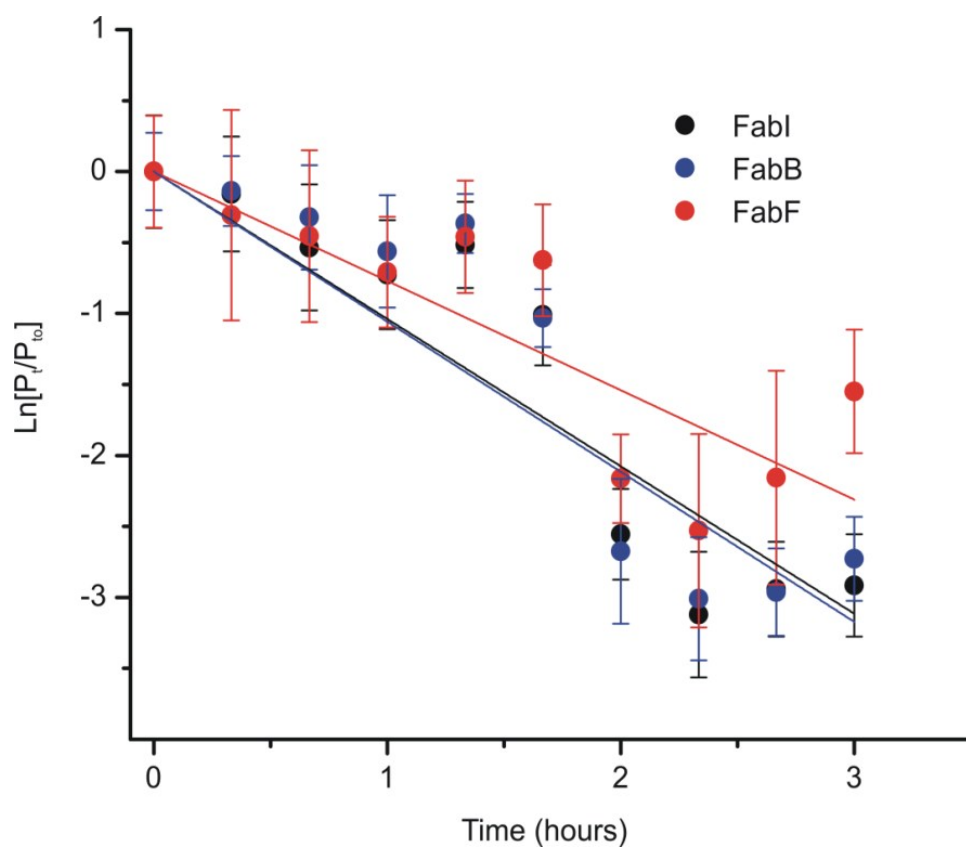


**Figure 5.7: Degradation of ecFabX using the non-steady state assumption.**

$\text{Ln}(f)$  (Equation 5.4) is plotted as a function of time. The solid line is the best fit of the data including the errors that were weighted using a direct weighting method. ecFabF data has higher errors than the other two enzymes due to an isobaric interference from the standard described subsequently.

<b>Table 5.10 : Rates of degradation of FabX using the non steady state assumption</b>					
<b>Target</b>	<b><math>k_{deg}</math> non steady state assumption</b>	<b>Adj. <math>R^2</math></b>	<b>Pearson's R</b>	<b><math>T_{1/2}</math> (hours)</b>	<b><math>T_{1/2}</math> (min)</b>
ecFabI	1.04 ± 0.09	0.93	-0.97	0.67	40.1
ecFabB	1.06 ± 0.09	0.93	-0.97	0.65	39.3
ecFabF	0.77 ± 0.08	0.89	-0.95	0.9	54.0

**Table 5.10: Rates of degradation of FabX (non-steady state assumption).**

The Spearman's correlation and protein half-lives obtained are reported.

As noted by Jayapal *et al* (227), for a monotonically decreasing protein concentration (anticorrelated), we get an underestimated rate of degradation using the steady state assumption. Since *E. coli* is a fast growing organism, this assumption is flawed due to the highly dynamic nature of the intracellular proteins. In fact our data does suggest fluctuations in the intracellular protein level over a period of time suggested by various workers (227, 228). The non-steady state analysis afforded by the AQUA methodology gives half lives in the range of ~40 min which fits in well with the doubling time for *E. coli* under the current experimental conditions (~38 min) unlike the steady state analysis.



Interestingly, the rate of degradation of ecFabF is slower resulting in a longer half-life of ~50 min.

**Protein Synthesis:** The  $^{14}\text{N}/^{15}\text{N}$  pulse-chase experiment allows us to measure the rate of protein synthesis by monitoring the increase in the  $^{15}\text{N}$  protein as a function of time. If  $F_n$  is the fraction of newly synthesized protein it can be described as follows (229, 230):

**Equation 5.5** 
$$F_n = \frac{I_H}{I_L + I_H}$$

Where  $I_H$  is the intensity of the  $^{15}\text{N}$  peptide and  $I_L$  is the  $^{14}\text{N}$  peptide. Since the AQUA method allows the quantitation of protein per cell, we use the amount of the heavy and the light peptide per cell to quantify the rate of protein synthesis. The rates of synthesis are measured by plotting the amount of newly synthesized  $^{15}\text{N}$  protein over the total protein pool. There is an initial lag in protein synthesis (**Figure 5.9**) in the first 20-40 min of the *chase* which is perhaps an artifact of transferring cells to fresh media (doubling time ~38 min). Moreover, the last few time points level off which is perhaps due to a competing degradation process. The rates observed in the lines of best fit (stem of the sigmoid) have been reported in units of percent new protein per hour. These rates observed fit in well with the preliminary experiments (data not shown) where we saw only ~ 50% incorporation of the  $^{15}\text{N}$  label in the protein after 90 minutes.

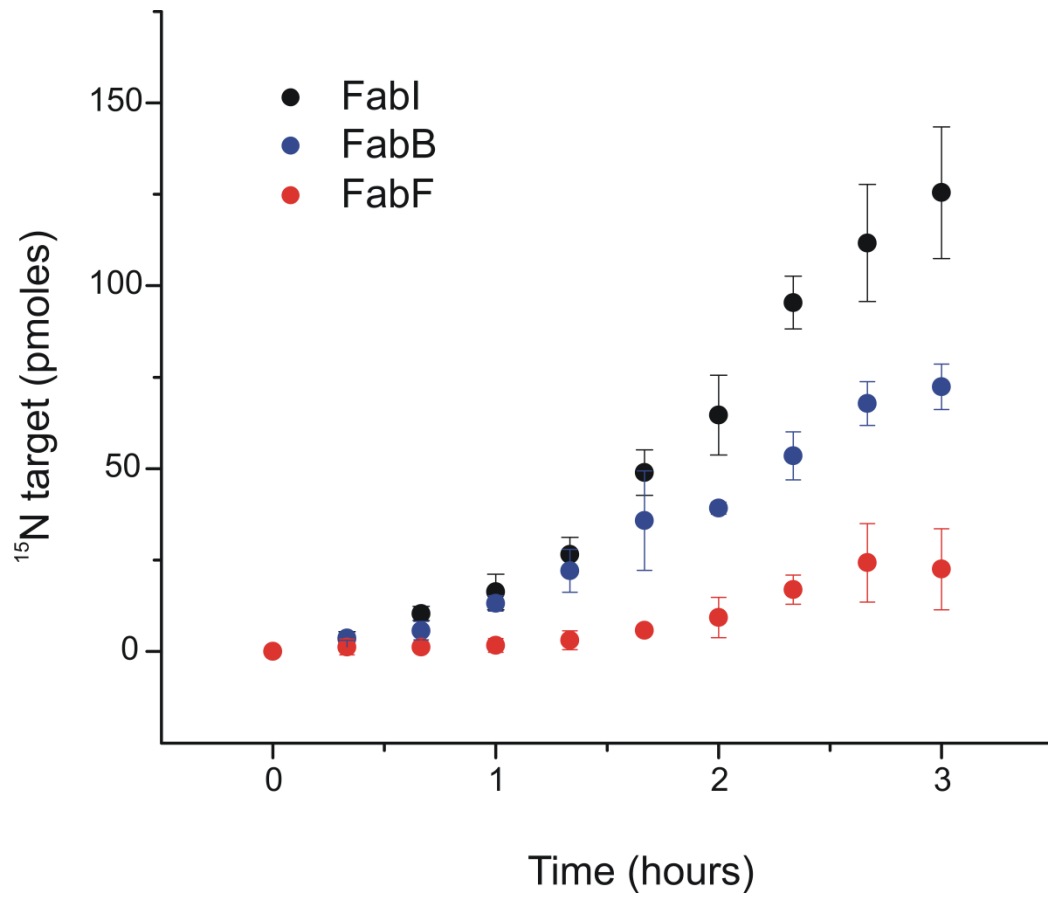
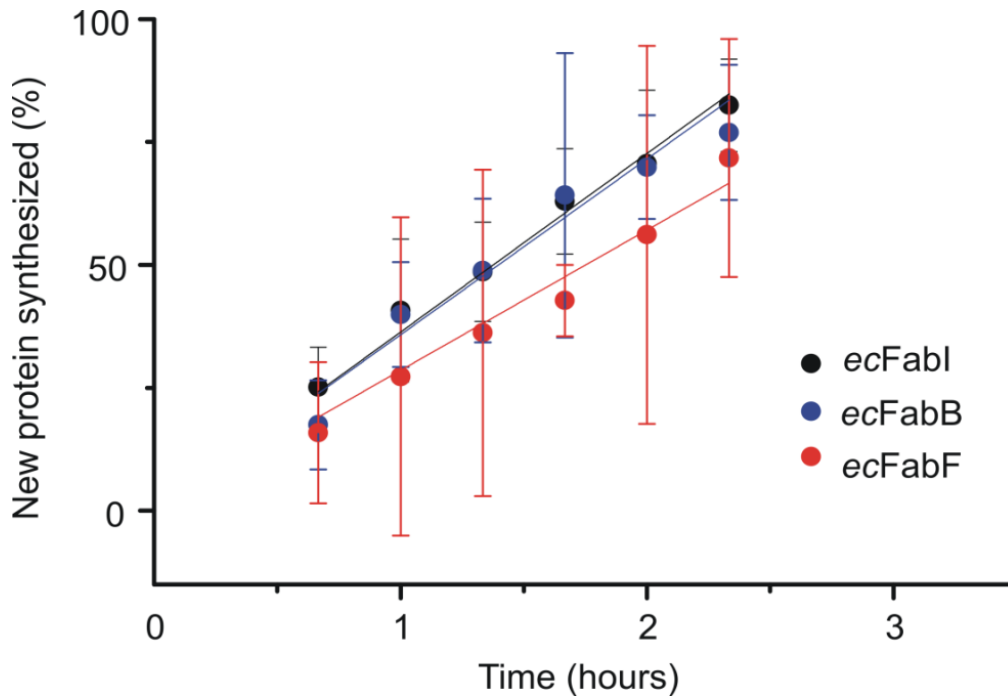


Figure 5.8: The amount of  $^{15}\text{N}$  protein synthesized as a function of time.



**Figure 5.9: Synthesis of the three FASII proteins.** The function  $F_n$  is plotted as a function of time (**Equation 5.5**). The solid line is the best fit of the data including the errors that were weighted using a direct weighting method. ecFabF data has higher errors than the other two enzymes due to an isobaric interference from the standard described subsequently.

<b>Table 5.11: Rates of synthesis of FabX.</b>				
<b>Target</b>	<b>Percent new protein synthesized per hour</b>	<b>Average total protein (<math>\mu\text{M}</math>)</b>	<b>Rate (<math>\text{nM min}^{-1}</math>)</b>	<b>Adj. <math>R^2</math></b>
<b>ecFabI</b>	$36.3 \pm 0.72$	0.5	3	0.99
<b>ecFabB</b>	$35.8 \pm 1.2$	0.4	2	0.99
<b>ecFabF</b>	$28.5 \pm 0.75$	0.1	0.4	0.99

**Table 5.11: The rates of synthesis of ecFabX.** The rates of synthesis are reported with the units of  $\% \text{ hr}^{-1}$  and  $\text{nM min}^{-1}$ . ecFabF data has higher errors than the other two enzymes due to an isobaric interference from the standard described subsequently.

Our data shows ecFabF is turned over more slowly than the other two enzymes with a slower rate of synthesis and a longer half-life in the cell. However, our analysis does not take into account the degradation of the newly synthesized  $^{15}\text{N}$  protein during the time course of the experiment. The degradation of the newly synthesized protein would be more pertinent at later time points where the amount of  $^{15}\text{N}$  protein is equal to or greater than the amount of  $^{14}\text{N}$  labeled protein. While, we are presently examining alternative ways of analyzing the data to get more absolute rates, a more rigorous analysis

would entail the use of *birth-death* ordinary differential equations to take into account the dynamics of the system.

It is important to note that in the current data, the quantitation of the  $^{15}\text{N}$  peptide of FabF is problematic as the peptide interference from the  $^{13}\text{C}$  (natural isotopic abundance) peptide of the native protein (**Figure 5.10**). This results in subtraction artifacts resulting in considerable errors. However, we can see that the rates of degradation and synthesis of *ecFabF* are slower than that of the other two proteins. Interestingly, *ecFabF* also has a lower rate of degradation and hence a longer half-life. This could perhaps give us some insight into the intracellular dynamics as it relates to protein essentiality.

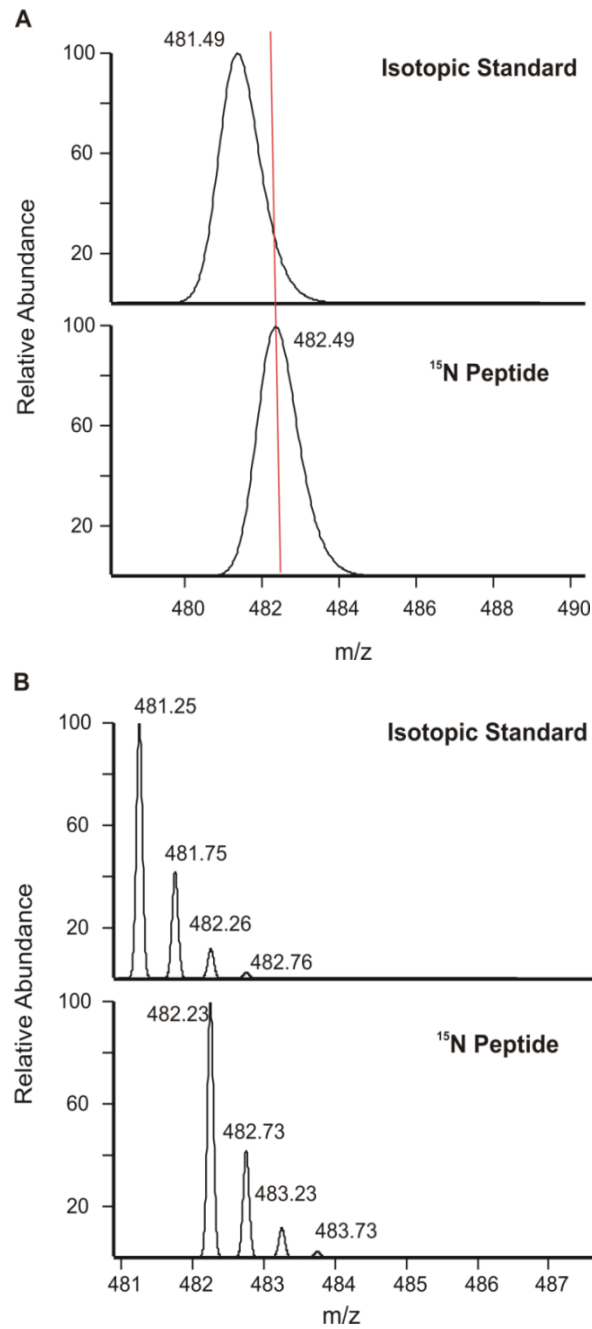


**Figure 5.10: Isobaric interference of the <sup>13</sup>C isotope of the FabF standard.**

**A)** Unit resolution, **B)** 5000 resolution.

## Conclusions:

We have successfully been able to quantify the concentration of proteins in a cell and measure their turnover in *E. coli* in log phase. We have also shown that administering TLM results in accumulation of FASII enzymes, with maximum accumulation observed for FabB followed by FabF and FabI which may correlate with FabB being the primary cellular target. This observation also explains the poor whole-cell activity of TLM against *E. coli*. Moreover, we see a very slight overexpression of FASII targets upon administering triclosan. We see a greater increase in the target concentration for FabB upon administering triclosan than for FabI implying an intricate regulatory mechanism that controls the expression of different FASII proteins in *E. coli*. Perhaps, the observation that triclosan does not result in as much accumulation of the target as TLM, might explain the 400 fold smaller whole cell activity in vitro.

Presently, we are measuring the post-antibiotic effect of triclosan in *E. coli* to examine the influence of protein turnover on the mechanism of triclosan's PAE. Moreover, experiments are underway to measure the rate of turnover for ecFabI in the presence of triclosan to understand the mechanism for the 5 fold accumulation of FabI that we observe. We hypothesize that while triclosan doesn't induce the overexpression of FabI (231), it stabilizes the drug-target complex against proteolysis thereby increasing the protein half-life (226).

Most standard PK/PD models used in antibacterial drug discovery assume that the pharmacological effects are mediated by time-independent effects at the target level and are driven by free fraction component of the drug at the site of action. We have been able to show that the target levels are not static, at a proteomic level, in the presence of a drug. Moreover, we have successfully designed and established a convenient handle on the absolute quantitation of targets in a cell and looking at their turnover. We plan to extend our studies to not only other pathogenic bacteria such as *P.aeruginosa*, *M.tuberculosis* etcetera but also different targets within these pathogens.



## References:

1. Drews, J. (2000) Drug discovery: a historical perspective, *Science* 287, 1960-1964.
2. Coates, A., Hu, Y., Bax, R., and Page, C. (2002) The future challenges facing the development of new antimicrobial drugs, *Nat Rev Drug Discov* 1, 895-910.
3. Dineeen, P., Homan, W. P., and Grafe, W. R. (1976) Tuberculous peritonitis: 43 years' experience in diagnosis and treatment, *Ann Surg* 184, 717-722.
4. Wright, G. D. (2007) The antibiotic resistome: the nexus of chemical and genetic diversity, *Nat Rev Microbiol* 5, 175-186.
5. (2007) News Feature: A call to arms, *Nat Rev Drug Discov* 6, 8-12.
6. Black, M. T., and Hodgson, J. (2005) Novel target sites in bacteria for overcoming antibiotic resistance, *Adv Drug Deliv Rev* 57, 1528-1538.
7. Bax, R. P., Anderson, R., Crew, J., Fletcher, P., Johnson, T., Kaplan, E., Knaus, B., Kristinsson, K., Malek, M., and Strandberg, L. (1998) Antibiotic resistance--what can we do?, *Nat Med* 4, 545-546.
8. McGowan, J. E., Jr. (2006) Resistance in nonfermenting gram-negative bacteria: multidrug resistance to the maximum, *Am J Infect Control* 34, S29-37; discussion S64-73.
9. Giamarellos-Bourboulis, E. J., Antonopoulou, A., Raftogiannis, M., Koutoukas, P., Tsaganos, T., Tziortzioti, V., Panagou, C., Adamis, T., and Giamarellou, H. (2006) Clarithromycin is an effective immunomodulator

- when administered late in experimental pyelonephritis by multidrug-resistant *Pseudomonas aeruginosa*, *BMC Infect Dis* 6, 31.
10. Pan, P., and Tonge, P. J. (2012) Targeting InhA, the FASII Enoyl-ACP Reductase: SAR Studies on Novel Inhibitor Scaffolds, *Curr Top Med Chem*, 672-693.
  11. Tonge, P. J., Kisker, C., and Slayden, R. A. (2007) Development of modern InhA inhibitors to combat drug resistant strains of *Mycobacterium tuberculosis*, *Current Topics in Medicinal Chemistry* 7, 489-498.
  12. Tonge, P. J. (2000) Another brick in the wall, *Nat Struct Biol* 7, 94-96.
  13. (2002) *Staphylococcus aureus* resistant to vancomycin--United States, 2002, *MMWR Morb Mortal Wkly Rep* 51, 565-567.
  14. Davies, J. (2006) Where have All the Antibiotics Gone?, *Can J Infect Dis Med Microbiol* 17, 287-290.
  15. Coates, A. (2003) *Dormancy and Low Growth States in Microbial Disease*, Cambridge University Press.
  16. So, A. D., Gupta, N., Brahmachari, S. K., Chopra, I., Munos, B., Nathan, C., Outterson, K., Paccaud, J. P., Payne, D. J., Peeling, R. W., Spigelman, M., and Weigelt, J. (2011) Towards new business models for R&D for novel antibiotics, *Drug Resist Updat* 14, 88-94.
  17. Lu, H., and Tonge, P. J. (2010) Drug-target residence time: critical information for lead optimization, *Curr Opin Chem Biol* 14, 467-474.
  18. Fishman, M. C., and Porter, J. A. (2005) Pharmaceuticals: a new grammar for drug discovery, *Nature* 437, 491-493.

19. Dimasi, J. A. (2001) New drug development in the United States from 1963 to 1999, *Clin Pharmacol Ther* 69, 286-296.
20. Smith, C. (2003) Drug target validation: Hitting the target, *Nature* 422, 341, 343, 345 passim.
21. Koul, A., Arnoult, E., Lounis, N., Guillemont, J., and Andries, K. (2011) The challenge of new drug discovery for tuberculosis, *Nature* 469, 483-490.
22. Rouhi, A. M. (2003) Betting on natural products for cures, *C & E News* 81, 93-103.
23. Darvas, F., Dorman, G., Urge, L., Szabo, I., Ronai, Z., and Sasvari-Szekely, M. (2001) Combinatorial chemistry. Facing the challenge of chemical genomics, *Pure and Applied Chemistry* 73, 1487-1498.
24. McDevitt, D., and Rosenberg, M. (2001) Exploiting genomics to discover new antibiotics, *Trends Microbiol* 9, 611-617.
25. Becker, D., Selbach, M., Rollenhagen, C., Ballmaier, M., Meyer, T. F., Mann, M., and Bumann, D. (2006) Robust Salmonella metabolism limits possibilities for new antimicrobials, *Nature* 440, 303-307.
26. Magnuson, K., Jackowski, S., Rock, C. O., and Cronan, J. E., Jr. (1993) Regulation of fatty acid biosynthesis in Escherichia coli, *Microbiol Rev* 57, 522-542.
27. Rock, C. O., and Cronan, J. E. (1996) Escherichia coli as a model for the regulation of dissociable (type II) fatty acid biosynthesis, *Biochim Biophys Acta* 1302, 1-16.

28. Payne, D. J., Warren, P. V., Holmes, D. J., Ji, Y. D., and Lonsdale, J. T. (2001) Bacterial fatty-acid biosynthesis: a genomics-driven target for antibacterial drug discovery, *Drug Discov Today* 6, 537-544.
29. Wright, H. T., and Reynolds, K. A. (2007) Antibacterial targets in fatty acid biosynthesis, *Curr Opin Microbiol* 10, 447-453.
30. Campbell, J. W., and Cronan, J. E. (2001) Bacterial fatty acid biosynthesis: Targets for antibacterial drug discovery, *Annual Review of Microbiology* 55, 305-332.
31. Balemans, W., Lounis, N., Gilissen, R., Guillemont, J., Simmen, K., Andries, K., and Koul, A. (2010) Essentiality of FASII pathway for *Staphylococcus aureus*, *Nature* 463, E3-E4.
32. Brinster, S., Lamberet, G., Staels, B., Trieu-Cuot, P., Gruss, A., and Poyart, C. (2009) Type II fatty acid synthesis is not a suitable antibiotic target for Gram-positive pathogens, *Nature* 458, 83-86.
33. Wang, H., and Cronan, J. E. (2004) Functional replacement of the FabA and FabB proteins of *Escherichia coli* fatty acid synthesis by *Enterococcus faecalis* FabZ and FabF homologues, *J Biol Chem* 279, 34489-34495.
34. Heath, R. J., White, S. W., and Rock, C. O. (2001) Lipid biosynthesis as a target for antibacterial agents, *Progress in Lipid Research* 40, 467-497.
35. Li, S. J., and Cronan, J. E., Jr. (1992) The genes encoding the two carboxyltransferase subunits of *Escherichia coli* acetyl-CoA carboxylase, *J Biol Chem* 267, 16841-16847.

36. Li, S. J., and Cronan, J. E., Jr. (1992) The gene encoding the biotin carboxylase subunit of *Escherichia coli* acetyl-CoA carboxylase, *J Biol Chem* 267, 855-863.
37. Cronan, J. E., Jr., and Waldrop, G. L. (2002) Multi-subunit acetyl-CoA carboxylases, *Progress in Lipid Research* 41, 407-435.
38. Li, Z. X., Huang, Y., Ge, J., Fan, H., Zhou, X. H., Li, S. T., Bartlam, M., Wang, H. H., and Rao, Z. (2007) The crystal structure of MCAT from *Mycobacterium tuberculosis* reveals three new catalytic models, *J Mol Biol* 371, 1075-1083.
39. Davies, C., Heath, R. J., White, S. W., and Rock, C. O. (2000) The 1.8 Å crystal structure and active-site architecture of beta-ketoacyl-acyl carrier protein synthase III (FabH) from *Escherichia coli*, *Structure* 8, 185-195.
40. Jackowski, S., and Rock, C. O. (1987) Acetoacetyl-acyl carrier protein synthase, a potential regulator of fatty acid biosynthesis in bacteria, *J Biol Chem* 262, 7927-7931.
41. Price, A. C., Zhang, Y. M., Rock, C. O., and White, S. W. (2001) Structure of beta-ketoacyl-[acyl carrier protein] reductase from *Escherichia coli*: negative cooperativity and its structural basis, *Biochemistry* 40, 12772-12781.
42. Price, A. C., Zhang, Y. M., Rock, C. O., and White, S. W. (2004) Cofactor-induced conformational rearrangements establish a catalytically competent active site and a proton relay conduit in FabG, *Structure* 12, 417-428.

43. Leesong, M., Henderson, B. S., Gillig, J. R., Schwab, J. M., and Smith, J. L. (1996) Structure of a dehydratase-isomerase from the bacterial pathway for biosynthesis of unsaturated fatty acids: Two catalytic activities in one active site, *Structure* 4, 253-264.
44. Kimber, M. S., Martin, F., Lu, Y., Houston, S., Vedadi, M., Dharamsi, A., Fiebig, K. M., Schmid, M., and Rock, C. O. (2004) The structure of (3R)-hydroxyacyl-acyl carrier protein dehydratase (FabZ) from *Pseudomonas aeruginosa*, *J Biol Chem* 279, 52593-52602.
45. Liu, N. N., Cummings, J. E., England, K., Slayden, R. A., and Tonge, P. J. (2011) Mechanism and inhibition of the FabI enoyl-ACP reductase from *Burkholderia pseudomallei*, *Journal of Antimicrobial Chemotherapy* 66, 564-573.
46. Roujeinikova, A., Sedelnikova, S., de Boer, G. J., Stuitje, A. R., Slabas, A. R., Rafferty, J. B., and Rice, D. W. (1999) Inhibitor binding studies on enoyl reductase reveal conformational changes related to substrate recognition, *J Biol Chem* 274, 30811-30817.
47. Roujeinikova, A., Levy, C. W., Rowsell, S., Sedelnikova, S., Baker, P. J., Minshull, C. A., Mistry, A., Colls, J. G., Camble, R., Stuitje, A. R., Slabas, A. R., Rafferty, J. B., Pauptit, R. A., Viner, R., and Rice, D. W. (1999) Crystallographic analysis of triclosan bound to enoyl reductase, *J Mol Biol* 294, 527-535.
48. Rock, C. O., and Cronan, J. E., Jr. (1979) Re-evaluation of the solution structure of acyl carrier protein, *J Biol Chem* 254, 9778-9785.

49. Rock, C. O., and Garwin, J. L. (1979) Preparative enzymatic synthesis and hydrophobic chromatography of acyl-acyl carrier protein, *J Biol Chem* 254, 7123-7128.
50. Rock, C. O., and Cronan, J. E., Jr. (1979) Solubilization, purification, and salt activation of acyl-acyl carrier protein synthetase from *Escherichia coli*, *J Biol Chem* 254, 7116-7122.
51. Bergler, H., Fuchsbichler, S., Hogenauer, G., and Turnowsky, F. (1996) The enoyl-[acyl-carrier-protein] reductase (FabI) of *Escherichia coli*, which catalyzes a key regulatory step in fatty acid biosynthesis, accepts NADH and NADPH as cofactors and is inhibited by palmitoyl-CoA, *European Journal of Biochemistry* 242, 689-694.
52. Lu, H., and Tonge, P. J. (2008) Inhibitors of FabI, an enzyme drug target in the bacterial fatty acid biosynthesis pathway, *Acc Chem Res* 41, 11-20.
53. Parikh, S., Moynihan, D. P., Xiao, G., and Tonge, P. J. (1999) Roles of tyrosine 158 and lysine 165 in the catalytic mechanism of InhA, the enoyl-ACP reductase from *Mycobacterium tuberculosis*, *Biochemistry* 38, 13623-13634.
54. Baldock, C., Rafferty, J. B., Sedelnikova, S. E., Baker, P. J., Stuitje, A. R., Slabas, A. R., Hawkes, T. R., and Rice, D. W. (1996) A mechanism of drug action revealed by structural studies of enoyl reductase, *Science* 274, 2107-2110.
55. Johnsson, K., King, D. S., and Schultz, P. G. (1995) Studies on the Mechanism of Action of Isoniazid and Ethionamide in the Chemotherapy

- of Tuberculosis, *Journal of the American Chemical Society* 117, 5009-5010.
56. Rawat, R., Whitty, A., and Tonge, P. J. (2003) The isoniazid-NAD adduct is a slow, tight-binding inhibitor of InhA, the *Mycobacterium tuberculosis* enoyl reductase: Adduct affinity and drug resistance, *Proc Natl Acad Sci U S A* 100, 13881-13886.
  57. Argyrou, A., Jin, L., Siconilfi-Baez, L., Angeletti, R. H., and Blanchard, J. S. (2006) Proteome-wide profiling of isoniazid targets in *Mycobacterium tuberculosis*, *Biochemistry* 45, 13947-13953.
  58. Argyrou, A., Vetting, M. W., Aladegbami, B., and Blanchard, J. S. (2006) *Mycobacterium tuberculosis* dihydrofolate reductase is a target for isoniazid, *Nat Struct Mol Biol* 13, 408-413.
  59. Sullivan, T. J., Truglio, J. J., Boyne, M. E., Novichenok, P., Zhang, X., Stratton, C. F., Li, H. J., Kaur, T., Amin, A., Johnson, F., Slayden, R. A., Kisker, C., and Tonge, P. J. (2006) High affinity InhA inhibitors with activity against drug-resistant strains of *Mycobacterium tuberculosis*, *ACS Chem Biol* 1, 43-53.
  60. McMurry, L. M., Oethinger, M., and Levy, S. B. (1998) Triclosan targets lipid synthesis, *Nature* 394, 531-532.
  61. Sivaraman, S., Sullivan, T. J., Johnson, F., Novichenok, P., Cui, G. L., Simmerling, C., and Tonge, P. J. (2004) Inhibition of the bacterial enoyl reductase FabI by triclosan: A structure-reactivity analysis of FabI



- inhibition by triclosan analogues, *Journal of Medicinal Chemistry* 47, 509-518.
62. Ward, W. H., Holdgate, G. A., Rowsell, S., McLean, E. G., Pauptit, R. A., Clayton, E., Nichols, W. W., Colls, J. G., Minshull, C. A., Jude, D. A., Mistry, A., Timms, D., Camble, R., Hales, N. J., Britton, C. J., and Taylor, I. W. (1999) Kinetic and structural characteristics of the inhibition of enoyl (acyl carrier protein) reductase by triclosan, *Biochemistry* 38, 12514-12525.
63. Boyne, M. E., Sullivan, T. J., Amende, C. W., Lu, H., Gruppo, V., Heaslip, D., Amin, A. G., Chatterjee, D., Lenaerts, A., Tonge, P. J., and Slayden, R. A. (2007) Targeting fatty acid biosynthesis for the development of novel chemotherapeutics against *Mycobacterium tuberculosis*: Evaluation of a-ring-modified diphenyl ethers as high-affinity InhA inhibitors, *Antimicrob Agents Chemother* 51, 3562-3567.
64. Luckner, S. R., Liu, N., am Ende, C. W., Tonge, P. J., and Kisker, C. (2010) A slow, tight binding inhibitor of InhA, the enoyl-acyl carrier protein reductase from *Mycobacterium tuberculosis*, *J Biol Chem* 285, 14330-14337.
65. Heath, R. J., and Rock, C. O. (2002) The Claisen condensation in biology, *Natural Product Reports* 19, 581-596.
66. Mathieu, M., Zeelen, J. P., Pauptit, R. A., Erdmann, R., Kunau, W. H., and Wierenga, R. K. (1994) The 2.8 Å crystal structure of peroxisomal 3-ketoacyl-CoA thiolase of *Saccharomyces cerevisiae*: a five-layered alpha

- beta alpha beta alpha structure constructed from two core domains of identical topology, *Structure* 2, 797-808.
67. Borgaro, J. G., Chang, A., Machutta, C. A., Zhang, X. J., and Tonge, P. J. (2011) Substrate Recognition by beta-Ketoacyl-ACP Synthases, *Biochemistry* 50, 10678-10686.
  68. Machutta, C. A., Bommineni, G. R., Luckner, S. R., Kapilashrami, K., Ruzsicska, B., Simmerling, C., Kisker, C., and Tonge, P. J. (2010) Slow onset inhibition of bacterial beta-ketoacyl-acyl carrier protein synthases by thiolactomycin, *J Biol Chem* 285, 6161-6169.
  69. Luckner, S. R., Machutta, C. A., Tonge, P. J., and Kisker, C. (2009) Crystal structures of Mycobacterium tuberculosis KasA show mode of action within cell wall biosynthesis and its inhibition by thiolactomycin, *Structure* 17, 1004-1013.
  70. Pappenberger, G., Schulz-Gasch, T., Kusznir, E., Muller, F., and Hennig, M. (2007) Structure-assisted discovery of an aminothiazole derivative as a lead molecule for inhibition of bacterial fatty-acid synthesis, *Acta Crystallogr D Biol Crystallogr* 63, 1208-1216.
  71. Young, K., Jayasuriya, H., Ondeyka, J. G., Herath, K., Zhang, C., Kodali, S., Galgoci, A., Painter, R., Brown-Driver, V., Yamamoto, R., Silver, L. L., Zheng, Y., Ventura, J. I., Sigmund, J., Ha, S., Basilio, A., Vicente, F., Tormo, J. R., Pelaez, F., Youngman, P., Cully, D., Barrett, J. F., Schmatz, D., Singh, S. B., and Wang, J. (2006) Discovery of FabH/FabF inhibitors from natural products, *Antimicrob Agents Chemother* 50, 519-526.

72. Ondeyka, J. G., Zink, D. L., Young, K., Painter, R., Kodali, S., Galgoci, A., Collado, J., Tormo, J. R., Basilio, A., Vicente, F., Wang, J., and Singh, S. B. (2006) Discovery of bacterial fatty acid synthase inhibitors from a *Phoma* species as antimicrobial agents using a new antisense-based strategy, *J Nat Prod* 69, 377-380.
73. Wang, J., Soisson, S. M., Young, K., Shoop, W., Kodali, S., Galgoci, A., Painter, R., Parthasarathy, G., Tang, Y. S., Cummings, R., Ha, S., Dorso, K., Motyl, M., Jayasuriya, H., Ondeyka, J., Herath, K., Zhang, C. W., Hernandez, L., Allocco, J., Basilio, A., Tormo, J. R., Genilloud, O., Vicente, F., Pelaez, F., Colwell, L., Lee, S. H., Michael, B., Felcetto, T., Gill, C., Silver, L. L., Hermes, J. D., Bartizal, K., Barrett, J., Schmatz, D., Becker, J. W., Cully, D., and Singh, S. B. (2006) Platensimycin is a selective FabF inhibitor with potent antibiotic properties, *Nature* 441, 358-361.
74. Wang, J., Kodali, S., Lee, S. H., Galgoci, A., Painter, R., Dorso, K., Racine, F., Motyl, M., Hernandez, L., Tinney, E., Colletti, S. L., Herath, K., Cummings, R., Salazar, O., Gonzalez, I., Basilio, A., Vicente, F., Genilloud, O., Pelaez, F., Jayasuriya, H., Young, K., Cully, D. F., and Singh, S. B. (2007) Discovery of platencin, a dual FabF and FabH inhibitor with in vivo antibiotic properties, *Proc Natl Acad Sci U S A* 104, 7612-7616.

75. Noto, T., Miyakawa, S., Oishi, H., Endo, H., and Okazaki, H. (1982) Thiolactomycin, a New Antibiotic .3. Invitro Antibacterial Activity, *Journal of Antibiotics* 35, 401-410.
76. Oishi, H., Noto, T., Sasaki, H., Suzuki, K., Hayashi, T., Okazaki, H., Ando, K., and Sawada, M. (1982) Thiolactomycin, a New Antibiotic .1. Taxonomy of the Producing Organism, Fermentation and Biological Properties, *Journal of Antibiotics* 35, 391-395.
77. Miyakawa, S., Suzuki, K., Noto, T., Harada, Y., and Okazaki, H. (1982) Thiolactomycin, a New Antibiotic .4. Biological Properties and Chemotherapeutic Activity in Mice, *Journal of Antibiotics* 35, 411-419.
78. Hamada, S., Fujiwara, T., Shimauchi, H., Ogawa, T., Nishihara, T., Koga, T., Nehashi, T., and Matsuno, T. (1990) Antimicrobial activities of thiolactomycin against gram-negative anaerobes associated with periodontal disease. f1, *Oral Microbiol Immunol* 5, 340-345.
79. Barry, C. E., 3rd, Lee, R. E., Mdluli, K., Sampson, A. E., Schroeder, B. G., Slayden, R. A., and Yuan, Y. (1998) Mycolic acids: structure, biosynthesis and physiological functions, *Progress in Lipid Research* 37, 143-179.
80. Schlesinger, L. S. (1996) Entry of Mycobacterium tuberculosis into mononuclear phagocytes, *Curr Top Microbiol Immunol* 215, 71-96.
81. Glickman, M. S., and Jacobs, W. R., Jr. (2001) Microbial pathogenesis of Mycobacterium tuberculosis: dawn of a discipline, *Cell* 104, 477-485.

82. Glickman, M. S., Cox, J. S., and Jacobs, W. R., Jr. (2000) A novel mycolic acid cyclopropane synthetase is required for cording, persistence, and virulence of *Mycobacterium tuberculosis*, *Mol Cell* 5, 717-727.
83. Dubnau, E., Chan, J., Raynaud, C., Mohan, V. P., Laneelle, M. A., Yu, K., Quemard, A., Smith, I., and Daffe, M. (2000) Oxygenated mycolic acids are necessary for virulence of *Mycobacterium tuberculosis* in mice, *Mol Microbiol* 36, 630-637.
84. Daffe, M., and Draper, P. (1998) The envelope layers of mycobacteria with reference to their pathogenicity, *Adv Microb Physiol* 39, 131-203.
85. Kremer, L., Douglas, J. D., Baulard, A. R., Morehouse, C., Guy, M. R., Alland, D., Dover, L. G., Lakey, J. H., Jacobs, W. R., Jr., Brennan, P. J., Minnikin, D. E., and Besra, G. S. (2000) Thiolactomycin and related analogues as novel anti-mycobacterial agents targeting KasA and KasB condensing enzymes in *Mycobacterium tuberculosis*, *J Biol Chem* 275, 16857-16864.
86. Smith, S., Witkowski, A., and Joshi, A. K. (2003) Structural and functional organization of the animal fatty acid synthase, *Progress in Lipid Research* 42, 289-317.
87. Kremer, L., Dover, L. G., Carrere, S., Nampoothiri, K. M., Lesjean, S., Brown, A. K., Brennan, P. J., Minnikin, D. E., Locht, C., and Besra, G. S. (2002) Mycolic acid biosynthesis and enzymic characterization of the beta-ketoacyl-ACP synthase A-condensing enzyme from *Mycobacterium tuberculosis*, *Biochem J* 364, 423-430.

88. Zhang, Y. M., White, S. W., and Rock, C. O. (2006) Inhibiting bacterial fatty acid synthesis, *J Biol Chem* 281, 17541-17544.
89. Boshoff, H. I., Barry, C.E. (2006) Is the mycobacterial cell wall a hopeless drug target for latent tuberculosis?, *Drug Discov. Today Dis Mech.* 3.
90. Haapalainen, A. M., Merilainen, G., and Wierenga, R. K. (2006) The thiolase superfamily: condensing enzymes with diverse reaction specificities, *Trends Biochem Sci* 31, 64-71.
91. Modis, Y., and Wierenga, R. K. (1999) A biosynthetic thiolase in complex with a reaction intermediate: the crystal structure provides new insights into the catalytic mechanism, *Structure* 7, 1279-1290.
92. Price, A. C., Choi, K. H., Heath, R. J., Li, Z., White, S. W., and Rock, C. O. (2001) Inhibition of beta-ketoacyl-acyl carrier protein synthases by thiolactomycin and cerulenin. Structure and mechanism, *J Biol Chem* 276, 6551-6559.
93. Lu, Y. J., White, S. W., and Rock, C. O. (2005) Domain swapping between *Enterococcus faecalis* FabN and FabZ proteins localizes the structural determinants for isomerase activity, *J Biol Chem* 280, 30342-30348.
94. von Wettstein-Knowles, P., Olsen, J. G., McGuire, K. A., and Henriksen, A. (2006) Fatty acid synthesis. Role of active site histidines and lysine in Cys-His-His-type beta-ketoacyl-acyl carrier protein synthases, *FEBS J* 273, 695-710.
95. Brown, M. S., Akopiants, K., Resceck, D. M., McArthur, H. A., McCormick, E., and Reynolds, K. A. (2003) Biosynthetic origins of the natural product,

- thiolactomycin: a unique and selective inhibitor of type II dissociated fatty acid synthases, *Journal of the American Chemical Society* 125, 10166-10167.
96. von Wettstein-Knowles, P., Olsen, J., Arnvig Mcguire, K., and Larsen, S. (2000) Molecular aspects of beta-ketoacyl synthase (KAS) catalysis, *Biochem Soc Trans* 28, 601-607.
97. Witkowski, A., Joshi, A. K., Lindqvist, Y., and Smith, S. (1999) Conversion of a beta-ketoacyl synthase to a malonyl decarboxylase by replacement of the active-site cysteine with glutamine, *Biochemistry* 38, 11643-11650.
98. Wang, J., Soisson, S. M., Young, K., Shoop, W., Kodali, S., Galgoci, A., Painter, R., Parthasarathy, G., Tang, Y. S., Cummings, R., Ha, S., Dorso, K., Motyl, M., Jayasuriya, H., Ondeyka, J., Herath, K., Zhang, C., Hernandez, L., Allocco, J., Basilio, A., Tormo, J. R., Genilloud, O., Vicente, F., Pelaez, F., Colwell, L., Lee, S. H., Michael, B., Felcetto, T., Gill, C., Silver, L. L., Hermes, J. D., Bartizal, K., Barrett, J., Schmatz, D., Becker, J. W., Cully, D., and Singh, S. B. (2006) Platensimycin is a selective FabF inhibitor with potent antibiotic properties, *Nature* 441, 358-361.
99. Surolia, A., Ramya, T. N., Ramya, V., and Surolia, N. (2004) 'FAS't inhibition of malaria, *Biochem J* 383, 401-412.
100. Sassetti, C. M., Boyd, D. H., and Rubin, E. J. (2003) Genes required for mycobacterial growth defined by high density mutagenesis, *Mol Microbiol* 48, 77-84.

101. Bhatt, A., Kremer, L., Dai, A. Z., Sacchettini, J. C., and Jacobs, W. R., Jr. (2005) Conditional depletion of KasA, a key enzyme of mycolic acid biosynthesis, leads to mycobacterial cell lysis, *J Bacteriol* 187, 7596-7606.
102. Hayashi, T., Yamamoto, O., Sasaki, H., Okazaki, H., and Kawaguchi, A. (1984) Inhibition of fatty acid synthesis by the antibiotic thiolactomycin, *J Antibiot (Tokyo)* 37, 1456-1461.
103. Nawata, Y., Sasaki, H., Oishi, H., Suzuki, K., Sawada, M., Ando, K., and Iitaka, Y. (1989) Structure of thiolactomycin, *Acta Crystallogr C* 45 ( Pt 6), 978-979.
104. Omura, S., Katagiri, M., Nakagawa, A., Sano, Y., and Nomura, S. (1967) Studies on cerulenin. V. Structure of cerulenin, *J Antibiot (Tokyo)* 20, 349-354.
105. Sato, Y., Nomura, S., Kamio, Y., Omura, S., and Hata, T. (1967) Studies on cerulenin, 3. Isolation and physico-chemical properties of cerulenin, *J Antibiot (Tokyo)* 20, 344-348.
106. Slayden, R. A., Lee, R. E., Armour, J. W., Cooper, A. M., Orme, I. M., Brennan, P. J., and Besra, G. S. (1996) Antimycobacterial action of thiolactomycin: an inhibitor of fatty acid and mycolic acid synthesis, *Antimicrob Agents Chemother* 40, 2813-2819.
107. Noto, T., Miyakawa, S., Oishi, H., Endo, H., and Okazaki, H. (1982) Thiolactomycin, a new antibiotic. III. In vitro antibacterial activity, *J Antibiot (Tokyo)* 35, 401-410.



108. Miyakawa, S., Suzuki, K., Noto, T., Harada, Y., and Okazaki, H. (1982) Thiolactomycin, a new antibiotic. IV. Biological properties and chemotherapeutic activity in mice, *J Antibiot (Tokyo)* 35, 411-419.
109. Kim, P., Zhang, Y. M., Shenoy, G., Nguyen, Q. A., Boshoff, H. I., Manjunatha, U. H., Goodwin, M. B., Lonsdale, J., Price, A. C., Miller, D. J., Duncan, K., White, S. W., Rock, C. O., Barry, C. E., 3rd, and Dowd, C. S. (2006) Structure-activity relationships at the 5-position of thiolactomycin: an intact (5R)-isoprene unit is required for activity against the condensing enzymes from *Mycobacterium tuberculosis* and *Escherichia coli*, *Journal of Medicinal Chemistry* 49, 159-171.
110. Oishi, H., Noto, T., Sasaki, H., Suzuki, K., Hayashi, T., Okazaki, H., Ando, K., and Sawada, M. (1982) Thiolactomycin, a new antibiotic. I. Taxonomy of the producing organism, fermentation and biological properties, *J Antibiot (Tokyo)* 35, 391-395.
111. Chen, J., Zhang, Z., Stebbins, J. L., Zhang, X., Hoffman, R., Moore, A., and Pellecchia, M. (2007) A fragment-based approach for the discovery of isoform-specific p38alpha inhibitors, *ACS Chem Biol* 2, 329-336.
112. Price, A. C., Choi, K. H., Heath, R. J., Li, Z., White, S. W., and Rock, C. O. (2001) Inhibition of beta-ketoacyl-acyl carrier protein synthases by thiolactomycin and cerulenin. Structure and mechanism, *J. Biol. Chem.* 276, 6551-6559.
113. Becattini, B., and Pellecchia, M. (2006) SAR by ILOEs: an NMR-based approach to reverse chemical genetics, *Chemistry* 12, 2658-2662.

114. Stott, K., Keeler, J., Van, Q. N., and Shaka, A. J. (1997) One-Dimensional NOE Experiments Using Pulsed Field Gradients, *J. Magn. Reson.* 125, 302-324.
115. Stott, K., Stonehouse, J., Keeler, J., Hwang, T.-L., and Shaka, A. J. (1995) Excitation Sculpting in High-Resolution Nuclear Magnetic Resonance Spectroscopy: Application to Selective NOE Experiments, *J. Am. Chem. Soc.* 117, 4199-4200.
116. Hu, H., and Krishnamurthy, K. (2006) Revisiting the initial rate approximation in kinetic NOE measurements, *J Magn Reson* 182, 173-177.
117. Marion, D., Ikura, M., Tschudin, R., and Bax, A. (1989) Rapid Recording of 2d Nmr-Spectra without Phase Cycling - Application to the Study of Hydrogen-Exchange in Proteins, *J. Magn. Reson.* 85, 393-399.
118. Sasaki, H., Oishi, H., Hayashi, T., Matsuura, I., Ando, K., and Sawada, M. (1982) Thiolactomycin, a new antibiotic. II. Structure elucidation, *J Antibiot (Tokyo)* 35, 396-400.
119. Edzes, H. T., and Samulski, E. T. (1977) Cross relaxation and spin diffusion in the proton NMR of hydrated collagen, *Nature* 265, 521-523.
120. DeLano, W. L. (2004) Use of PYMOL as a communications tool for molecular science., *Abstracts of Papers of the American Chemical Society* 228, U313-U314.
121. Oishi, H., Noto, T., Sasaki, H., Suzuki, K., Hayashi, T., Okazaki, H., Ando, K., and Sawada, M. (1982) Thiolactomycin, a new antibiotic. I. Taxonomy

- of the producing organism, fermentation and biological properties, *J. Antibiot.* **35**, 391-395.
122. Slayden, R. A., Lee, R. E., Armour, J. W., Cooper, A. M., Orme, I. M., Brennan, P. J., and Besra, G. S. (1996) Antimycobacterial action of thiolactomycin: an inhibitor of fatty acid and mycolic acid synthesis, *Antimicrob. Agents Chemother.* **40**, 2813-2819.
123. Hayashi, T., Yamamoto, O., Sasaki, H., Kawaguchi, A., and Okazaki, H. (1983) Mechanism of action of the antibiotic thiolactomycin inhibition of fatty acid synthesis of *Escherichia coli*, *Biochem. Biophys. Res. Commun.* **115**, 1108-1113.
124. Jackowski, S., Zhang, Y. M., Price, A. C., White, S. W., and Rock, C. O. (2002) A missense mutation in the *fabB* (beta-ketoacyl-acyl carrier protein synthase I) gene confers thiolactomycin resistance to *Escherichia coli*, *Antimicrob. Agents Chemother.* **46**, 1246-1252.
125. Tsay, J. T., Rock, C. O., and Jackowski, S. (1992) Overproduction of beta-ketoacyl-acyl carrier protein synthase I imparts thiolactomycin resistance to *Escherichia coli* K-12, *J. Bacteriol.* **174**, 508-513.
126. Miyakawa, S., Suzuki, K., Noto, T., Harada, Y., and Okazaki, H. (1982) Thiolactomycin, a new antibiotic. IV. Biological properties and chemotherapeutic activity in mice, *J. Antibiot.* **35**, 411-419.
127. Lipinski, C. A., Lombardo, F., Dominy, B. W., and Feeney, P. J. (2001) Experimental and computational approaches to estimate solubility and

- permeability in drug discovery and development settings, *Adv. Drug Deliv. Rev.* **46**, 3-26.
128. Nishida, I., Kawaguchi, A., and Yamada, M. (1986) Effect of thiolactomycin on the individual enzymes of the fatty acid synthase system in *Escherichia coli*, *J. Biochem.* **99**, 1447-1454.
129. Kim, P., Zhang, Y. M., Shenoy, G., Nguyen, Q. A., Boshoff, H. I., Manjunatha, U. H., Goodwin, M. B., Lonsdale, J., Price, A. C., Miller, D. J., Duncan, K., White, S. W., Rock, C. O., Barry, C. E., and Dowd, C. S. (2006) Structure-activity relationships at the 5-position of thiolactomycin: An intact (5R)-isoprene unit is required for activity against the condensing enzymes from *Mycobacterium tuberculosis* and *Escherichia coli*, *J. Med. Chem.* **49**, 159-171.
130. Machutta, C. A., Bommineni, G. R., Luckner, S. R., Kapilashrami, K., Ruzsicska, B., Simmerling, C., Kisker, C., and Tonge, P. J. (2010) Slow onset inhibition of bacterial beta-ketoacyl-acyl carrier protein synthases by thiolactomycin, *J. Biol. Chem.* **285**, 6161-6169.
131. Swinney, D. C. (2004) Biochemical mechanisms of drug action: what does it take for success?, *Nat Rev Drug Discov* **3**, 801-808.
132. Copeland, R. A., Pompliano, D. L., and Meek, T. D. (2006) Drug-target residence time and its implications for lead optimization, *Nat Rev Drug Discov* **5**, 730-739.
133. Sakya, S. M., Suarez-Contreras, M., Dirlam, J. P., O'Connell, T. N., Hayashi, S. F., Santoro, S. L., Kamicker, B. J., George, D. M., and Ziegler,

- C. B. (2001) Synthesis and structure-activity relationships of thiotetronic acid analogues of thiolactomycin, *Bioorg Med Chem Lett* 11, 2751-2754.
134. Jones, S. M., Urch, J. E., Brun, R., Harwood, J. L., Berry, C., and Gilbert, I. H. (2004) Analogues of thiolactomycin as potential anti-malarial and anti-trypanosomal agents, *Bioorg. Med. Chem.* 12, 683-692.
135. Kim, P., Barry, C. E., and Dowd, C. S. (2006) Novel route to 5-position vinyl derivatives of thiolactomycin: Olefination vs. deformylation, *Tetrahedron Lett.* 47, 3447-3451.
136. Jones, A. L., Herbert, D., Rutter, A. J., Dancer, J. E., and Harwood, J. L. (2000) Novel inhibitors of the condensing enzymes of the type II fatty acid synthase of pea (*Pisum sativum*), *Biochem. J.* 347, 205-209.
137. Samel, S. A., Wagner, B., Marahiel, M. A., and Essen, L. O. (2006) The thioesterase domain of the fengycin biosynthesis cluster: a structural base for the macrocyclization of a non-ribosomal lipopeptide, *J Mol Biol* 359, 876-889.
138. McFadden, J. M., Medghalchi, S. M., Thupari, J. N., Pinn, M. L., Vadlamudi, A., Miller, K. I., Kuhajda, F. P., and Townsend, C. A. (2005) Application of a flexible synthesis of (5R)-thiolactomycin to develop new inhibitors of type I fatty acid synthase, *J. Med. Chem.* 48, 946-961.
139. Kao, S. M., Asanov, A. N., and Oldham, P. B. (1998) A comparison of fluorescence inner-filter effects for different cell configurations, *Instrumentation Science & Technology* 26, 375-387.

140. Tsai, Y. C., and Johnson, K. A. (2006) A new paradigm for DNA polymerase specificity, *Biochemistry* 45, 9675-9687.
141. Lang, P. T., Brozell, S. R., Mukherjee, S., Pettersen, E. F., Meng, E. C., Thomas, V., Rizzo, R. C., Case, D. A., James, T. L., and Kuntz, I. D. (2009) DOCK 6: Combining techniques to model RNA-small molecule complexes, *Rna-a Publication of the Rna Society* 15, 1219-1230.
142. Mukherjee, S., Balius, T. E., and Rizzo, R. C. (2010) Docking validation resources: protein family and ligand flexibility experiments, *J Chem Inf Model* 50, 1986-2000.
143. Witkowski, A., Joshi, A. K., and Smith, S. (2002) Mechanism of the beta-ketoacyl synthase reaction catalyzed by the animal fatty acid synthase, *Biochemistry* 41, 10877-10887.
144. Dalvit, C., Fogliatto, G., Stewart, A., Veronesi, M., and Stockman, B. (2001) WaterLOGSY as a method for primary NMR screening: practical aspects and range of applicability, *J Biomol NMR* 21, 349-359.
145. Baldock, C., Rafferty, J. B., Stuitje, A. R., Slabas, A. R., and Rice, D. W. (1998) The X-ray structure of Escherichia coli enoyl reductase with bound NAD<sup>+</sup> at 2.1 Å resolution, *J Mol Biol* 284, 1529-1546.
146. Stewart, M. J., Parikh, S., Xiao, G., Tonge, P. J., and Kisker, C. (1999) Structural basis and mechanism of enoyl reductase inhibition by triclosan, *J Mol Biol* 290, 859-865.

147. Rozwarski, D. A., Grant, G. A., Barton, D. H., Jacobs, W. R., Jr., and Sacchettini, J. C. (1998) Modification of the NADH of the isoniazid target (InhA) from *Mycobacterium tuberculosis*, *Science* 279, 98-102.
148. Rozwarski, D. A., Vilcheze, C., Sugantino, M., Bittman, R., and Sacchettini, J. C. (1999) Crystal structure of the *Mycobacterium tuberculosis* enoyl-ACP reductase, InhA, in complex with NAD<sup>+</sup> and a C16 fatty acyl substrate, *J Biol Chem* 274, 15582-15589.
149. Xu, H., Sullivan, T. J., Sekiguchi, J., Kirikae, T., Ojima, I., Stratton, C. F., Mao, W., Rock, F. L., Alley, M. R., Johnson, F., Walker, S. G., and Tonge, P. J. (2008) Mechanism and inhibition of saFabI, the enoyl reductase from *Staphylococcus aureus*, *Biochemistry* 47, 4228-4236.
150. Lu, H., England, K., am Ende, C., Truglio, J. J., Luckner, S., Reddy, B. G., Marlenee, N. L., Knudson, S. E., Knudson, D. L., Bowen, R. A., Kisker, C., Slayden, R. A., and Tonge, P. J. (2009) Slow-onset inhibition of the FabI enoyl reductase from *Francisella tularensis*: residence time and in vivo activity, *ACS Chem Biol* 4, 221-231.
151. Zhang, Y., Heym, B., Allen, B., Young, D., and Cole, S. (1992) The catalase-peroxidase gene and isoniazid resistance of *Mycobacterium tuberculosis*, *Nature* 358, 591-593.
152. Rawat, R., Whitty, A., and Tonge, P. J. (2003) The isoniazid-NAD adduct is a slow, tight-binding inhibitor of InhA, the *Mycobacterium tuberculosis* enoyl reductase: Adduct affinity and drug resistance, *P Natl Acad Sci USA* 100, 13881-13886.

153. Banerjee, A., Dubnau, E., Quemard, A., Balasubramanian, V., Um, K. S., Wilson, T., Collins, D., de Lisle, G., and Jacobs, W. R., Jr. (1994) inhA, a gene encoding a target for isoniazid and ethionamide in *Mycobacterium tuberculosis*, *Science* 263, 227-230.
154. White, S. W., Zheng, J., Zhang, Y. M., and Rock. (2005) The structural biology of type II fatty acid biosynthesis, *Annu Rev Biochem* 74, 791-831.
155. Parikh, S. L., Xiao, G., and Tonge, P. J. (2000) Inhibition of InhA, the enoyl reductase from *Mycobacterium tuberculosis*, by triclosan and isoniazid, *Biochemistry* 39, 7645-7650.
156. Boyne, M. E., Sullivan, T. J., Amende, C. W., Lu, H., Gruppo, V., Heaslip, D., Amin, A. G., Chatterjee, D., Lenaerts, A., Tonge, P. J., and Slayden, R. A. (2007) Targeting fatty acid biosynthesis for the development of novel chemotherapeutics against *Mycobacterium tuberculosis*: Evaluation of a-ring-modified diphenyl ethers as high-affinity InhA inhibitors, *Antimicrobial Agents and Chemotherapy* 51, 3562-3567.
157. O'Shea, R., and Moser, H. E. (2008) Physicochemical properties of antibacterial compounds: implications for drug discovery, *Journal of Medicinal Chemistry* 51, 2871-2878.
158. Lipinski, C. A., Lombardo, F., Dominy, B. W., and Feeney, P. J. (2001) Experimental and computational approaches to estimate solubility and permeability in drug discovery and development settings, *Adv Drug Deliv Rev* 46, 3-26.



159. Zhang, R., and Monsma, F. (2009) The importance of drug-target residence time, *Current Opinion in Drug Discovery & Development* 12, 488-496.
160. Eyles, S. J., and Kaltashov, I. A. (2004) Methods to study protein dynamics and folding by mass spectrometry, *Methods* 34, 88-99.
161. Krukenberg, K. A., Street, T. O., Lavery, L. A., and Agard, D. A. (2011) Conformational dynamics of the molecular chaperone Hsp90, *Q Rev Biophys* 44, 229-255.
162. Yan, B. X., and Sun, Y. Q. (1997) Glycine residues provide flexibility for enzyme active sites, *J Biol Chem* 272, 3190-3194.
163. Beechem, J. M., and Brand, L. (1985) Time-Resolved Fluorescence of Proteins, *Annu Rev Biochem* 54, 43-71.
164. Lakowicz, J. R. (2006) Introduction to Fluorescence, (Lakowicz, J. R., Ed.), pp 1-26, Springer US.
165. Wang, L., Xie, J., and Schultz, P. G. (2006) Expanding the genetic code, *Annu Rev Biophys Biomol Struct* 35, 225-249.
166. Ross, J. B., Szabo, A. G., and Hogue, C. W. (1997) Enhancement of protein spectra with tryptophan analogs: fluorescence spectroscopy of protein-protein and protein-nucleic acid interactions, *Methods Enzymol* 278, 151-190.
167. Chin, J. W., Cropp, T. A., Anderson, J. C., Mukherji, M., Zhang, Z. W., and Schultz, P. G. (2003) An expanded eukaryotic genetic code, *Science* 301, 964-967.

168. Jackson, J. C., Hammill, J. T., and Mehl, R. A. (2007) Site-specific incorporation of a F-19-amino acid into proteins as an NMR probe for characterizing protein structure and reactivity, *Journal of the American Chemical Society* 129, 1160-1166.
169. Taskent-Sezgin, H., Marek, P., Thomas, R., Goldberg, D., Chung, J., Carrico, I., and Raleigh, D. P. (2010) Modulation of p-cyanophenylalanine fluorescence by amino acid side chains and rational design of fluorescence probes of alpha-helix formation, *Biochemistry* 49, 6290-6295.
170. Aprilakis, K. N., Taskent, H., and Raleigh, D. P. (2007) Use of the novel fluorescent amino acid p-cyanophenylalanine offers a direct probe of hydrophobic core formation during the folding of the N-terminal domain of the ribosomal protein L9 and provides evidence for two-state folding, *Biochemistry* 46, 12308-12313.
171. Taskent-Sezgin, H., Chung, J., Patsalo, V., Miyake-Stoner, S. J., Miller, A. M., Brewer, S. H., Mehl, R. A., Green, D. F., Raleigh, D. P., and Carrico, I. (2009) Interpretation of p-cyanophenylalanine fluorescence in proteins in terms of solvent exposure and contribution of side-chain quenchers: a combined fluorescence, IR and molecular dynamics study, *Biochemistry* 48, 9040-9046.
172. Park, H., Suquet, C., Savenkova, M. I., Satterlee, J. D., and Kang, C. (2002) Cloning, purification, crystallization and preliminary X-ray analysis of DOS heme domain, a new heme oxygen sensor in Escherichia coli, *Acta Crystallogr D Biol Crystallogr* 58, 1504-1506.

173. Lundqvist, T., Fisher, S. L., Kern, G., Folmer, R. H., Xue, Y., Newton, D. T., Keating, T. A., Alm, R. A., and de Jonge, B. L. (2007) Exploitation of structural and regulatory diversity in glutamate racemases, *Nature* 447, 817-822.
174. Wiesner, S., Wybenga-Groot, L. E., Warner, N., Lin, H., Pawson, T., Forman-Kay, J. D., and Sicheri, F. (2006) A change in conformational dynamics underlies the activation of Eph receptor tyrosine kinases, *EMBO J* 25, 4686-4696.
175. Kovacs, J. M., Hannan, J. P., Eisenmesser, E. Z., and Holers, V. M. (2009) Mapping of the C3d ligand binding site on complement receptor 2 (CR2/CD21) using nuclear magnetic resonance and chemical shift analysis, *J Biol Chem* 284, 9513-9520.
176. Pellecchia, M., Meininger, D., Dong, Q., Chang, E., Jack, R., and Sem, D. S. (2002) NMR-based structural characterization of large protein-ligand interactions, *J Biomol NMR* 22, 165-173.
177. Griswold, I. J., and Dahlquist, F. W. (2002) Bigger is better: megadalton protein NMR in solution, *Nat Struct Biol* 9, 567-568.
178. Fiaux, J., Bertelsen, E. B., Horwich, A. L., and Wuthrich, K. (2002) NMR analysis of a 900K GroEL GroES complex, *Nature* 418, 207-211.
179. Salzmann, M., Pervushin, K., Wider, G., Senn, H., and Wuthrich, K. (2000) NMR assignment and secondary structure determination of an octameric 110 kDa protein using TROSY in triple resonance experiments, *Journal of the American Chemical Society* 122, 7543-7548.

180. Tugarinov, V., Choy, W. Y., Orekhov, V. Y., and Kay, L. E. (2005) Solution NMR-derived global fold of a monomeric 82-kDa enzyme, *Proceedings of the National Academy of Sciences of the United States of America* 102, 622-627.
181. Vogtherr, M., Saxena, K., Hoelder, S., Grimme, S., Betz, M., Schieberr, U., Pescatore, B., Robin, M., Delarbre, L., Langer, T., Wendt, K. U., and Schwalbe, H. (2006) NMR characterization of kinase p38 dynamics in free and ligand-bound forms, *Angew Chem Int Ed Engl* 45, 993-997.
182. Jacobs, D. M., Langer, T., Elshorst, B., Saxena, K., Fiebig, K. M., Vogtherr, M., and Schwalbe, H. (2006) NMR backbone assignment of the N-terminal domain of human HSP90, *J Biomol NMR* 36 Suppl 1, 52.
183. Huntley, J. J., Scrofani, S. D., Osborne, M. J., Wright, P. E., and Dyson, H. J. (2000) Dynamics of the metallo-beta-lactamase from *Bacteroides fragilis* in the presence and absence of a tight-binding inhibitor, *Biochemistry* 39, 13356-13364.
184. Osborne, M. J., Schnell, J., Benkovic, S. J., Dyson, H. J., and Wright, P. E. (2001) Backbone dynamics in dihydrofolate reductase complexes: role of loop flexibility in the catalytic mechanism, *Biochemistry* 40, 9846-9859.
185. Isaacson, R. L., Simpson, P. J., Liu, M., Cota, E., Zhang, X., Freemont, P., and Matthews, S. (2007) A new labeling method for methyl transverse relaxation-optimized spectroscopy NMR spectra of alanine residues, *Journal of the American Chemical Society* 129, 15428-15429.

186. Quemard, A., Sacchettini, J. C., Dessen, A., Vilcheze, C., Bittman, R., Jacobs, W. R., Jr., and Blanchard, J. S. (1995) Enzymatic characterization of the target for isoniazid in *Mycobacterium tuberculosis*, *Biochemistry* 34, 8235-8241.
187. Hammill, J. T., Miyake-Stoner, S., Hazen, J. L., Jackson, J. C., and Mehl, R. A. (2007) Preparation of site-specifically labeled fluorinated proteins for <sup>19</sup>F-NMR structural characterization, *Nat Protoc* 2, 2601-2607.
188. Weljie, A. M., Yamniuk, A. P., Yoshino, H., Izumi, Y., and Vogel, H. J. (2003) Protein conformational changes studied by diffusion NMR spectroscopy: application to helix-loop-helix calcium binding proteins, *Protein Sci* 12, 228-236.
189. Pervushin, K., Riek, R., Wider, G., and Wuthrich, K. (1997) Attenuated T-2 relaxation by mutual cancellation of dipole-dipole coupling and chemical shift anisotropy indicates an avenue to NMR structures of very large biological macromolecules in solution, *Proceedings of the National Academy of Sciences of the United States of America* 94, 12366-12371.
190. Delaglio, F., Grzesiek, S., Vuister, G. W., Zhu, G., Pfeifer, J., and Bax, A. (1995) NMRPipe: a multidimensional spectral processing system based on UNIX pipes, *J Biomol NMR* 6, 277-293.
191. Marek, P., Gupta, R., and Raleigh, D. P. (2008) The fluorescent amino acid p-cyanophenylalanine provides an intrinsic probe of amyloid formation, *Chembiochem* 9, 1372-1374.

192. Jones, J. A., Wilkins, D. K., Smith, L. J., and Dobson, C. M. (1997) Characterisation of protein unfolding by NMR diffusion measurements, *J Biomol NMR* 10, 199-203.
193. Wilkins, D. K., Grimshaw, S. B., Receveur, V., Dobson, C. M., Jones, J. A., and Smith, L. J. (1999) Hydrodynamic radii of native and denatured proteins measured by pulse field gradient NMR techniques, *Biochemistry* 38, 16424-16431.
194. Kruh, N. A., Rawat, R., Ruzsicska, B. P., and Tonge, P. J. (2007) Probing mechanisms of resistance to the tuberculosis drug isoniazid: Conformational changes caused by inhibition of InhA, the enoyl reductase from *Mycobacterium tuberculosis*, *Protein Sci* 16, 1617-1627.
195. Putnam, C. D., Hammel, M., Hura, G. L., and Tainer, J. A. (2007) X-ray solution scattering (SAXS) combined with crystallography and computation: defining accurate macromolecular structures, conformations and assemblies in solution, *Q Rev Biophys* 40, 191-285.
196. Schuyler, A. D., Maciejewski, M. W., Arthanari, H., and Hoch, J. C. (2011) Knowledge-based nonuniform sampling in multidimensional NMR, *J Biomol NMR* 50, 247-262.
197. Tugarinov, V., and Kay, L. E. (2003) Ile, Leu, and Val methyl assignments of the 723-residue malate synthase G using a new labeling strategy and novel NMR methods, *Journal of the American Chemical Society* 125, 13868-13878.

198. Iskar, M., Campillos, M., Kuhn, M., Jensen, L. J., van Noort, V., and Bork, P. (2010) Drug-induced regulation of target expression, *PLoS Comput Biol* 6.
199. Tummino, P. J., and Copeland, R. A. (2008) Residence time of receptor-ligand complexes and its effect on biological function, *Biochemistry* 47, 5481-5492.
200. Vauquelin, G., and Van Liefde, I. (2006) Slow antagonist dissociation and long-lasting in vivo receptor protection, *Trends in Pharmacological Sciences* 27, 355-359.
201. Champney, W. S., and Tober, C. L. (1999) Molecular investigation of the postantibiotic effects of clarithromycin and erythromycin on *Staphylococcus aureus* cells, *Antimicrob Agents Chemother* 43, 1324-1328.
202. Copeland, R. A. (2010) The dynamics of drug-target interactions: drug-target residence time and its impact on efficacy and safety, *Expert Opinion on Drug Discovery* 5, 305-310.
203. MacKenzie, F. M., and Gould, I. M. (1993) The post-antibiotic effect, *J Antimicrob Chemother* 32, 519-537.
204. Bundtzen, R. W., Gerber, A. U., Cohn, D. L., and Craig, W. A. (1981) Post-Antibiotic Suppression of Bacterial-Growth, *Reviews of Infectious Diseases* 3, 28-37.

205. Isaksson, B., Nilsson, L., Maller, R., and Soren, L. (1988) Postantibiotic Effect of Aminoglycosides on Gram-Negative Bacteria Evaluated by a New Method, *J Antimicrob Chemother* 22, 23-33.
206. Gerber, A. U., and Craig, W. A. (1981) Growth-Kinetics of Respiratory Pathogens after Short Exposures to Ampicillin and Erythromycin Invitro, *J Antimicrob Chemother* 8, 81-91.
207. Kirkpatrick, D. S., Gerber, S. A., and Gygi, S. P. (2005) The absolute quantification strategy: a general procedure for the quantification of proteins and post-translational modifications, *Methods* 35, 265-273.
208. Gerber, S. A., Rush, J., Stemman, O., Kirschner, M. W., and Gygi, S. P. (2003) Absolute quantification of proteins and phosphoproteins from cell lysates by tandem MS, *Proc Natl Acad Sci U S A* 100, 6940-6945.
209. Ong, S. E., Foster, L. J., and Mann, M. (2003) Mass spectrometric-based approaches in quantitative proteomics, *Methods* 29, 124-130.
210. Mirgorodskaya, O. A., Kozmin, Y. P., Titov, M. I., Korner, R., Sonksen, C. P., and Roepstorff, P. (2000) Quantitation of peptides and proteins by matrix-assisted laser desorption/ionization mass spectrometry using (18)O-labeled internal standards, *Rapid Commun Mass Spectrom* 14, 1226-1232.
211. Yao, X., Freas, A., Ramirez, J., Demirev, P. A., and Fenselau, C. (2001) Proteolytic 18O labeling for comparative proteomics: model studies with two serotypes of adenovirus, *Anal Chem* 73, 2836-2842.



212. Barr, J. R., Maggio, V. L., Patterson, D. G., Jr., Cooper, G. R., Henderson, L. O., Turner, W. E., Smith, S. J., Hannon, W. H., Needham, L. L., and Sampson, E. J. (1996) Isotope dilution--mass spectrometric quantification of specific proteins: model application with apolipoprotein A-I, *Clin Chem* 42, 1676-1682.
213. Barnidge, D. R., Dratz, E. A., Martin, T., Bonilla, L. E., Moran, L. B., and Lindall, A. (2003) Absolute quantification of the G protein-coupled receptor rhodopsin by LC/MS/MS using proteolysis product peptides and synthetic peptide standards, *Anal Chem* 75, 445-451.
214. Heath, R. J., and Rock, C. O. (2000) A triclosan-resistant bacterial enzyme, *Nature* 406, 145-146.
215. Furukawa, H., Tsay, J. T., Jackowski, S., Takamura, Y., and Rock, C. O. (1993) Thiolactomycin resistance in *Escherichia coli* is associated with the multidrug resistance efflux pump encoded by *emrAB*, *J Bacteriol* 175, 3723-3729.
216. Kubitschek, H. E., and Friske, J. A. (1986) Determination of bacterial cell volume with the Coulter Counter, *J Bacteriol* 168, 1466-1467.
217. Washburn, M. P., Wolters, D., and Yates, J. R., 3rd. (2001) Large-scale analysis of the yeast proteome by multidimensional protein identification technology, *Nat Biotechnol* 19, 242-247.
218. Mengin-Lecreulx, D., Flouret, B., and van Heijenoort, J. (1982) Cytoplasmic steps of peptidoglycan synthesis in *Escherichia coli*, *J Bacteriol* 151, 1109-1117.

219. Link, A. J., Robison, K., and Church, G. M. (1997) Comparing the predicted and observed properties of proteins encoded in the genome of *Escherichia coli* K-12, *Electrophoresis* 18, 1259-1313.
220. Ishihama, Y., Schmidt, T., Rappsilber, J., Mann, M., Hartl, F. U., Kerner, M. J., and Frishman, D. (2008) Protein abundance profiling of the *Escherichia coli* cytosol, *BMC Genomics* 9, 102.
221. Sivaraman, S., Sullivan, T. J., Johnson, F., Novichenok, P., Cui, G., Simmerling, C., and Tonge, P. J. (2004) Inhibition of the bacterial enoyl reductase FabI by triclosan: a structure-reactivity analysis of FabI inhibition by triclosan analogues, *Journal of Medicinal Chemistry* 47, 509-518.
222. Stock, J. B., Rauch, B., and Roseman, S. (1977) Periplasmic space in *Salmonella typhimurium* and *Escherichia coli*, *J Biol Chem* 252, 7850-7861.
223. Wenzel, M., Patra, M., Albrecht, D., Chen, D. Y., Nicolaou, K. C., Metzler-Nolte, N., and Bandow, J. E. (2011) Proteomic signature of fatty acid biosynthesis inhibition available for in vivo mechanism-of-action studies, *Antimicrob Agents Chemother* 55, 2590-2596.
224. Laubacher, M. E., and Ades, S. E. (2008) The Rcs phosphorelay is a cell envelope stress response activated by peptidoglycan stress and contributes to intrinsic antibiotic resistance, *J Bacteriol* 190, 2065-2074.

225. Kaldalu, N., Mei, R., and Lewis, K. (2004) Killing by ampicillin and ofloxacin induces overlapping changes in *Escherichia coli* transcription profile, *Antimicrob Agents Chemother* 48, 890-896.
226. Lomenick, B., Hao, R., Jonai, N., Chin, R. M., Aghajan, M., Warburton, S., Wang, J., Wu, R. P., Gomez, F., Loo, J. A., Wohlschlegel, J. A., Vondriska, T. M., Pelletier, J., Herschman, H. R., Clardy, J., Clarke, C. F., and Huang, J. (2009) Target identification using drug affinity responsive target stability (DARTS), *Proc Natl Acad Sci U S A* 106, 21984-21989.
227. Jayapal, K. P., Sui, S., Philp, R. J., Kok, Y. J., Yap, M. G., Griffin, T. J., and Hu, W. S. (2010) Multitagging proteomic strategy to estimate protein turnover rates in dynamic systems, *J Proteome Res* 9, 2087-2097.
228. Taniguchi, Y., Choi, P. J., Li, G. W., Chen, H., Babu, M., Hearn, J., Emili, A., and Xie, X. S. (2010) Quantifying *E. coli* proteome and transcriptome with single-molecule sensitivity in single cells, *Science* 329, 533-538.
229. Doherty, M. K., Whitehead, C., McCormack, H., Gaskell, S. J., and Beynon, R. J. (2005) Proteome dynamics in complex organisms: using stable isotopes to monitor individual protein turnover rates, *Proteomics* 5, 522-533.
230. Pratt, J. M., Petty, J., Riba-Garcia, I., Robertson, D. H., Gaskell, S. J., Oliver, S. G., and Beynon, R. J. (2002) Dynamics of protein turnover, a missing dimension in proteomics, *Mol Cell Proteomics* 1, 579-591.
231. Betts, J. C., McLaren, A., Lennon, M. G., Kelly, F. M., Lukey, P. T., Blakemore, S. J., and Duncan, K. (2003) Signature gene expression

profiles discriminate between isoniazid-, thiolactomycin-, and triclosan-treated *Mycobacterium tuberculosis*, *Antimicrob Agents Chemother* 47, 2903-2913.